UNIVERSITÀ DEGLI STUDI DI TRIESTE

XXX CICLO DEL DOTTORATO DI RICERCA IN

NANOTECNOLOGIE

CHARACTERIZATION OF THE ANTIMICROBIAL EFFECT OF BLUE LASER ON PSEUDOMONAS AERUGINOSA IN VITRO AND IN VIVO

Settore scientifico-disciplinare: **MED/28**

DOTTORANDO / A
KATIA RUPEL

COORDINATORE
PROF. LUCIA PASQUATO

SUPERVISORE DI TESI
PROF. ROBERTO DI LENARDA

TUTORE DI TESI
PROF. SERENA ZACCHIGNA

ANNO ACCADEMICO 2016/2017

CONTENTS

Abstract

The development of novel antimicrobial strategies has returned of crucial importance due to increasing resistance to conventional antibiotics. The antimicrobial effect of blue light has been recently described in several research works, but it needs further validation to be safely used in clinical practice and to find appropriate fields of application.

The aims of this study were to evaluate the antimicrobial properties of blue laser light on *Pseudomonas aeruginosa* (PAO), to explore the mechanisms underlying the antimicrobial activity, to evaluate possible toxicity on human keratinocytes, to validate this effect in vivo and to evaluate the use of blue laser in antimicrobial photodynamic therapy (PDT) using free curcumin and curcumin embedded in three types of amphiphilic nanomicelles.

The results of our study demonstrated how blue laser irradiation alone is able to exert antimicrobial effects towards PAO grown in different conditions (PAO grown in planktonic state and on solid surfaces) and we identified several effective irradiation parameters. Furthermore, we described also an antibiofilm activity both in disrupting a mature biofilm and in inhibiting biofilm formation. Although further and more molecular-based investigation is warranted, our results suggest, according with literature, a possible role of oxidative stress stimulation for the explanation of bacterial inhibition/death. Comparing blue laser source with LED, laser was significantly more effective.

When investigating the possible toxic effects on keratinocytes, we observed slightly different effects on two keratinocyte cell lines in terms of cell viability and metabolic activity after irradiation, and identified several protocols which proved both antimicrobial efficacy and safety towards human cells.

Furthermore, we highlighted a stimulation of inflammosome molecules expression as expected, but also an overexpression of highly active antimicrobial peptides (defensins), which persists hours after irradiation (especially defensin b3 and b4).

When applying the protocol with wavelength 445nm, power 0,3W, spot size 7cm^2, irradiance 0,105W/cm^2, and fluence 60J/cm^2 *in vivo* on a mouse model of infected abrasion, we obtained a significant reduction in bacterial load in laser treated mice, but not the complete eradication as we were expecting basing on our previous results.

But on the other hand, when observing histological samples to evaluate possible thermal damage, we noticed a huge difference among samples: while non treated displayed a high inflammation rate permeating epidermal and dermal layers, the laser treated ones had minimum epidermal damage and were almost free of inflammatory infiltrate.

Finally, we explored the possible potentiating effect of blue laser sublethal irradiation on three types of amphiphilic nanomicelles loaded with curcumin. We obtained the lowest MIC of curcumin nanoparticles described so far, which further decreased after sublethal blue laser irradiation.

Introduction

1. Antibiotic resistance and novel antimicrobial strategies

The beginning of the treatment of infections with antibiotics has revolutionized modern medicine and dramatically improved the success of a wide range of diseases and interventions such as surgical procedures, organ transplantations and cancer chemotherapy, among others. Unfortunately, the overuse and misuse of these medications, as well as a lack of novel drug development by the pharmaceutical industry, are most likely the responsible factors for the increase in antimicrobial resistance among common bacterial pathogens. In fact, there is an ever increasing number of patients suffering from infections caused by multi-resistant pathogens. It is understandable that the World Health Organization has named antibiotic resistance as one of the three most important public health threats of the 21st century (World Health Organization, 2014).

There is a high proportion of antibiotic resistance within bacteria that cause common infections, including urinary tract infections, pneumonia, cutaneous and mucosal infections. Several hospital-acquired infections are caused by highly resistant bacteria, such as methicillin-resistant *Staphylococcus aureus* (MRSA) or multidrug-resistant Gram-negative bacteria such as *Pseudomonas aeruginosa*. These infections are even more aggressive in immune-compromised and oncological patients, negatively impacting on their prognosis (Rossolini et al, 2014; Taylor et al, 2014). Therefore, alternative antimicrobial strategies are urgently needed.

Bacteria use two major genetic strategies to develop antimicrobial resistance: mutations in genes often associated with the mechanism of action of the compound, and acquisition of foreign DNA coding for resistance determinants through horizontal gene transfer. These strategies lead to several possible resistance mechanisms: modifications of the antimicrobial molecule, prevention to reach the antibiotic target (by decreasing penetration or actively extruding the antimicrobial compound), changes and/or bypass of target sites, and resistance due to global cell adaptive processes (Munita et al, 2016).

To face growing resistance, several novel approaches have been described: weak organic acids, bacteriophages, antimicrobial peptides, predatory bacteria,

gene editing enzymes, metals, photodynamic therapy and phototherapy (the latter two will be described later).

- Weak organic acids (WOA) such as acetic acid contain a carboxyl group COOH and unlike „strong" mineral/inorganic acids they do not completely dissociate in water (Hirshfield et al, 2003); several works describe their strong antimicrobial activity (Sloss et al, 1993; Nagoba et al, 2013), which is probably promoted by their high lipid permeability, allowing to enter into bacterial cells where they dissociate lowering bacterial pH, increasing osmolarity and consequently leading to microbial death (Roe et al, 1998). Despite case series studies on humans show promising results, no systematic clinical trial to test efficacy and tolerability in humans have been performed yet.

- Bacteriophages are viruses which target bacteria and can cause cell death. Bacteriophage have been studied and clinically used to treat various infections before antibiotics were discovered and became widespread (Kutter et al, 2015), including infections from *Pseudomonas aeruginosa* and *Staphylococcus aureus*. They are still used in food industry to eliminate specific pathogens (Bai et al, 2016). Their evaluation for use in human infections has began to increase again in recent years, and several studies with promising results *in vitro* and *in vivo* have been performed on *Pseudomonas aeruginosa* wound infections (McVay et al, 2007) or on infected catheters (Fu et al, 2010). However, there are very limited data on possible toxicity.

- Antimicrobial peptides (AMPs) are endogenous short peptides that exhibit antimicrobial activity and play an important role in the innate immune response. They act directly inactivating infective agents, or through the stimulation and modulation of the host immune response (Ganz et al, 1999; Yount et al, 2006). They act prevalently damaging the bacterial membrane, causing the release of ions and metabolites ending in cell death. However, a small subgroup is able to penetrate inside the microorganisms without damaging the membranes, and to block the

bacterial protein synthesis interacting with the ribosomes (Mardirossian et al, 2014). AMPs are characterized by a broad spectrum antimicrobial activity against both Gram-positive and Gram-negative bacteria even at the micromolar concentrations (Zanetti et al., 2005). Their peptidic nature and moderate toxicity make them more suitable for topical application than for systemic delivery. Many efforts have been put in decreasing the cytotoxicity of some of these peptides, ending in much more safe optimized antimicrobial peptides (Tomasinsig et al., 2006).

- Predatory bacteria (Myxobacteria) are gram-negative bacteria colonizing the soil which prey on other microorganisms both as solitary hunters, or grouping together in large consortia. They often utilize antibiotics as predatory weapons. In the 1980's sorangicin was isolated from a Sorangium strain as the first myxobacterial antibiotic with high potential for market development (Irschik et al., 1987). Since then many new compounds have been described. Myxobacteria are believed to be potent resources for novel anti-infectives, a probable consequence of the habitat where they live in competition with other bacteria and fungi, making the production of bioactive compounds an obvious strategy for survival (Müller et al, 2014). Antimicrobial peptides synthetized by bacteria are categorized as bacteriocins. It is believed that more than 99% of bacteria can produce at least one bacteriocin, to reduce the number of competitors in conditions of lack of nutrients (Riley and Wertz, 2002).

- Bacterial genome engeneering has become a concrete possibility thanks to the rapid development of genetic engeneering techniques. Together with gene insertions, deletions or mutations for modification of the genome, one of the main goals is to build and integrate gene circuits which process signals within a living cell for a desired output. Genetically modified bacteria offer great hope for finding novel solutions to detect and treat infections. However, the field is very young and it needs important assessment of biosafety before clinical application (Krishnamurthy et al, 2016).

- Metal nanoparticles (NPs) are nanosized metals with dimensions (length, width or thickness) within the size range 1-100 nm. They are derived mostly from heavy metals, having a density > 5 g/cm^3. The bactericidal activity of metal NPs is ascribed mainly to their ability to generate reactive oxygen species (ROS) and their affinity to associate closely with R-SH groups, impairing the function of specific enzymes or break S–S bridges necessary to maintain the integrity of folded proteins, causing detrimental effects to the metabolism and physiology of the cell. Ag is the most extensively used element to synthesize NPs. In addition, other elements have been used including Al (Al2O3), Au, Bi, Ce, Cu (CuI, CuO, and Cu2O), Fe (Fe2O3), Mg (MgO), Ti (TiO2), and Zn (ZnO). An important slowdown for their clinical application is toxicity against human cells, which will hopefully be strongly reduced by using specific ligands and bacterial cell receptors, making their activity as specific as possible (Slavin et al, 2017).

2. Photodynamic therapy (PDT) and nanovectors

Photodynamic therapy (PDT) is a treatment that requires a photosensitizing agent (PS), a low intensity light source (e.g. laser, intense pulsed laser, light-emitting diodes) of suitable wavelength to match the PS absorption peak and molecular oxygen. Hematoporphyrin derivative or Photofrin was the first PS to be studied in detail, while the most frequently employed clinically are the 5-aminolevulinic acid (ALA) and its methyl ester 5-aminolevulinate (MAL), which are metabolized to the photo-active protoporphyrin IX (Gold et al, 2009).

After exposure to light, the excited triplet PS can undergo two types of reaction: type 1 photoprocesses involve hydrogen or electron-transfer reactions between the excited state PS and other molecules in the environment (frequently oxygen), which produce ROS such as superoxide (O_2•−), hydrogen peroxide (H_2O_2), hydroxyl radicals (HO•) and hydroperoxyl radicals (HOO•); type 2 photoprocess is an energy transfer mechanism involving electron spin exchange between the excited triplet state PS and ground state oxygen ($^3O_2$), itself a triplet. Type I and type II reactions produce both ROS that cause oxidation of biomolecules (lipids, proteins and nucleic acids) in the cell. The damage involves prevalently the cell wall, causing permeabilization so that essential components such as nucleic acids leak out (Almeida et al, 2004; Yin et al, 2015).

Antimicrobial PDT presents several advantages: it can inactivate all known classes of microorganisms, including Gram-positive, Gram-negative bacteria, fungi, protozoa and viruses; it is effective also against resistant strains (Hamblin et al, 2004); it is unlikely to cause resistance; the effect is rapid (seconds) while the action of antibiotics can take hours or days, giving a potential advantage against fast-spreading infections. In addition, thanks to the broad-spectrum activity, the treatment can be performed before the identification of the infectuous species (Ferreyra et al, 2016).

In the last decade, PDT has also been combined with nanotechnology techniques, as the photochemical effectiveness can be greatly enhanced by the use of nanoparticles. For instance, many PS have poor water solubility and they tend to aggregate in the aqueous environment in physiological conditions.

Curcumin (diferuloylmethane) is a polyphenolic compound isolated by *Curcuma longa*. It is a hydrophobic yellow powder soluble in ethanol, dimethylsulfoxide (DMSO), and acetone. The molecular formula of Curcumin is $C_{21}H_{20}O_6$, and the molecular weight is 368.37 g/mol. It has been used throughout centuries as a medication, food pigment, and as a spice. Many medical properties have been described so far, and several are under scientific investigation to confirm them: in particular anti-inflammatory, anti-tumoral and antimicrobial effects are among the most extensively studied (Goel et al, 2008).

The absorption peak of curcumin is within the range 300-500nm with maximum at 430nm. When excited by light emitted with such wavelengths, it produces singlet oxygen ($^1O_2$) exerting potent phototoxic effects in micromolar amounts. Therefore, curcumin has the potential to be used as a photosensitizer for the treatment of microbial infections. One of the main problems for its application is hydrophobicity, which strongly decreases bioavailability limiting its action (Araujo et al, 2012).

Appropriately chosen nanoparticles can increase the solubility of hydrophobic PS including curcumin by encapsulation in delivery agents such as liposomes, micelles, gold nanoparticles, polymer nanoparticles, ceramic-based nanoparticles and carbon nanotubes.

- Liposomes are small artificial vesicles of spherical shape, with a wide size range 25nm-2,5μm, that can be created from cholesterol and natural non-toxic phospholipids. Liposomes can differ considerably due to several controllable factors: lipid composition, surface charge, size, and the method of preparation. Thanks to their biocompatibility, biodegradability, low toxicity, possibility to embed both hydrophilic and lipophilic drugs/compounds and capability to be modified with target-specific ligands, they are extensively investigated and already used in several fields: in medicine for target therapies, but also in food and cosmetic industry (Akbarzadeh et al, 2013).

- Nanomicelles (polymeric micelles) are colloidal structures formed from amphiphilic monomers/molecules, which tend to self-assembly at a critical micellar concentration, forming structures in a size range 5-

200nm, possibly embedding hydrophobic compounds. Advantages of nanomicelle use include simplicity of preparation, reproducibility at small scale, and the possibility to conjugate the surface side of the monomers with ligands for molecular targeting. Possible disadvantages are rapid dilution in aqueous medium and their inability to be loaded with hydrophilic molecules (Mitra et al, 2015).

- Gold nanoparticles (AuNPs) are the most extensively studied among metal nanoparticles due to their versatility and characteristics, evaluating several possible clinical applications such as biosensing, photothermal therapy, molecular imaging and drug carrying. Various shapes (such as spherical) and sizes (1-100nm) can be easily synthetized. Consequently, their optical and electrical properties depend on their shape and size. The negative charge on the surface permits functionalization with many kinds of biomolecules, such as drugs, DNA, and targeting ligands. Finally, they have distinct surface effect, ultra-small size, macroscopic quantum tunneling effect, and the presence of surface plasmon resonance (SPR) bands (Kong et al, 2017). However, toxicity studies against cells, tissues, organins and organisms have produced contrasting results, so this aspect still warrants further investigations (Alkilany et al, 2010).

- Polymer nanoparticles (PNPs) are nanosized hybrid protein/synthetic species (3–200 nm) used as drug delivery systems. The synthetic component can be a (bio)degradable or nondegradable polymer, and combined with proteins forms novel biohybrid materials with unprecedented properties. These include tissue-penetrating ability, high payload, a sustained drug release profile, drug protection from enzymatic digestion, passive targeting, etc. However, PNPs possess some limitations that include use of toxic solvents in the production process, polymer degradation, drug release outside the diseased tissue, and possible polymer cytotoxicity. A frequently used approach to reduce opsonins' adsorption and recognition by macrophages is PEGylation, that is binding with poly(ethylene glycol) (PEG), drastically increasing

biological inertness and hydrophilicity, which has already been approved by the U.S. Food and Drug Administration (FDA) (Koseva et al, 2015).

- Ceramic-based nanoparticles are nanoscale ceramic materials such as hydroxyapatite (HA), zirconia (ZrO_2), silica (SiO_2), titanium oxide (TiO_2), and alumina (Al_2O_3) made through novel synthesis methods to improve their physical-chemical properties seeking to reduce their cytotoxicity in biological systems (Moreno-Vega et al, 2012). Ceramic nanocarriers can easily transport drug entities in volume-confined administration routes (such as blood vessels, the digestive tract, across cell membranes, etc.) and deliver drugs in minimally invasive methods just as their polymeric counterparts. They are also easy to fabricate and inexpensive to produce. However, two major challenges remain: targeted drug delivery and precise control of drug release kinetics (Biondi et al, 2008).

- Carbon nanotubes (CNTs) are cylindrical molecules made of carbon atoms, with a lowest diameter of 1nm and variable length up to μm range. CNTs are hydrophobic, but can be easily functionalized to become water soluble and be used as carriers of both small drug molecules as well as macromolecules such as genes and proteins via covalent or noncovalent bonding. The needle-like shape of the CNTs enables them to penetrate cellular membranes via endocytosis and transport the carried therapeutic molecules. Due to safety issues, CNTs need extensive amounts of further research to explore their potential (Elhissi et al, 2012).

3. Antimicrobial effect of blue light

An emerging, novel approach to control antibiotic-resistant bacterial infections is based on the use of light, in particular blue wavelengths. The antimicrobial effect of blue light has been recently described, showing that exposure to light in the range of 400-470 nm with low irradiance (below 500mW/cm^2) decreases the viability of various bacterial species, including *Pseudomonas aeruginosa*, *Porphyromonas gingivalis*, *Helicobacter pylori*, and methicillin-resistant *Staphylococcus aureus* (MRSA) (Dai et al, 2012; Enwemeka et al, 2009). However, to date the clinical application of these approaches is currently limited to the topical treatment of acne vulgaris (Wheeland et al, 2011).

The antimicrobial mechanism of blue light is still unclear and under investigation, but it seems to rely on a photochemichal effect rather than a photothermal one. The interaction of blue light with endogenous photosensitizing molecules, especially porphyrins and flavins, is believed to provoke the generation of ROS. Specifically, absorption of light brings porphyrin molecules into an excited triplet state, leading to a non-radiative transfer of energy to the chemically stable molecular oxygen. The excited oxygen molecule dissociates into two highly reactive atomic species that damage the integrity of cells, leading eventually to microbial death (Yang et al, 1995).

Considering that the power and energy densities required to obtain antimicrobial effects are lower than in the case of the photothermal effect using other wavelengths, it seems that such approach may be used safely without provoking burn lesions on treated areas. In a recent study, Dai et al performed an *in vivo* study using a 415nm LED light applied on mouse burns infected with Pseudomonas aeruginosa using an irradiance of 19.5 mW/cm^2 and energy density of 55.8 J/cm^2. Histological analyses indicated no significant damage in the mouse skin exposed to blue light at the effective antimicrobial dose. In addition, survival analyses revealed that blue light significantly increased the survival rate of the infected mice (Dai et al, 2013). While the majority of such studies have been performed using LED sources of light, there is growing evidence that blue lasers have the same antimicrobial efficacy (Masson-Meyers et al, 2015; Biener et al, 2017).

4. Laser-tissue and laser-bacteria interactions

L.a.s.e.r. is the acronym for: Light Amplification by Stimulated Emission of Radiation. The laser is a source of electromagnetic radiation, which is distinguished from other light sources by its coherence. Other peculiar characteristics include monochromaticity, directivity and brightness. Lasers are characterized according to their wavelength in a vacuum, which depends mainly on the gain medium and the pumping modality. Laser light is massively employed in multiple fields including industry, manufacturing and medicine.
In particular, our team has accumulated experience on the clinical and experimental use of class IV laser therapy exploring and using this approach to reduce the severity of oral mucositis and skin dermatitis, two major side effects of anticancer therapies. This type of therapeutic approach has been recently included in the term Photobiomodulation (PBM).

Laser irradiation modality is defined with the following parameters:
Wavelength: is the distance between the crests of an electromagnetic wave; defined in nm, in lasers ranges between 0.1 nm and 1 mm
Power: The rate at which energy is emitted from a laser
Irradiance (Power density): The quotient of incident laser power on a unit surface area, expressed as W/cm^2
Fluence: The energy contained within light is expressed in joules (J). The energy fluence determines the amount of laser energy delivered in a single pulse and is expressed in J/cm^2
Pulse duration/ repetition rate: Lasers can emit light in three modalities: continuous wave (CW), pulsed and ultrafast. Throughout our study, we will use a CW diode laser, which is able to produce a continuous beam of light, with a very stable output power. The continuous wave can be provided in interrupted modality, generating pulsed irradiation with pulse length in the range of ms.
Frequency of the pulses is measured in Hz.
The combination of these parameters can lead to three types of tissue responses to laser irradiation: thermal, mechanical and chemical. PBM works through photochemical reactions, initiated by the interaction of the laser beam with specific photosensitizers/cromophores.

a. Laser-tissue interactions

The exact laser-tissue interactions underlying PBM remain still under investigation, but recently great scientific efforts have been made to clarify the molecular mechanisms. In fact, several macroscopic effects of PBM have been described (anti-inflammatory, analgesic, stimulation of neoangiogenesis, and recently modulation of innate immune system response), but the lack of precise explanation prevents the full acceptance of such techniques in clinical practice.
PBM employs mainly red (600–700 nm) and near-infrared (NIR, 770–1200 nm) spectral regions, which can reach also maximal tissue penetration, since the highest peaks of absorption of the principal tissue chromophores (haemoglobin and melanin), are below 600 nm, while water absorbs light in the infrared (IR) region.
Several intracellular cromophores responsible for biological effects have been described, such as Cytochrome C Oxidase. Light-enzyme interaction stimulates an increase in ATP production, modulation of ROS production and activation of transcription factors, ultimately leading to an increase in cell proliferation and migration, regulation of cytokine expression, and augmentation of tissue oxygenation. All these reactions contribute to the promotion of wound healing (Passarella et al, 2014; Hamblin, 2017).
Unlike red and NIR wavelengths, blue laser light is absorbed by major tissue chromophores (melanin and haemoglobin) as shown in Figure 1, limiting its action to the most superficial layers of the dermis.

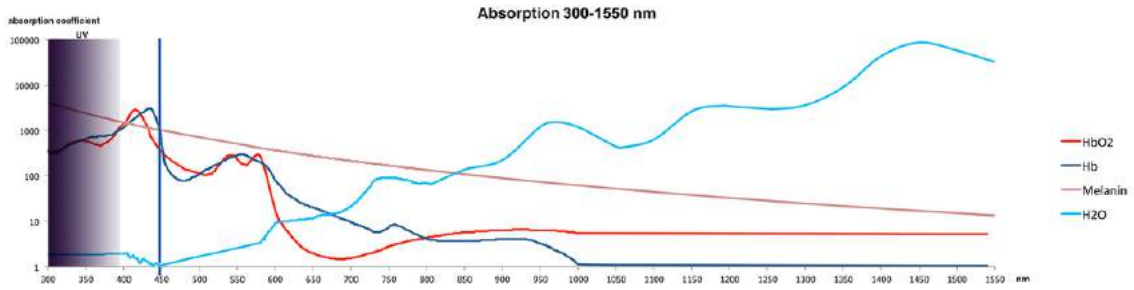

Figure 1. Absorption spectra of major tissue chromophores (modified from http://www.klaser.eu/wavelenghts1.html).

While these properties, used with high power parameters, make blue wavelengths suitable for tissue cutting and coagulation, the PBM performed with blue wavelengths remains poorly explored.

b. Laser-bacteria interactions

It is well known from several years that laser irradiation is able to eliminate bacteria and is been demonstrated in both in vitro and *in vivo* studies, and using different wavelengths and sources of laser light ranging from 193 nm in the ultraviolet (UV) region emitted by excimer laser to 10.6 μm in the far infrared (IR) region of the spectrum emitted by CO_2 lasers.
It is usually believed that the bactericidal action of the laser is due to thermal heating. In fact, it is known that temperatures above 60°C can cause thermal damage and subsequent killing of bacteria. Grönqvist et al demonstrated antimicrobial effect using an 1064 nm Nd:YAG laser with 1000 J/cm2 on *Staphylococcus epidermidis*, registering an agar temperature of approximately 70°C (Grönqvist A et al, 2000). Schoop et al. have explored the antimicrobial effect of four laser systems: Nd:YAG (1064nm), diode (810nm), Er:YAG (2940 nm), and Er:YSGG (2780 nm). Concerning all the wavelengths investigated, using radiant powers greater than 1.5 W was capable of significant reductions of *Escherichia coli* viability, while only diode and the Er:YAG laser were capable of complete eradication of *Enterococcus faecalis* (Schoop et al, 2004). Jawhara et al conducted a study in vitro and in vivo on wound infections sustained by *Escherichia coli* using a 810nm diode laser and showed that bacterial killing depends also on laser fluence. They obtained a complete killing of bacteria colonizing infected wounds at 260 J/cm2 registering a local temperature of 45°C, therefore hypothesizing that chromophores inside bacteria which may be sensitive to infrared light may cause a local intracaterial temperature increase, leading eventually to bacterial death (Jawhara S, 2006). It is unfortunately difficult to compare the results of different studies because of several differences in experimental settings. It is not correct to consider only the total delivered energy, because other connected parameters such as wavelength, spot size, time of application and operating mode (continuous wave or pulsed) may be different.

An important limitation to the use of lasers as topical antimicrobial tools is the nature of their effect: temperature increase at site of irradiation would provoke burn wounds and further tissue damage. For this reason, its use is now limited to the oral cavity, where several types of lasers are used for the sterilization of root canals during tooth endodontic therapy or to decrease bacterial load in infected periodontal pockets. For this purpose, two studies by Moritz et al. (1997, 1998) using the 805nm diode laser, reported reductions in total subgingival bacterial loads and decreases in *Aggregatibacter actinomycetemcomitans*, *Porphyromonas gingivalis* and *Prevotella intermedia*. The study performed by Kamma et al, using a 980nm diode laser, confirmed this results extending it also on other bacterial species (*Tannerella forsythia* and *Treponema denticola*) (Kamma et al, 2009).

Aims of the study

Considering the state of the art described so far, we performed a study regarding the use of blue laser light as a novel antimicrobial strategy against *Pseudomonas aeruginosa*. The specific aims of this study were:

- to evaluate the antimicrobial properties of blue laser light on *Pseudomonas aeruginosa* (PAO)
- to explore the mechanisms underlying the antimicrobial activity
- to evaluate possible toxicity on human keratinocytes
- to validate this effect *in vivo*
- to evaluate the use of blue laser in antimicrobial photodynamic therapy (PDT) using free curcumin and curcumin embedded in three types of amphiphilic nanomicelles.

Materials and Methods

Laser device

A prototype of class IV diode laser (K-Laser Blue, Eltech S.r.l. K-Laser, Treviso, Italy) has been used to perform all the experiments described. The laser is associated to a programmable scanner conveniently designed by Eltech S.r.l. K-Laser to provide uniform irradiation to different multiwell plates (12, 24 and 96-well plates) as shown in Figure 1.

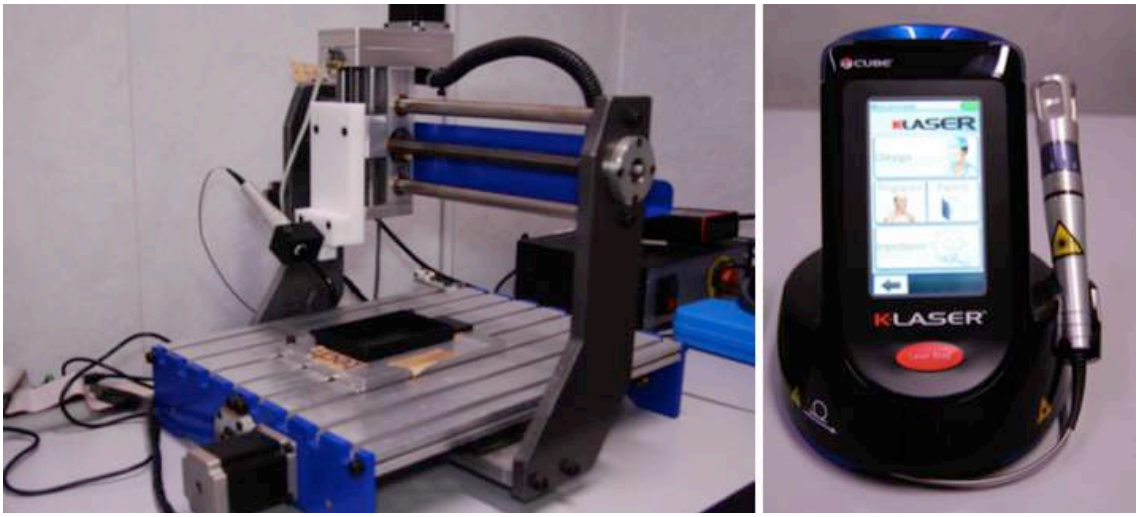

Figure 1. Eltech S.r.l. K-Laser prototype with an adapted probe directly connected to irradiate wells/plates in a programmed and controlled way.

Plate covers were removed during irradiation and the emission tip was hold perpendicular above the cells/animals. The diode area laser source consisted of equal diodes, which emitted an elliptic laser field with a Gaussian distribution of irradiance. The emitted light completely covered the irradiated field of each culture plate, as shown in Figure 2, and power was adapted to the spot size to provide the desired irradiance and fluence using an optical power meter (LaserPoint Plus+, Via Burona, 51 - 20090 Vimodrone (MI), Italy).

Figure 2. Irradiation of single wells with different diameters.

Two types of tips were used basing on the needed spot size, which will be called “ENT” (used for spot sizes ≤ 1 cm^2) and “ZOOM” (used for spot sizes > 1 cm^2) tip as showed in Figure 2. The device is able to provide 445nm, 660nm and 970nm wavelength laser light in different combinations of power and energy.

Figure 3. a) ENT tip; B) ZOOM tip for the K-Laser Blue device.

1. Antimicrobial effect of blue laser on *Pseudomonas aeruginosa* (PAO)

1.1 Antimicrobial effect of blue laser on planktonic PAO

To perform all experiments, a *Pseudomonas aeruginosa* strain (ATCC 27853) has been employed. To test anti-microbial activity on bacteria in planktonic state, bacterial strains were grown to 0.5 McFarland's standard approximately corresponding to 1×10^8 CFU/mL and then diluted 1:1000 in fresh Luria-Bertani (LB) broth growth medium and inoculated in 96-well plates. The wells have been irradiated testing multiple protocols in terms of power and energy fluence, all in continuous wave (CW). The spot size was 1 cm^2. While all protocols have been tested using blue laser light (445nm), the protocols with the fluence 120 J/cm^2 have been tested also with red (660nm) and infrared (970nm) laser wavelengths.

Power (W)	**Irradiance at sample (W/cm^2)**	**Fluence (J/cm^2)**	**Power (W)**	**Irradiance at sample (mW/cm^2)**	**Fluence (J/cm^2)**
0,3	0,12	40 60 120	1	0,49	40 60 120
0,5	0,18	40 60 120	1,5	0,73	40 60 120
0,7	0,24	40 60 120	2	1,040	40 60 120

Table 1. Scheme of all tested laser protocols employed with blue laser (445nm). The protocols with the fluence 120 J/cm^2 have been tested also with red (660nm) and infrared (970nm) lasers.

The optical density of the wells have been measured using a spectrophotometer with OD_{600} immediately after irradiation (T0) and after 6, 12, 18 and 24 hours. The experiment has been performed in triplicate for a total of 280 samples for each wavelength.

Statistical analysis has been performed using the Mann-Whitney U-test to evaluate differences between treated and untreated samples and at each time point, and the Friedman test has been used to evaluate changes over time for each protocol. A p-value <0,05 has been used for the rejection of the null hypothesis.

1.2 Antimicrobial effect of blue laser on PAO grown on agar plates

To test anti-microbial activity on bacteria grown on solid surfaces, the same PAO strain has been grown to 0.5 McFarland's standard approximately corresponding to 1×10^8 CFU/mL and then 100µl of bacterial suspension has been swabbed on sterile petri dishes carrying Mueller-Hinton agar obtaining a uniform distribution on the surface of the plates. Afterwards, the plates have been irradiated in a standardized manner using a programmable scanner carrying the laser tip.

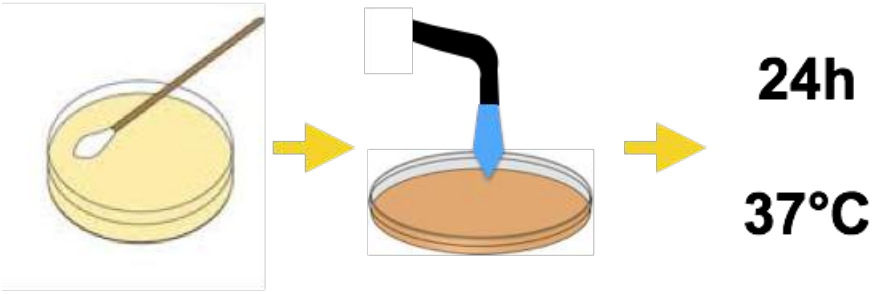

Figure 4. Schematical representation of the experiment.

The following protocols (each protocol is defined as follows: power, irradiance at sample level, fluence) have been tested in blue and infrared wavelengths (445nm, 970nm): 0,2W 0,12W/cm^2 40J/cm^2, 0,3W 0,18W/cm^2 40J/cm^2, 0,4W 0,24W/cm^2 40J/cm^2, 0,5W 0,3W/cm^2 40J/cm^2, 1W 0,49W/cm^2 40J/cm^2, all in CW. The spot size was 1 cm^2. The plates have been then incubated at 37°C and then checked after 24 hours.

To verify the abscence of a possible degradating effect of the laser on the growth medium possibly inhibiting bacterial growth, we performed an experiment irradiating the plates with the same protocols before the inoculation of bacteria as shown in Figure 5. Afterwards, the plates were incubated at 37°C and then checked after 24 hours.

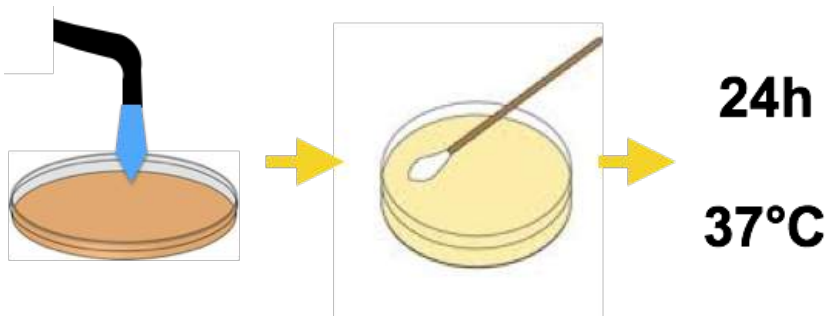

Figure 5. Schematical representation of the experiment. Agar plates were irradiated before inoculation of bacteria to test possible effects on growth medium.

1.3 Antimicrobial effect of blue laser on PAO biofilms

a. Biofilms grown on Calgary biofilm devices

To test the efficacy of blue laser to disrupt PAO biofilms, bacteria have been grown on Calgary biofilm devices (ASTM E2799-17, Standard Test Method for Testing Disinfectant Efficacy against Pseudomonas aeruginosa Biofilm using the MBEC Assay, ASTM International, West Conshohocken, PA, 2017, www.astm.org), which allows bacterial growth in biofilms and performing high throughput screening for antimicrobial efficacy of different agents. The assay device consists of a plastic lid with ninety-six (96) pegs and a corresponding receiver plate with ninety-six (96) individual wells that have a maximum 200 µL working volume. After resuspension of a PAO culture, the bacteria have been diluted to a 30-fold dilution of the 1.0 McFarland standard (1.0 x 10^7 CFU ml^{-1}) in fresh LB broth growth medium and 200 µL have been inoculated into each well, subsequently covered by the peg lid. Biofilm was established on the pegs under batch conditions (that is, no flow of nutrients into or out of an individual well) with gentle mixing for 24 hours, as shown in Figure 6.

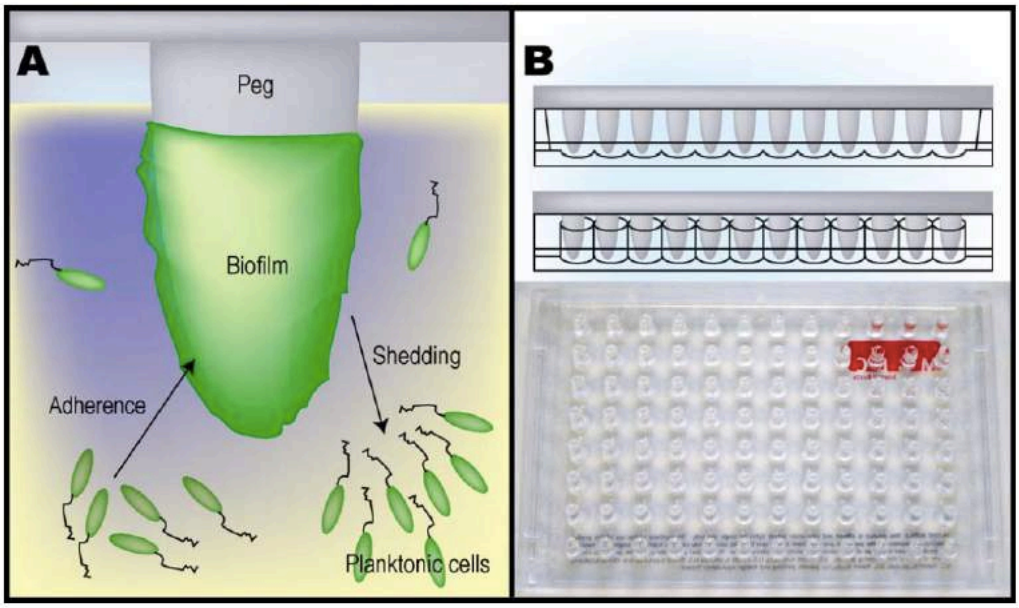

Figure 6. A) Biofilms form on the polystyrene pegs of the MBEC™ device when planktonic bacteria adsorb to the surface. These bacteria become irreversibly attached and grow to form mature biofilms. B) The peg lid has 96 identical plastic pegs and fits into a standard 96-well microtiter plate. (Modified from http://www.innovotech.ca/products_mbec.php)

After 24 hours and biofilm formation, the device with 96 pegs was overturned and exposed to blue laser irradiation. Each peg was irradiated singularly holding the tip perpendicularly above it. Several blue lase protocols have been tested, all in CW, as shown in Table 2. The spot size was 1 cm^2.

Power (W)	Irradiance at sample (W/cm^2)	Fluence (J/cm^2)	Power (W)	Irradiance at sample (W/cm^2)	Fluence (J/cm^2)
0,3	0,18	20 60	0,5	0,3	20 40 60
0,4	0,24	20 40 60	0,6	0,36	20 40 60

Table 2. Scheme of all tested laser protocols employed with blue laser (445nm).

After irradiation, the device has been put into a recovery plate carrying fresh LB growth medium and incubated at 37°C. After 24 hours, bacterial growth has

been assessed through sonication of the plate to transform biofilms in planktonic cultures (as shown in Figure 7) and subsequent reading using an automated plate reader to obtain optical density measurements at 600nm (OD_{600}).

Alongside, the effect of the laser protocol 0,3W 0,18W/cm^2 20J/cm^2, CW has been evaluated on changes in MIC (Minimum Inhibitory Concentration) of the antibiotics Tobramycin and Gentamicin, which are currently used in clinical practice on PAO lung infections in cystic fibrosis patients. Antibiotics have been added in serial dilutions in the recovery plate as shown in Figure 7B and processed as described above. Serial dilutions were prepared at the following concentrations:

Tobramycin: 5µg/mL, 2.5µg/mL, 1.25 µg/mL, 0.75µg/mL, 0.5µg/mL, 0.4µg/mL, 0.3µg/mL, 0.2µg/mL, 0.1µg/mL, 0.05µg/mL, 0.025µg/mL, 0µg/mL.

Gentamicin: 10µg/mL, 5µg/mL, 2.5µg/mL, 1.8µg/mL, 1.25µg/mL, 0.9µg/mL, 0.62µg/mL, 0.45µg/mL, 0.31µg/mL, 0.22µg/mL, 0.15µg/mL, 0µg/mL.

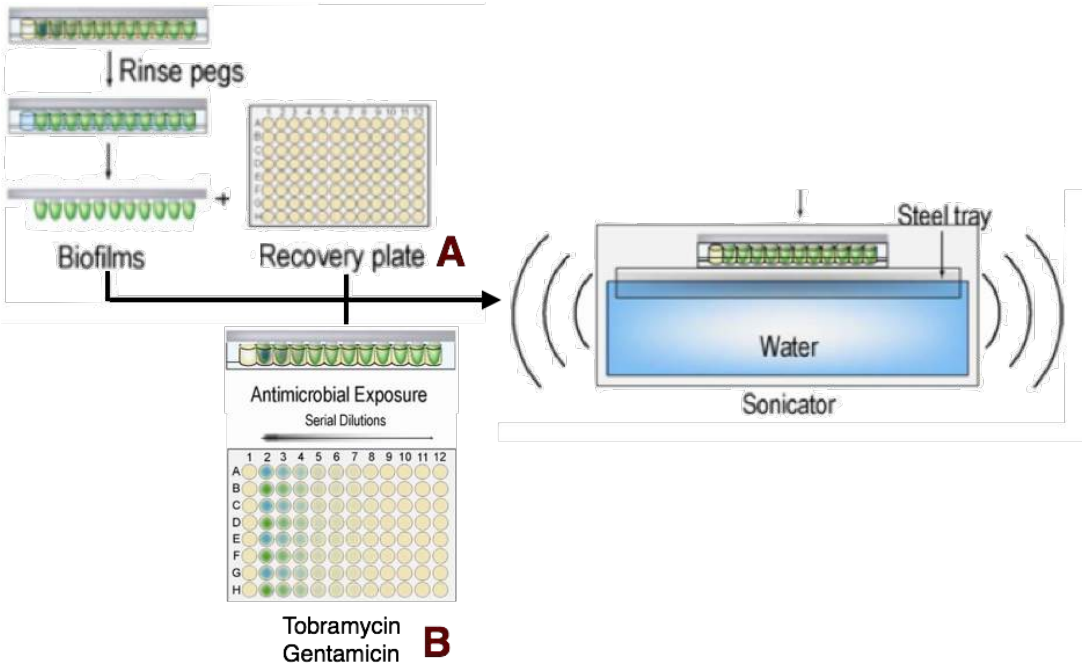

Figure 7. After exposure, biofilms were rinsed twice in physiological saline. The biofilms were then transferred to a microtiter recovery plate containing fresh LB broth (A) or to a recovery plate containing serial antibiotic dilutions (B). The biofilms were disrupted by sonication. (Modified from http://www.innovotech.ca/products_mbec.php)

Clear wells (OD_{600} < 0.1) are considered evidence of biofilm eradication. The antimicrobial effect has been evaluated comparing them with non treated control cultures. The experiment has been performed in triplicate for a total of 600 samples.

Statistical analysis has been performed using the Mann-Whitney U-test to evaluate differences between treated and untreated samples. A p-value <0,05 has been used for the rejection of the null hypothesis.

b. Laser Scanning Confocal Microscopy on biofilms grown in flow cells

To visualize the effect on mature PAO biofilms, we performed imaging experiments using the Laser Scanning Confocal Microscopy in collaboration with the Department of Microbiology at the University of Washington, Seattle, USA. Biofilms were cultivated in flow cell chambers inoculating flow cells from a mid-log LB culture to an OD_{600} of 0.01, allowed to attach under static conditions and then grown on glucose minimal media for 4 days at room temperature under a constant flow rate (10 mL/h).

Before setting the protocols, the interference and diffraction of laser light passing through the plexiglass flow cells was measured using a power meter (Laser Point Plus, Opto-Electronic, Singapore) and a decrease of 50% in power density was assessed from one side to the other of the flow cell, which was thick 0,5cm. Therefore, the protocols will be described using the power, the irradiance at the top of the flow cell, and the irradiance at the opposite side of the flow cell. The following experiments were performed:

- Wavelength 445nm, power 0,5W, top irradiance 0,3W/cm^2, bottom irradiance 0,15 W/cm^2, fluence 120 J/cm^2 , CW
- Wavelength 445nm, power 1W, top irradiance 0,6W/cm^2, bottom irradiance 0,3 W/cm^2, fluence 150 J/cm^2, CW
- Wavelength 970nm, power 1W, top irradiance 0,6W/cm^2, bottom irradiance 0,3 W/cm^2, fluence 150 J/cm^2, CW

- To evaluate biofilm growth inhibition, a flow cell has been irradiated shortly after inoculation with the protocol Wavelength 445nm, power 1W, top irradiance 0,6W/cm^2, bottom irradiance 0,3 W/cm^2, fluence 150 J/cm^2, CW and then biofilm growth has been monitored over time using optical microscopy with different magnifications.

After irradiation, biofilms were stained using Syto9 green fluorescent stain for whole biomass (5 μM; Life Technologies) and Propidium Iodide purple fluorescent stain (30 μM; Life Technologies) for extracellular DNA (dead cells) and then visualized on a Zeiss LSM 510 scanning confocal laser microscope (Carl Zeiss Microscopy, Carl-Zeiss-Promenade 10, 07745 Jena, Germany). Images were acquired in triplicates and 3D reconstructions of the biofilms were performed. Image analysis was conducted using Volocity software (Improvision, Coventry, England). Voxel counting for every stain has been performed calculating the sum of the voxels containing each stain in every volume stack, allowing to calculate the total biomass and the % of dead cells in every sample. In every flow cell, the central part was irradiated since it is considered as the most representative area of the biofilm, as shown in Figure 8.

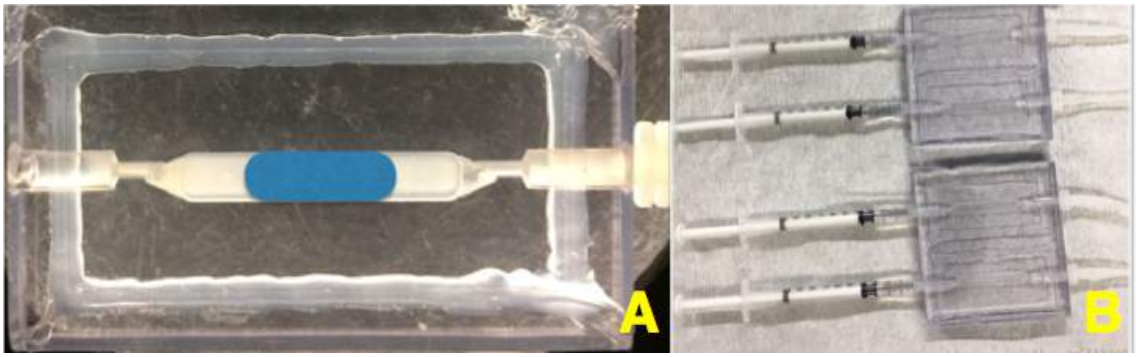

Figure 8. Showing A) A flow cell and the area of laser irradiation coloured in blue. B) Staining of the biofilm after irradiation.

Statistical analysis has been performed using the Mann-Whitney U-test to evaluate differences between treated and untreated samples. A p-value <0,05 has been used for the rejection of the null hypothesis.

1.4 Scanning Electron Microscopy imaging and analysis

To characterize further the effect of blue laser, an experiment using high resolution Scanning Electron Microscope (SEM) imaging has been performed (Quanta250 SEM; FEI, Hillsboro, OR). The specimens have been prepared growing PAO on sterile 13mm diameter cover glasses (Fisher Scientific, Hampton, New Hampshire, USA) on the bottom of plastic wells in LB broth growth medium to a density of 10^8 CFU/ml and then diluted 1:100. Bacteria have been incubated at 37°C for 2 hours before irradiation to enable adherence to the glasses. Spot size was 1,32cm^2. The plates have been irradiated using the following protocols:

- Wavelength 445nm, power 1W, irradiance 0,3W/cm^2, fluence 150 J/cm^2 and 75 J/cm^2, CW;
- Wavelength 970nm, power 1W, irradiance 0,3W/cm^2, fluence 150 J/cm^2 and 75 J/cm^2, CW.

Afterwards, the plates have been washed twice with Phosphate Buffer Saline (PBS) solution in order to remove the dead cells that detached from the surface, fixed with Paraformaldehyde (PFA) 4% for 1 hour, dehydrated using ethanol solutions at increasing concentrations (30%, 50%, 70%, 95% (twice) and 100% (twice) - 30 min in each solution) and 1,1,1,3,3,3-hexamethyldisilazane (HMDS; Acros Organics, Springfield, NJ, USA) for 90 min. The cover glasses were then mounted on metallic stubs, sputter-coated with gold and SEM images have been obtained using different magnifications (300x, 2400x, 20.000x). The working distance and the accelerating voltage were adjusted to obtain the suitable magnification.

The 300x magnification images have been analyzed using the ImageJ software to calculate the density of the remaining bacteria. The experiment has been performed in quadruplicate. Statistical analysis has been performed using the Mann-Whitney U-test to evaluate differences between treated and untreated samples. A p-value <0,05 has been used for the rejection of the null hypothesis.

2. Evaluation of the antimicrobial mechanism of action

Although the anti-microbial action of blue light has been described by a number of research works, the molecular mechanism responsible for such effect hasn't been clearly identified yet. We performed several experiments to understand the possible photothermal/photochemical mechanism responsible for bacterial inhibition following blue laser exposure.

2.1 Monitoring of the temperature at sites of irradiation

To exclude a possible photothermal effect, we evaluated the temperatures on site of irradiations when irradiating petri dishes carrying Mueller-Hinton agar and bacteria. The temperature was measured using the Ti20 Thermal Imager (Fluke, Everett, Washington, U.S.A.). The following protocols were tested: power 0,2W irradiance 0,12W/cm^2, power 0,3W irradiance 0,18W/cm^2, power 0,4W irradiance 0,24W/cm^2, power 0,5W irradiance 0,3W/cm^2, power 1W irradiance 0,49W/cm^2 and the temperature at sites of irradiation has been compared to the surrounding temperature on the plate.

2.2 Measurement of the Total Oxidant Status

Since several research works hypotesized that the antimicrobial mechanism involves the interaction of blue light with endogenous porphyrins leading to the generation of Reactive Oxygen Species (ROS) and subsequently to microbial death, an experiment involving the measurement of ROS generation after irradiation has been performed on planktonic bacteria. Bacteria were grown to a 0,5 McFarland's standard concentration in LB broth. 100 µL of bacterial suspension were inoculated to a 96-well sterile plate and irradiated using the blue laser protocol power 0,3W irradiance 0,18W/cm^2, fluence 120 J/cm^2, CW. 1 hour after irradiation, the Total Oxidant Status (TOS) assay has been performed as described elsewhere (Erel, 2005).

The principle of the assay is that oxidants present in the sample oxidize the ferrous ion–o-dianisidine complex to ferric ion. The oxidation reaction is

enhanced by glycerol molecules, which are abundantly present in the reaction medium. The ferric ion makes a coloured complex with xylenol orange in an acidic medium. The color intensity, which can be measured spectro-photometrically, is related to the total amount of oxidant molecules present in the sample as shown in Figure 9.

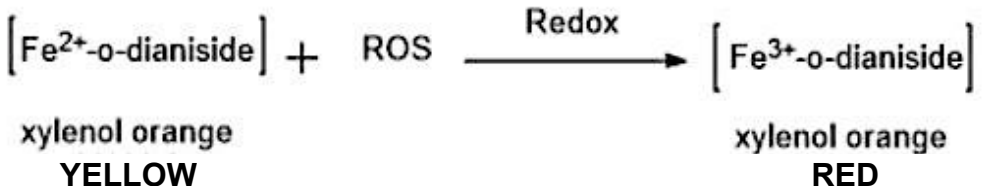

Figure 9. Scheme summarizing the chemical reaction.

35µL of bacterial suspension have been added to Reagent 1 (Reagent 1: xylenol orange 150 µM, NaCl 140 mM and glycerol 1.35 M in 25 mM H_2SO_4 solution, pH 1.75). The absorbance of the mixture was then read spectro-photometrically at OD_{560}. Subsequently, 11 µL of Reagent 2 (ferrous ion 5 mM and o-dianisidine 10 mM in 25 mM H_2SO_4 solution) have been added. After 5 minutes the solutions have been gently mixed and a second end-point absorbance measurement at OD_{560} has been performed.

The experiment has been performed in triplicate. Statistical analysis has been performed using the Mann-Whitney U-test to evaluate differences between treated and untreated samples. A p-value <0,05 has been used for the rejection of the null hypothesis.

2.3 Evaluation of the antimicrobial effect adding an antioxidant compound

Ascorbic acid is a naturally occurring organic compound with antioxidant properties. It is oxidized with loss of one electron to form a radical cation and then with loss of a second electron to form dehydroascorbic acid. It typically reacts with oxidants of the reactive oxygen species by electron transfer. It is a natural scavenger molecule already present in bacteria. The oxidized forms of

ascorbate are relatively unreactive and do not cause cellular damage, as shown in Figure 10.

The net reaction is:

$RO\bullet + C_6H_7O_{-6} \rightarrow RO^- + C_6H7O\bullet_6 \rightarrow ROH + C_6H_6O_6$

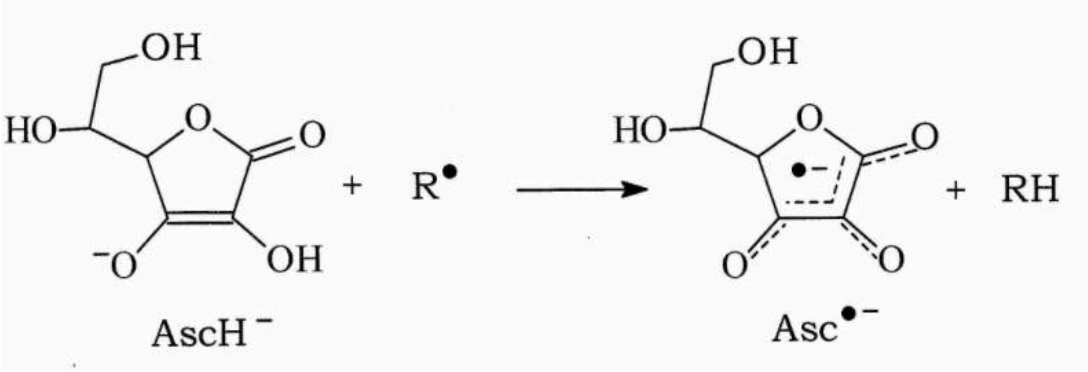

Figure 10. Vitamin C (ascorbate, AscH-) can donate a hydrogen atom to a free radical molecule (R.) neutralizing the free radical while becoming an ascorbate radical itself (Asc·-), which is very stable because of its resonance structure as shown in the figure above.

We decided to prove the oxidative stress generation mechanism of antimicrobial action of blue laser light by repeating a survival experiment on planktonic bacteria using a protocol which has been effective before, with the addition of ascorbic acid as natural scavenger of reactive oxygen species.

Bacteria were grown to a 0,5 McFarland's standard concentration in LB broth and divided into four groups which have been inoculated into 96-well plates (100 µL of bacterial suspension for each well):

1) Non treated bacteria
2) Non treated bacteria with the addition of ascorbic acid (40 µM)
3) Laser-treated bacteria
4) Laser treated bacteria with the addition of ascorbic acid (40 µM)

Groups 3 and 4 were then irradiated using the blue laser protocol power 0,3W irradiance 0,18W/cm^2 fluence 120 J/cm^2. The optical density of the wells has been measured using a spectrophotometer with OD_{600} immediately after irradiation (T0) and after 24 hours. The experiment has been performed in triplicate.

Statistical analysis has been performed using the Kruskal-Wallis test to evaluate differences among groups, and Mann-Whitney U-test has been employed to evaluate differences between the group treated with laser therapy and ascorbic acid and each other group. A p-value <0,05 has been used for the rejection of the null hypothesis.

2.4 Evaluation of the antimicrobial effect of blue LED light

To test whether another source of blue light could exert a similar antimicrobial activity, thus confirming a possible photochemical effect rather than photothermal, a planktonic growth curve assay has been performed using a blue LED light source providing 380-490nm light (VALO LED curing light, Ultradent Products, Inc., South Jordan, UT 84095). PAO bacterial strains were grown to 0.5 McFarland's standard approximately corresponding to 1×10^8 CFU/mL and then diluted 1:1000 in fresh LB broth growth medium and inoculated in 96-well plates. The following irradiation protocols have been tested: power 0,3W irradiance 0,18W/cm^2 fluence 60J/cm^2 and 120J/cm^2, power 0,5W irradiance 0,3W/cm^2 fluence 60J/cm^2 and 120J/cm^2, all in CW. The optical density at OD_{600} of the wells has been measured using a spectrophotometer at several time points: T0 (immediately after irradiation), and after 6, 12, 18 and 24 hours.

Statistical analysis has been performed using the Mann-Whitney U-test to evaluate differences between treated and untreated samples and at each time point, and the Friedman test has been used to evaluate changes over time for each protocol. Subsequently, the results have been compared to the ones of the bacterial growth curve performed with 445nm blue laser light using the same protocols in terms of power and fluence. Mann-Whitney U-Test has been used to evaluate differences between laser and LED at each time point for every protocol. A p-value <0,05 has been used for the rejection of the null hypothesis.

2.5 Irradiation of a mutant library of PAO

To identify one or a pool of candidate genes encoding for proteins responsible for bacterial susceptibility to blue laser light, we performed the screening of a gene mutant library of PAO. A non-redundant transposon promoter-probe genomic mutant library of PAO has been generated. The miniTn5-GNm transposon has been introduced in PAO by biparental conjugation. The transconjugants, harboring the mTn5-GNm into the chromosome, have be selected on LB plates containing nalidixic acid (25µg/ml), Ampicillin (100µg/ml) and Kanamycin (300µg/ml). Several conjugations have been performed in order to obtain more than 100.000 independent transposon insertions. The mutant library has been saved at -80°C as a pool of mutants.

The library has been grown to a 0,5 McFarland concentration, and the bacterial suspension has been inoculated in Petri dishes carrying LB km agar. The plates have been irradiated in a standardized manner using the protocol power 0,5W irradiance 0,3W/cm^2 fluence 120J/cm^2 CW which has proved to be effective in the previous experiments. After irradiation, the plates have been incubated at 37°C and checked after 24 hours for the growth of single colonies in the irradiated areas. In case of detection of grown colonies, they would be processed to identify the mutated locus by arbitrary PCR (O'Toole and Kolter, 1998) or cloning techniques. Involvement of the mutated locus in the susceptibility to blue laser light would be confirmed by mutant regeneration and/or complementation experiments.

3. Safety/Toxicity of blue light irradiation on eukaryotic cell lines

Since the aim of the research project is to provide laser light directly to mucosa and skin, it is crucial to prove its safety on mammalian cells and tissues. We have started exploring the safety of the proposed approach, by evaluating cell metabolism, viability, cell cycle and mitochondrial membrane potential changes after blue laser irradiation, using the protocols that exerted the highest antimicrobial activity. We also performed a gene expression analysis to evaluate the possible stimulation of innate immunity and inflammasome molecules in keratinocytes.

3.1 Cell viability and metabolism assays

We tested the effect of several blue laser protocols including those that proved to have the best anti-microbial activity during previous experiments on human oral mucosa keratinocytes (TR146, model of oral buccal epithelium derived from well-differentiated keratinizing squamous cell carcinoma) and human skin keratinocytes (HaCaT, model of human skin derived from spontaneously transformed aneuploid immortal keratinocyte cell line) cell types. Both cell lines were maintained in Ham's F12 culture medium supplemented with 10% fetal bovine serum, 100 U/ml Penicillin/Streptomycin, 2 mM Glutamine (Euroclone, Pero, Milan, Italy). Cells were incubated at 37°C in 95% air - 5% CO_2 in a humidified incubator for 2 to 3 days until the cell monolayer became confluent. All experiments were conducted in passages between 2 and 10-12 to avoid outcomes due to cellular senescence. Cells were treated after seeding 10.000 cells/well into 24 or 96-well plates, which were irradiated leaving the plate cover open.

a. Cell viability assays

To test cell viability and proliferation after blue laser irradiation, MTT assays (Trevigen, Gaithersburg, Maryland, U.S.A.) have been performed. It is based on the reduction of the yellow tetrazolium salt 3-[4,5-di-methylthiazol-2yl]-2,5-diphenyl-tetrazolium bromide (MTT) by metabolically active cells, generating

intracellular purple formazan which can be solubilized and quantified spectrophotometrically with OD_{570}.

Several blue laser protocols have been tested. MTT has been executed 24 hours after irradiation:

- power 0,3W irradiance 0,18W/cm^2 fluences 30J/cm^2, 60J/cm^2 and 120J/cm^2; power 0,5W irradiance 0,3W/cm^2 fluences 30J/cm^2, 60J/cm^2 and 120J/cm^2; power 1W irradiance 0,49W/cm^2 fluences 30J/cm^2, 60J/cm^2 and 120J/cm^2 on both cell types
- power 0,5W irradiance 0,175W/cm^2 fluence 40J/cm^2 has been employed testing different frequencies: 10Hz, 100Hz, 1000Hz, 10.000Hz, CW on TR146 cells;

Statistical analysis has been performed using the Kruskal-Wallis test to evaluate differences among groups, and Dunn's multiple comparison test as post hoc to compare each pair of groups. A p-value <0,05 has been used for the rejection of the null hypothesis.

b. Cell metabolism assays

Cell metabolic activity has been assessed through ATP production using the ATPlite luciferase test (PerkinElmer, Waltham, Massachusetts, U.S.A.). The ATPlite assay system is based on the production of light caused by the reaction of ATP with added luciferase and d-luciferin. The emitted light is proportional to the ATP concentration.

Several blue laser protocols have been tested:

- power 0,3W irradiance 0,18W/cm^2 fluence 40J/cm^2 has been tested at different time points: 30', 2h and 6h after irradiation on both cell types
- power 0,2W irradiance 0,12W/cm^2 fluence 40J/cm^2; power 0,3W irradiance 0,18W/cm^2 fluence 40J/cm^2; power 0,4W irradiance 0,24W/cm^2 fluence 40J/cm^2; power 0,5W irradiance 0,3W/cm^2 fluence 40J/cm^2; power 1W irradiance 0,49W/cm^2 fluence 40J/cm^2 with and

without growth medium (to test possible interference of the medium with laser light) at 30' and 24h on TR146 cells

Statistical analysis has been performed using the Kruskal-Wallis test to evaluate differences among groups, and Dunn's multiple comparison test as post hoc to compare each pair of groups. The Mann-Whitney U test has been employed to testt difference between two groups when appropriate. A p-value <0,05 has been used for the rejection of the null hypothesis.

c. Cell cycle analysis

The cell cycle is the process by which eukaryotic cells duplicate and divide. The cell cycle consists of two specific and distinct phases: interphase, consisting of G1 (Gap 1), S (synthesis), and G2 (Gap 2), and a mitotic M phase. Each phase of the cell cycle is tightly regulated, and checkpoints exist to detect potential DNA damage and allow it to be repaired before a cell divides. If the damage cannot be repaired, a cell becomes targeted for apoptosis.

We performed a cell cycle flow cytometry analysis of DNA content following cell staining with Propidium Iodide (a stoichiometric dye which binds in proportion to the amount of DNA present in the cell) to reveal the distribution of cells in three major phases of the cycle (G1 vs S vs G2/M) and to detect apoptotic cells with fractional DNA content 4 hours and 24 hours after laser treatment.

We performed the analysis on both cell types. After treatment with the blue laser protocol wavelength 445nm, power 0,5W irradiance 0,175W/cm^2 fluence 40J/cm^2, cells were processed as follows: cells were fixed in 70°C ethanol, treated with RNAase to maintain only DNA, and then stained with Propidium Iodide (50µg/ml). Cell suspension was then transferred to a flow cytometer and cell fluorescence was measured. Maximum excitation of PI bound to DNA is at 536 nm, and emission is at 617 nm. Data were subsequently analyzed using DNA content frequency histogram deconvolution software and reported as % of cells in the different cell cycle phases: G0/G1, S, G2/M, cells with fragmented

DNA (apoptotic cells) and multinucleate cells (possible presence of cell aggregates).

d. Mitochondrial transmembrane potential

Cell viability has been measured also employing the JC-1 mitochondrial potential sensor. JC-1 s a cationic dye that exhibit potential-dependent accumulation in mitochondria, indicated by a fluorescence emission shift from green (~525 nm) to red (~590 nm). Red fluorescence indicates healthy mitochondria, while green fluorescence indicates mitochondria in poor health. Consequently, mitochondrial depolarization is indicated by a decrease in the red/green fluorescence intensity ratio.

Cells have been treated with the laser protocol 445nm power 0,5W irradiance 0,175W/cm^2 fluence 40J/cm^2 and subsequently stained following manufacturer's instructions. Red/green emission was measured in flow citometry. Results are reported in red/green fluorescence intensity ratio.

The experiment has been performed in triplicate. Statistical analysis has been performed employing the Mann-Whitney U-test to evaluate differences between treated and non treated samples. A p-value <0,05 has been used for the rejection of the null hypothesis.

3.2 Gene expression analysis

Gene expression analysis for innate immunity (Defensin beta1, beta4, beta103) and inflammosome (Caspase 1, Interleukin-1b, NLRP3) molecules has been performed on the HaCaT cell line, since TR146 is derived from an oral squamous cell carcinoma and is therefore not suitable for such experiments.

Cells have been treated with the blue laser protocol 445nm power 0,5W irradiance 0,175W/cm^2 fluence 40J/cm^2. Total cellular RNA was extracted after 30 minutes and 6 hours using RNAqueous®-Micro Kit Micro Scale RNA Isolation Kit (Thermo Fisher Scientific, Waltham, Massachusetts, U.S.A.)

following manufacturer's instructions and retro-transcribed using High-Capacity cDNA Reverse transcription kit (Thermo Fisher Scientific). To quantify mRNA, Taq-man™ probes for DEFB1 (Hs00608345_m1), DEFB4A (Hs00608345_m1), DEFB103 (Hs00218678_m1), CASP1 (Hs00354836_m1), IL1B (Hs01555410_m1), NLRP3 (Hs00918082_m1) genes and β-Actin (as calibrator and reference, ACTB: Hs99999903_m1) were used on Applied Biosystems 7900HT Fast Real-Time PCR System (Thermo Fisher Scientific) platform. Raw fluorescent data were collected and converted in fold-increase with the Relative Quantification manager software (Thermo Fisher Scientific) using the ΔΔCt method. Untreated cells were used as references for the comparison.

4. Assessment of the antimicrobial effect on PAO in vivo in a mouse model of wound infection

Animal care and treatment were conducted in conformity with institutional guidelines in compliance with national and international laws and policies (European Economic Community Council Directive 86/609, OJL 358, December 12, 1987). Animals were housed under controlled environmental conditions for 5 days with a 12 hours light/dark cycle.

15 adult 7- to 8-week-old female C57BL/6 mice were shaved on the dorsal surfaces and subsequently skin abrasions measuring approximately 13mmx13mm were performed using a sterile scalpel. Then, 20µl of a PAO bacterial suspension containing 10^6 CFU was topically applied to each abrasion. Mice were randomely assigned to a laser treated (8) and non treated (7) group and 30min after the infection, a laser irradiation has been performed using the protocol wavelength 445nm power 0,3W irradiance 0,105W/cm^2 fluence 60J/cm^2. The zoom tip has been employed as the spot size was 1,5cm^2. Experimental procedures are shown in Figure 11.

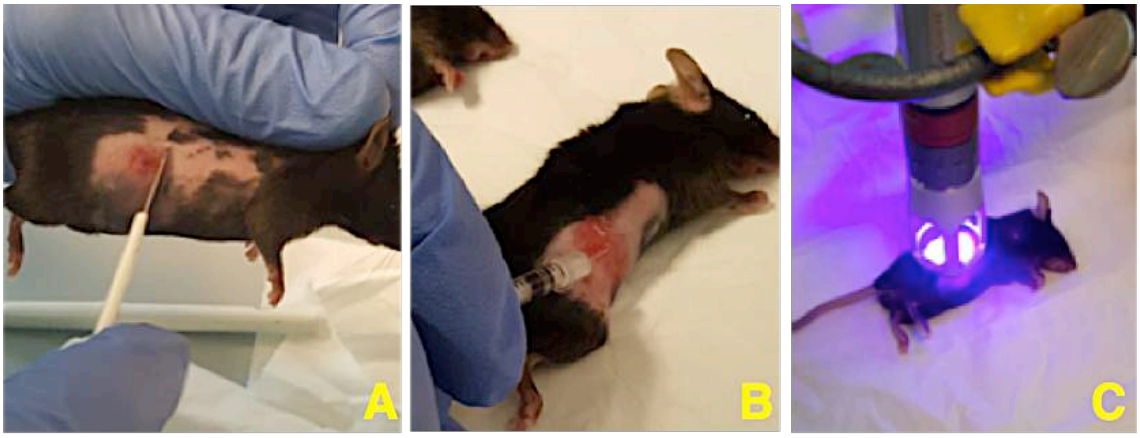

Figure 11. A) Inducing the skin abrasions on the shaved dorsal skin; B) Infection applying 10^6 CFU/ml of PAO on the abrasions; C) Laser treatment following anesthesia by intraperitoneal injection of a ketamine-xylazine cocktail.

After 24 hours, mice have been sacrificed and skin specimens have been obtained. For each mice, the infected abrasion area has been marked to obtain a square area with dimensions 10mmx10mm which has been then harvested using a sterile scalpel. The specimen has been then divided in two identical

halves as shown in Figure 12. One half has been placed into LB bacterial growth medium, sonicated, and then 10µl have been plated on Petri dishes and incubated at 37°C. After 24 hours, the plates have been checked and colonies have been counted. Colony count has been converted into CFU/ml. The other one has been fixed in Paraformaldehyde 4% and stained with hematoxylin and eosin for histopathological examination, which was conducted by an expert pathologist. When possible, the depth of heat/laser damage has been measured in laser treated samples.

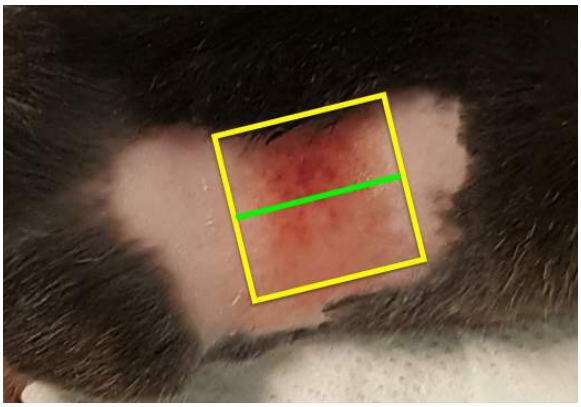

Figure 12. Scheme of the skin harvesting to obtain standardized specimens for analysis.

Statistical analysis has been performed employing the Mann-Whitney U-test to evaluate differences in CFU/ml between treated and non treated samples. A p-value <0,05 has been used for the rejection of the null hypothesis.

5. Photodynamic therapy (PDT) using amphiphilic nanomicells loaded with curcumin activated by sublethal blue laser irradiation

A photodynamic therapy (PDT) experiment preparing amphiphilic nanomicelles was performed. The micelles had palmitic acid (C_{16}), with different amines as ligands: C_{16}-DAPMA had N,N-di-(3-aminopropyl)-N-methylamine), C_{16}-SPD had Spermidine and C_{16}-SPM had Spermine. The compounds have been characterized elsewhere and the chemical structure of the compounds is shown in Figure 12 (Fechner et al, 2016). The nanomicelles were loaded with curcumin, which acted as photosensitizing molecule for blue light irradiation.

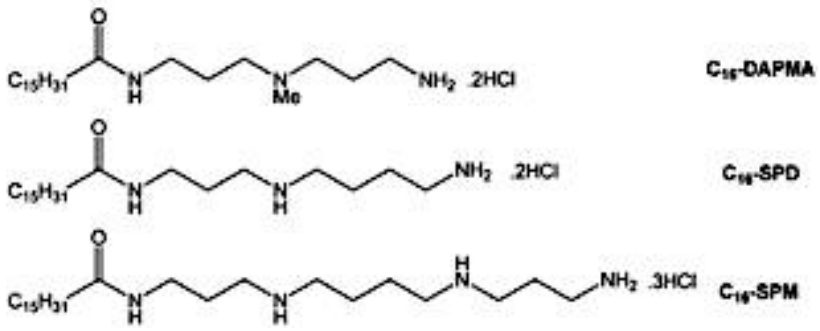

Compound	N_{agg}	D_m (nm)	ψ_s (mV)	ζ (mV)
C_{16}-DAPMA	16 ± 2	6.0 ± 0.3	172.4	50.2
C_{16}-SPD	13 ± 1	6.3 ± 0.1	153.3	45.1
C_{16}-SPM	10 ± 1	5.8 ± 0.2	144.6	41.8

Figure 13. Compounds investigated in this study. Nagg aggregation number; Dm diameter; Ψs surface electrostatic potential; ζ zeta potential (Modified from Fechner et al, 2016).

5.1 Loading of the nanomicelles

Curcumin (0.32mg) (C1386, Sigma-Aldrich, Munich, Germany) was dissolved in 1.0 ml mixed solvent (chloroform:methanol = 3:2, vol/vol) and then mixed with 3 mg of nanomicelles in 3.0 ml of mixed solvent. The solvent was then removed by dry heated nitrogen evaporator (VLM GmbH, Bielefeld, Germany) to form a dry film, which was hydrated adding Hepes buffer (10 mM, pH 7.4) at 60 °C for

30 minutes under stirring. Nonencapsulated curcumin was separated by filtration through a 0.45-μm polycarbonate membrane (Millipore Co.) followed by 9h dialysis (changing water every hour) using a membrane with molecular weight cutoff of 2,000 Da. The product in the dialysis tube was subsequently lyophilized by means of a concentrator plus (Eppendorf, Hamburg, Germany). The amount of curcumin encapsulated in the nanomicelles was measured using a spectrophotometer (Ultrospec 3100pro, Amersham Bioscience, GE Healthcare, Buckinghamshire, UK) with wavelength at 420 nm. Blank nanomicelles were prepared using the same procedures without curcumin addition. The drug-loading content was calculated using a standard curve made on specific curcumin concentrations dissolved into the same mixed solvent.

5.2 PAO irradiation

PAO bacterial strains were grown to 0.5 McFarland's standard approximately corresponding to 1×10^8 CFU/mL and then diluted 1:1000 in fresh LB broth growth medium and inoculated in 96-well plates. Planktonic PAO suspensions have been treated with free curcumin in different concentrations (50μM, 20μM, 10μM), and with 3 types of curcumin nanomicelles (DAPMA, SPD, SPM) in different concentrations (1μM, 500nM, 250nM, 100nM, 50nM). For every treatment, 4 wells have been irradiated with a subletal blue laser protocol (wavelength 445nm, power 0,2W irradiance 0,1W/cm^2, fluence 6J/cm^2) and 4 weren't. Subsequently, the most effective nanomicelles have been selected and other laser protocols with increasing fluences have been tested (wavelength 445nm, power 0,2W, irradiance 0,1W/cm^2, fluence 18J/cm^2, and wavelength 445nm, power 0,2W, irradiance 0,1W/cm^2, fluence 30J/cm^2)

Statistical analysis has been performed using the Kruskal-Wallis test to evaluate differences among groups, and Dunn's multiple comparison test as post hoc to compare each pair of groups. A p-value <0,05 has been used for the rejection of the null hypothesis.

Results

1. Antimicrobial effect of blue laser on Pseudomonas aeruginosa (PAO)

1.1 Antimicrobial effect of blue laser on planktonic PAO

To evaluate the antimicrobial effect of blue laser (445nm) irradiation on planktonic PAO, we performed a planktonic growth curve experiment over time evaluating three fluences (40J/cm^2, 60J/cm^2 and 120J/cm^2) reached with the combination of different powers, irradiances and irradiation times. Table 1 and Figure 1 show the results of the protocols with Fluence 40J/cm^2.

40J/cm^2 445nm	**0,3W**	**0,5W**	**0,7W**	**1W**	**1,5W**	**2W**	**NT**
T0	0	0	0	0	0	0	0
T6	0	0	0	0	0	0	0,012
T12	0***	0***	0***	0***	0***	0***	0,177
T18	0,175	0,171	0,176	0,179	0,167	0,166	0,45
T24	0,454	0,433	0,41	0,432	0,373	0,401	0,515
p-value (Friedman)	**<0,0001**	**<0,0001**	**<0,0001**	**<0,0001**	**<0,0001**	**<0,0001**	**<0,0001**

Table 1. T0-24 represent time points (hours) after irradiation. Values represent OD_{600} of bacterial suspensions. NT non treated. *** Mann-Whitney U test vs. NT p<0,0001.

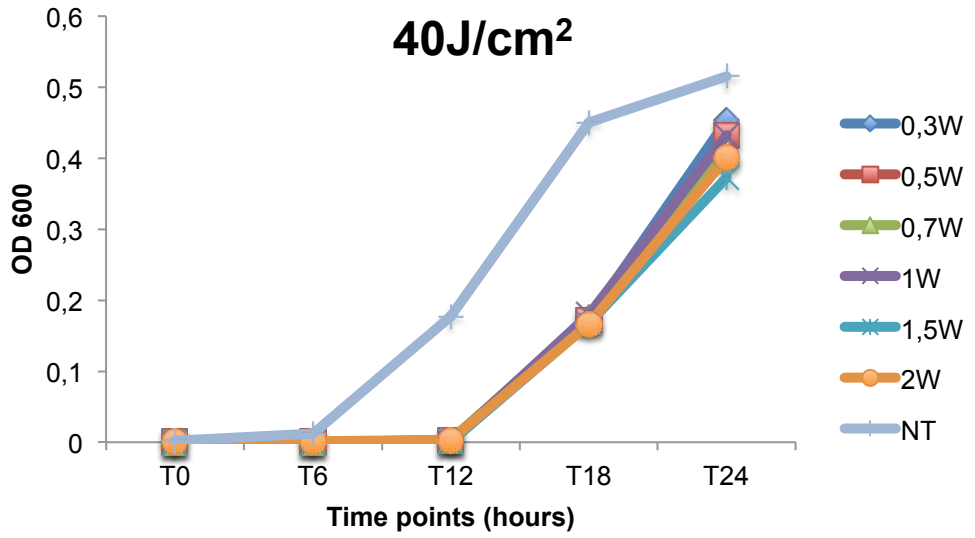

Figure 1. Graph summarizing the results of 40J/cm^2 protocols.

All the protocols employed with 40J/cm^2 fluence have shown to be able to partially inhibit bacterial growth, considering that at T12 (12 hours after irradiation) there is a significant difference between every protocol and non treated wells ($p<0,0001$). However, at T18 bacteria started to grow in all wells (no significant differences between every protocol and non treated wells) and reached the plateau of the curve at T24. Statistical analysis regarding the changes in well turbidity over time performed employing the Friedman test showed a significant increase in bacterial growth in all the tested protocols ($p<0,0001$). Therefore, we can conclude that 40J/cm^2 protocols were able to decrease bacterial viability, but weren't enough effective in eradicating completely planktonic bacteria.

Table 2 and Figure 2 summarize the results of the protocols with Fluence 60J/cm^2.

60J/cm^2 445nm	**0,3W**	**0,5W**	**0,7W**	**1W**	**1,5W**	**2W**	**NT**
T0	0	0	0	0	0	0	0
T6	0	0	0	0	0	0	0,006
T12	0***	0***	0***	0***	0***	0***	0,177
T18	0***	0***	0***	0***	0***	0,155***	0,288
T24	0***	0***	0,2***	0,111***	0,145**	0,267	0,288
p-value (Friedman)	**NS**	**NS**	**NS**	**NS**	**NS**	**NS**	**<0,0001**

Table 2. T0-24 represent time points (hours) after irradiation. Values represent OD_{600} of bacterial suspensions. NT non treated. *** Mann-Whitney U test vs. NT $p<0,0001$. ** Mann-Whitney U test vs. NT $p<0,001$.

All the protocols with fluence 60J/cm^2 have shown an inhibition of bacterial growth over time (Friedman for differences in bacterial growth over time non significant for all tested protocols, while non treated increased significantly with $p<0,0001$). While 0,2W and 0,5W protocols maintained bacterial inhibition up to 24 hours after irradiation, the other protocols showed a slight increase in bacterial density, even if significantly lower compared to non treated samples. The 2W protocol proved to be the less effective, showing a complete recovery of bacterial growth at T24 (Test vs. NT statistically not significant).

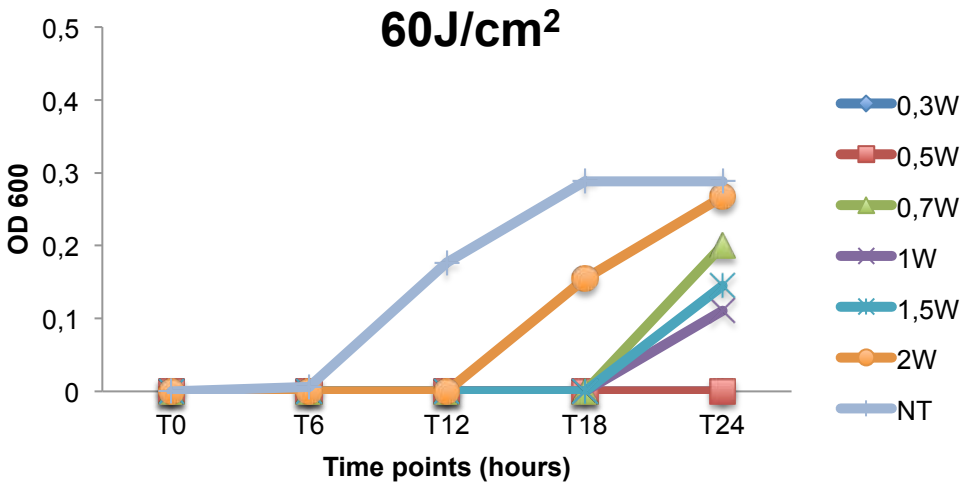

Figure 2. Graph summarizing the results of 60J/cm^2 protocols.

Table 3 and Figure 3 summarize the results of the protocols with Fluence 120J/cm^2.

120J/cm^2 445nm	**0,3W**	**0,5W**	**0,7W**	**1W**	**1,5W**	**2W**	**NT**
T0	0	0	0	0	0	0	0
T6	0	0	0	0	0	0	0,006
T12	0***	0***	0***	0***	0***	0***	0,177
T18	0***	0***	0***	0***	0***	0***	0,288
T24	0***	0***	0***	0***	0***	0,09	0,288
p-value (Friedman)	**NS**	**NS**	**NS**	**NS**	**NS**	**NS**	**<0,0001**

Table 3. T0-24 represent time points (hours) after irradiation. Values represent OD_{600} of bacterial suspensions. NT non treated. *** Mann-Whitney U test vs. NT p<0,0001. ** Mann-Whitney U test vs. NT p<0,001.

When samples were irradiated with protocols reaching 120J/cm^2 fluence, they were all able to significantly inhibit bacterial growth (Friedman test not significant for all tested protocols). At every time point from T12 to T24 the difference of each protocol compared to non treated samples was significant with p<0,0001 except fo the 2W protocol at T24, when bacteria started to recovery. Interestingly, the 2W protocol (characterized by the fact that blue

laser is applied for the shortest time compared to the other protocols) was the less effective in all three fluences tested.

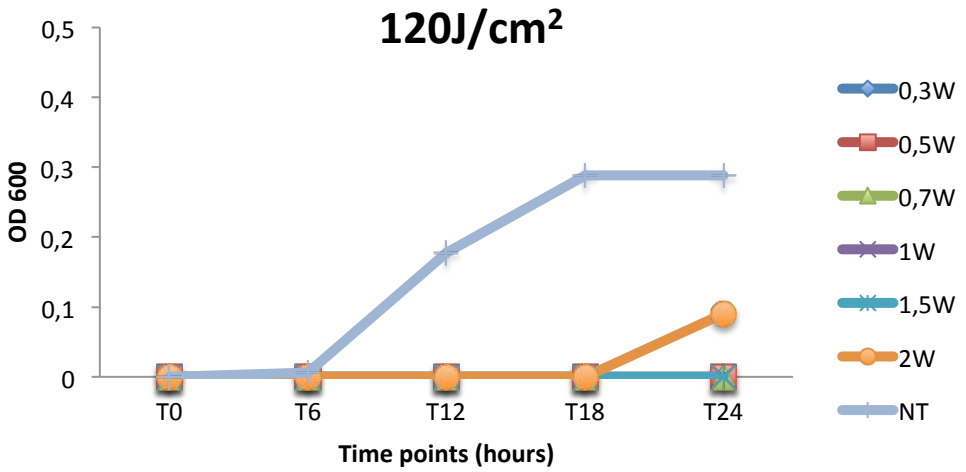

Figure 3. Graph summarizing the results of 120J/cm^2 protocols.

Tables 4 and 5 and Figures 4 and 5 summarize the results of the protocols with red (660nm) and infrared (970nm) laser wavelength, applied with Fluence 120J/cm^2 which proved to be the most effective during tests with blue (445nm) laser irradiation.

120J/cm^2 660nm	**0,3W**	**0,5W**	**0,7W**	**1W**	**1,5W**	**2W**	**NT**
T0	0	0	0	0	0	0	0
T6	0,005	0,006	0,004	0,007	0,006	0,004	0,006
T12	0,134	0,188	0,193	0,156	0,178	0,187	0,177
T18	0,25	0,28	0,27	0,29	0,31	0,34	0,288
T24	0,26	0,29	0,28	0,28	0,32	0,35	0,288
p-value (Friedman)	**<0,0001**	**<0,0001**	**<0,0001**	**<0,0001**	**<0,0001**	**<0,0001**	**<0,0001**

Table 4. T0-24 represent time points (hours) after irradiation. Values represent OD_{600} of bacterial suspensions. NT non treated.

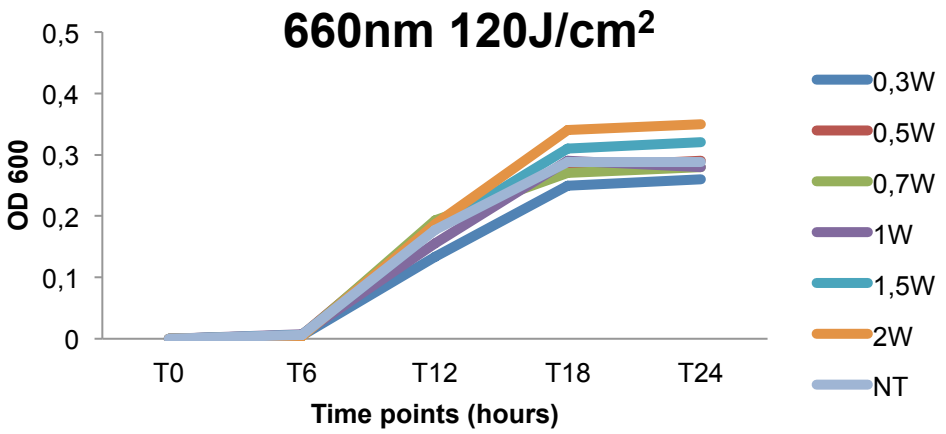

Figure 4. Graph summarizing the results of 120J/cm^2 protocols.

120J/cm^2 970nm	0,3W	0,5W	0,7W	1W	1,5W	2W	NT
T0	0	0	0	0	0	0	0
T6	0,004	0,007	0,005	0,003	0,006	0,003	0,004
T12	0,124	0,178	0,196	0,156	0,187	0,178	0,177
T18	0,28	0,34	0,27	0,31	0,33	0,34	0,288
T24	0,3	0,27	0,29	0,29	0,31	0,34	0,288
p-value (Friedman)	**<0,0001**	**<0,0001**	**<0,0001**	**<0,0001**	**<0,0001**	**<0,0001**	**<0,0001**

Table 5. T0-24 represent time points (hours) after irradiation. Values represent OD_{600} of bacterial suspensions. NT non treated.

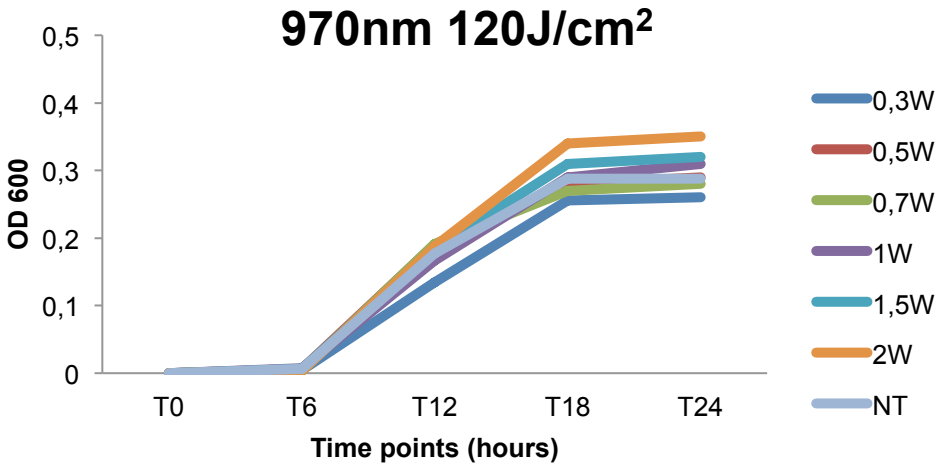

Figure 5. Graph summarizing the results of 120J/cm^2 protocols.

All protocols with the highest fluence (120J/cm^2) have been tested in the same conditions using two different laser wavelengths: red (660nm) and infrared (970nm) and neither of them showed any antimicrobial activity compared to non treated samples. Microbial density increased significantly over time (Friedman test significant with p<0,0001 for all protocols and non treated samples) and there were not significant differences between tested protocols and non treated samples at each time point.

1.2 Antimicrobial effect of blue laser on PAO grown on agar plates

To evaluate the effect of blue laser on PAO grown on solid surfaces, we performed several experiments on bacteria grown on agar using the Kirby-Bauer protocol, conventionally employed to perform antibiograms and MIC (Minimum Inhibitory Concentration) measurements. Plates were irradiated shortly after bacterial inoculation, and afterwards incubated at 37°C. After 24 hours, all blue (445nm) laser protocols tested (0,2W 0,12W/cm^2 40J/cm^2, 0,3W 0,18W/cm^2 40J/cm^2, 0,4W 0,24W/cm^2 40J/cm^2, 0,5W 0,3W/cm^2 40J/cm^2, 1W 0,49W/cm^2 40J/cm^2, all in CW) have shown to be able to completely inhibit bacterial growth inside the spot size of irradiation, surrounded by a homogeneous layer of grown bacteria as shown in Figure 6. In particular, Figure 6B shows also the lack of antimicrobial effect exerted by the protocols conventionally used to treat oral mucositis (660nm and 970nm, 0,1W 0,06W/cm^2 6J/cm^2).

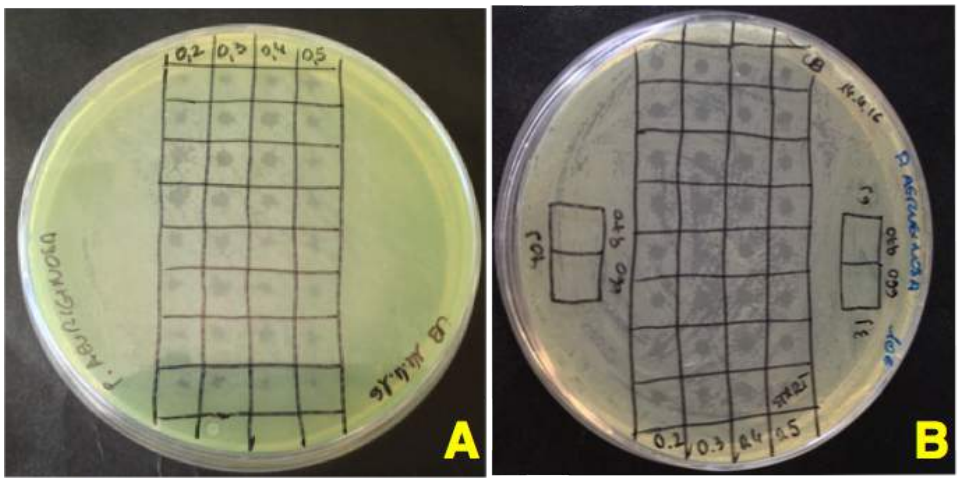

Figure 6. Pictures showing the effect of several blue laser protocols on PAO grown on solid Mueller-Hinton Agar.

When PAO in agar plates were irradiated with the same protocols but exerted by infrared laser light (970nm), we haven't observed any inhibition of bacterial growth, but obtained a homogenous layer of bacterial colonies as shown in Figure 7A. As described in the Materials and Methods part, we wanted to verify whether laser could exert a degradating effect on the growth medium thus inhibiting bacterial growth. For this means, we performed an experiment irradiating the plate before bacterial inoculation. After 24 hours of incubation at 37°C, we obtained a uniform bacterial growth forming a homogenous layer, as shown in Figure 7B.

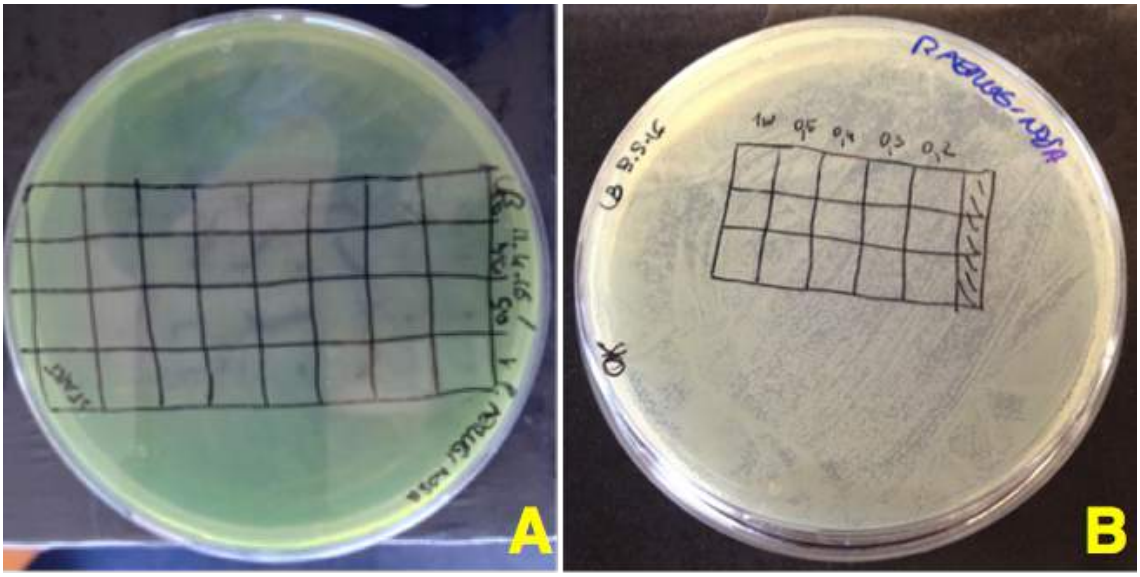

Figure 7. Picture showing the effect of infrared laser protocols on PAO grown on solid Mueller-Hinton Agar (A). When agar was irradiated before inoculation of bacteria, we haven't observed any changes in bacterial growth (B).

1.3 Antimicrobial effect of blue laser on PAO biofilms

a. Biofilms grown on Calgary biofilm devices

Eleven different blue laser protocols were tested on PAO biofilm grown on plastic pegs of the Calgary biofilm devices. 24 hours after irradiation, bacterial growth was assessed measuring optical density of the wells inside the recovery plates after sonication. Figure 8 shows the mean optical density for each protocol: 7 of the tested protocols significantly reduced bacterial growth

compared to non treated bacteria ($p<0,0001$ for 8 protocols by Mann-Whitney U-test): specifically 0,4W 40J/cm^2 and 60J/cm^2, 0,5W 20J/cm^2, 40J/cm^2 and 60J/cm^2, 0,6W 40J/cm^2 and 60J/cm^2. 4 out of these 7 protocols were able to completely eradicate bacteria, being their mean OD_{600} <0.1: 0,4W 60J/cm^2, 0,5W 20J/cm^2, 40J/cm^2 and 60J/cm^2.

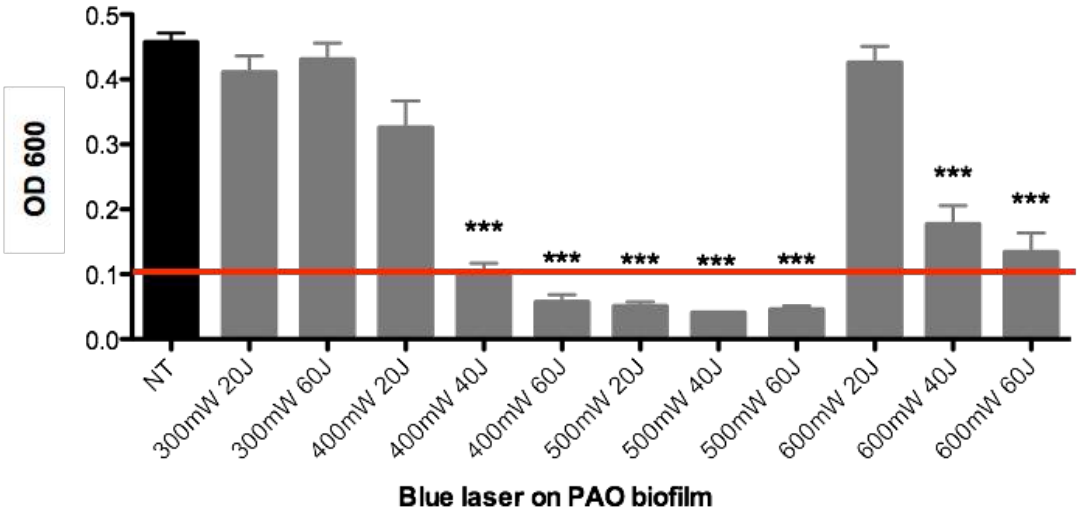

Figure 8. Graph summarizing optical density measurements of PAO samples after different protocols of blue laser irradiation compared to non treated samples. A value of 0,1 is considered as evidence of bacterial eradication. Data are shown as mean ±SD. *** Mann-Whitney U test vs. NT $p<0,0001$.

This experiment allowed us to identify lethal and sublethal blue laser protocols towards PAO biofilms. In the next phase, we evaluated whether a sublethal laser protocol could enhance the effect of antibiotic treatments which are currently employed in clinical practice for the treatment of PAO infections. Specifically, the changes in MIC (Minimum Inhibitory Concentration) of the antibiotics Tobramycin and Gentamicin after irradiation with the protocol power 0,3W irradiance 0,18W/cm^2 fluence 20J/cm^2 have been investigated. The results of the experiment are shown in Figures 9 and 10.

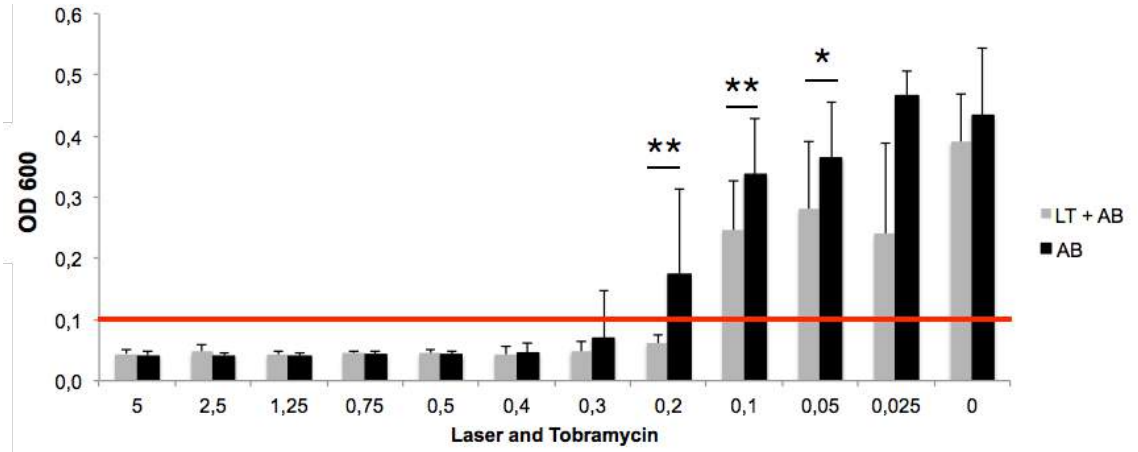

Figure 9. Graph summarizing optical density measurements of PAO samples treated with increasing concentrations of Tobramycin (concentrations are expressed in µg/mL) with and without sublethal blue laser irradiation. A value of 0,1 is considered as evidence of bacterial eradication. Mann-Whitney U test has been employed to compare laser treated and non treated samples at each concentration. Data are shown as mean ±SD. ** LT+AB vs. AB p<0,001. * LT+AB vs. AB p<0,01.

In PAO samples treated with Tobramycin alone, the MIC was 0,3µg/mL while in samples pre-treated with blue laser the MIC was 0,2µg/mL (p<0,001). Bacterial growth was significantly lower in the laser treated group with 0,1µg/mL and 0,05µg/mL concentrations of Tobramycin.

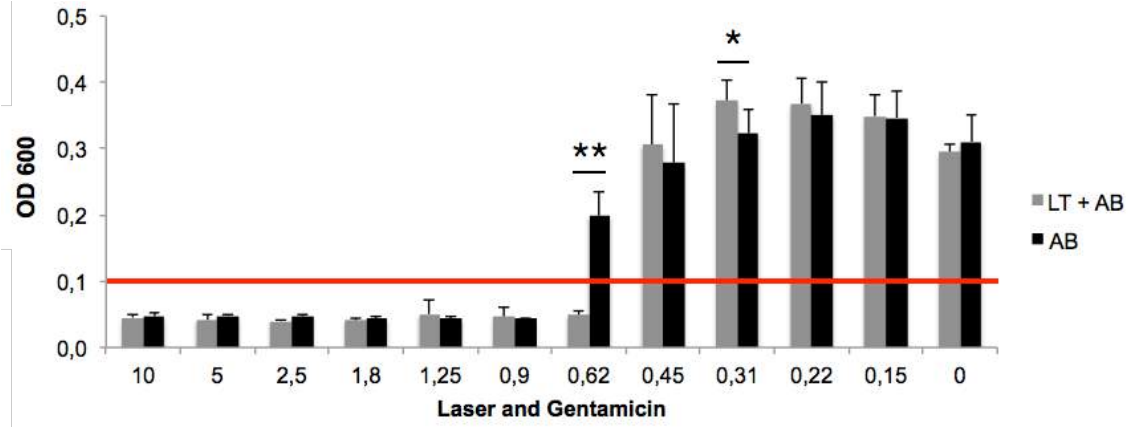

Figure 10. Graph summarizing optical density measurements of PAO samples treated with increasing concentrations of Gentamicin (concentrations are expressed in µg/mL) with and without sublethal blue laser irradiation. A value of 0,1 is considered as evidence of bacterial eradication. Mann-Whitney U test has been employed to compare laser treated and non treated samples at each concentration. Data are shown as mean ±SD.** LT+AB vs. AB p<0,001. * LT+AB vs. AB p<0,01.

In PAO samples treated with Gentamicin alone, the MIC was 0,9μg/mL while in samples pre-treated with blue laser the MIC was 0,62μg/mL ($p<0,001$). Bacterial growth was significantly higher in the laser treated group with 0,31μg/mL concentrations of Gentamicin.

In both experiments, a single session of laser irradiation on PAO biofilms with a sub-lethal protocol was able to increase susceptibility to both Gentamicin and Tobramycin and decrease significantly the MIC ($p<0,001$).

b. Laser Scanning Confocal Microscopy on biofilms grown in flow cells

To visualize the effect on mature PAO biofilms and on biofilm development, we performed several experiments using the Laser Scanning Confocal Microscopy in collaboration with the Department of Microbiology at the University of Washington, Seattle, USA. As described in the Materials and Methods part, a decrease in power density of laser irradiation passing through the flow cells was assessed. Therefore, the protocols are described using the emitted power, the irradiance on the top of the flow cell, and the irradiance measured by the power meter at the opposite side of the flow cell. For every flow cell, 3 volumetric acquisitions were made in 3 different areas. Results are reported showing four representative images: Syto9 (green, whole biomass), PI (purple, dead cells), Merged (showing both stainings together) and a 3Dimensional reconstruction of whole volume acquired.

The non treated samples' representative images are showed in Figure 11. The 3Dimensional reconstruction is showing how the mature PAO biofim grows forming hill-like biomass structures called "mushrooms", where a decreasing gradient of O_2 and nutrients towards the base of the mushroom causes both the death of some bacteria, but also the selection and proliferation of more resistant mutants. Therefore, the presence of structures stained with PI (extracellular DNA, showing the dead cells' presence) in non treated samples is expected.

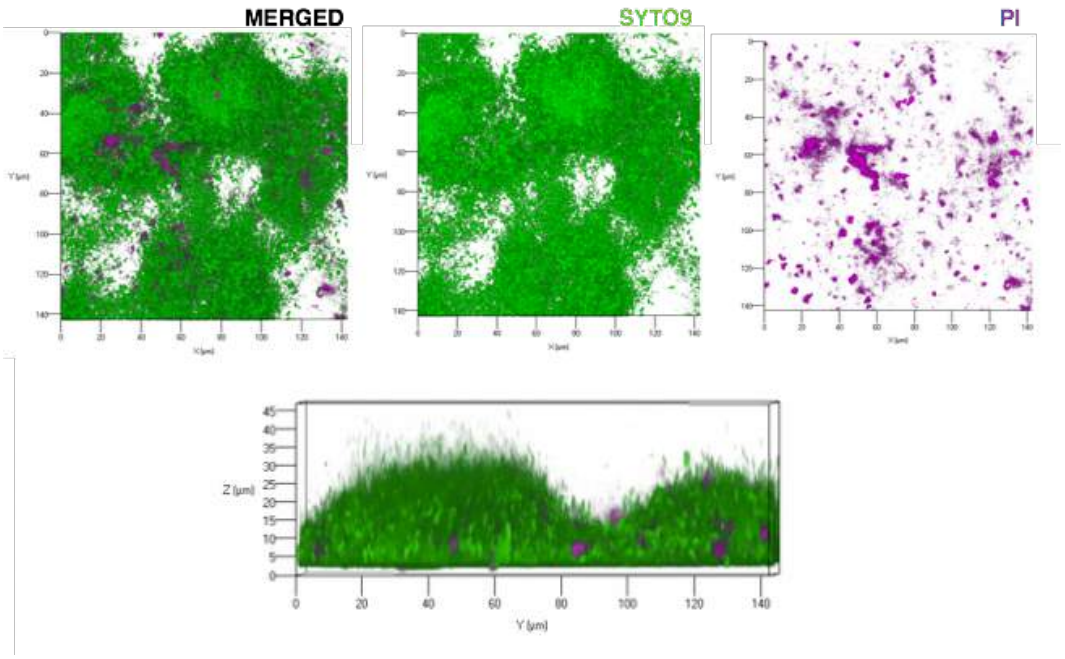

Figure 11. Non treated PAO biofilm, stained and visualized using Laser Scanning Confocal Microscopy.

Figure 12 is showing representative images of the stainings and the 3Dimensional reconstruction of the biofilm treated with diode laser with the following parameters: Wavelength 445nm, power 0,5W, top irradiance 0,3W/cm^2, bottom irradiance 0,15 W/cm^2, fluence 120 J/cm^2 , CW.

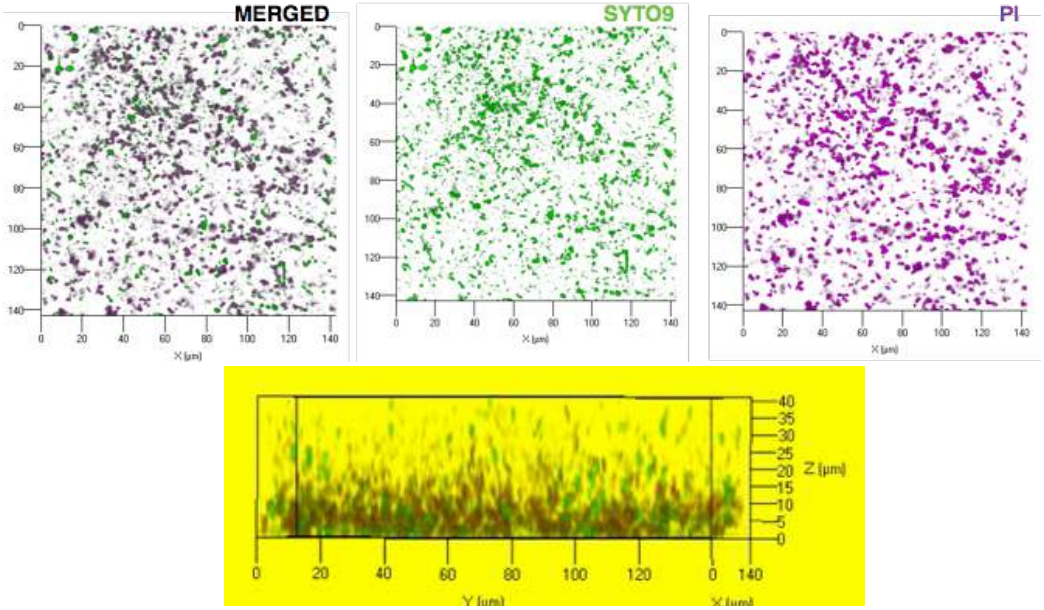

Figure 12. PAO biofilm treated with blue laser protocol Wavelength 445nm, power 0,5W, top irradiance 0,3W/cm^2, bottom irradiance 0,15 W/cm^2, fluence 120 J/cm^2 , CW, stained and visualized using Laser Scanning Confocal Microscopy.

In this case, it is clearly visible how the mushroom structures are not detectable and the distribution of living and dead bacteria is homogenous and random.

To obtain a numerical value representing the biomass and dead cells to compare treated and non treated samples, voxel counting for every acquired volume stack has been performed as described in the Materials and Methods part. Therefore, the mean total biomass and the proportion of dead cells on biomass has been calculated and plotted as shown in Figure 13.

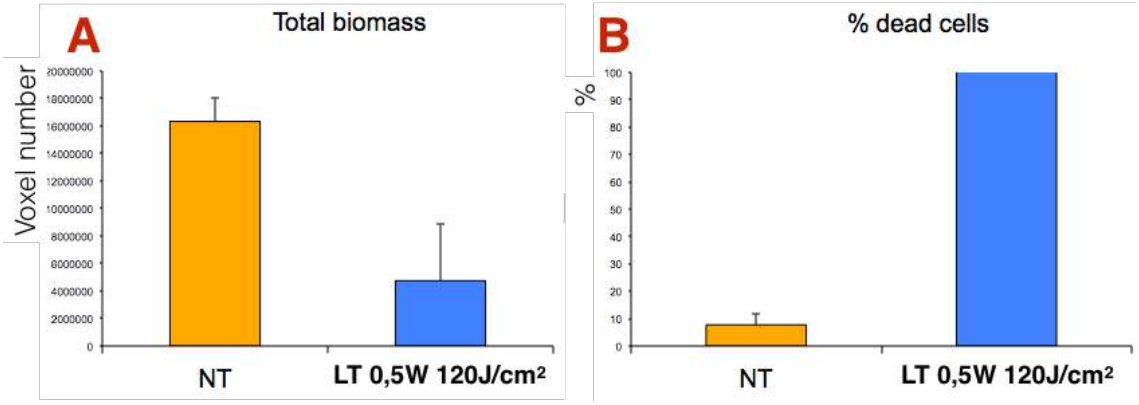

Figure 13. Graph A is showing the total biomass in treated and non treated samples, while Graph B is showing the % of dead cells on total biomass in each group. Data are shown as mean ±SD. Mann-Whitney U Test LT versus NT significant with p<0,0001 for both total biomass and % of dead cells.

The results of this experiments show how blue laser irradiation with the protocol Wavelength 445nm, power 0,5W, top irradiance 0,3W/cm^2, bottom irradiance 0,15 W/cm^2, fluence 120 J/cm^2 , CW was able to significanlty reduce the whole biofilm biomass and to obtain a 100% of dead cells.

A second experiment has been performed irradiating the PAO biofilm with the protocol Wavelength 445nm, power 1W, top irradiance 0,6W/cm^2, bottom irradiance 0,3 W/cm^2, fluence 150 J/cm^2, CW. The representative images of the stainings and the 3Dimensional reconstruction of the PAO biofilm are shown in Figure 14. The mean total biomass and the proportion of dead cells on biomass have been calculated and plotted in the graphs in Figure 15, comparing the values with those obtained in non treated samples. This protocol has been able to completely disrupt the biofilm structure and kill all the remaining bacteria.

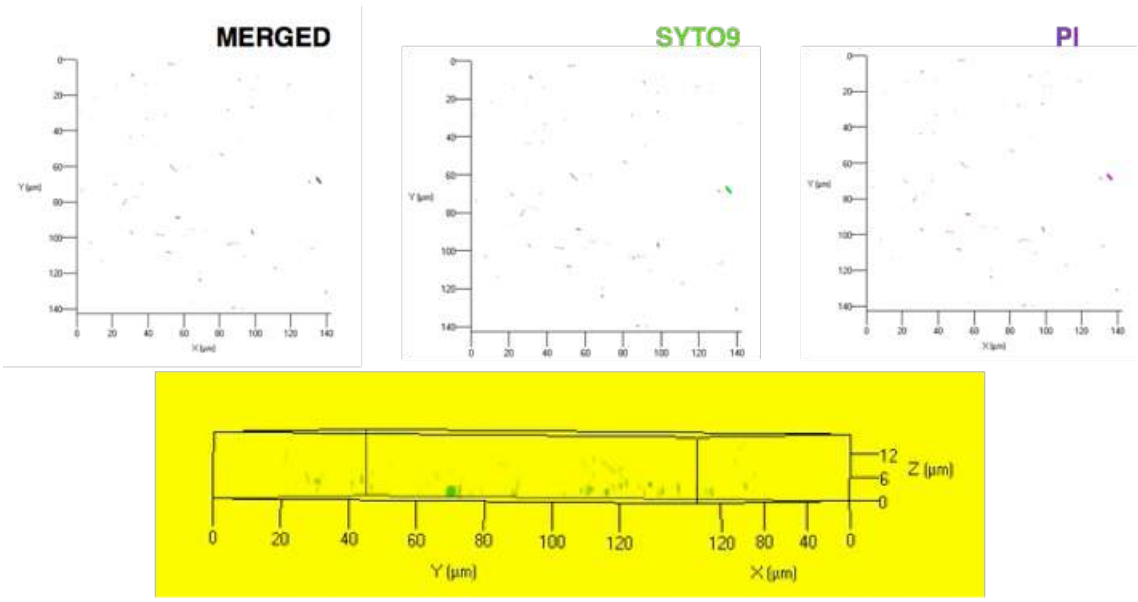

Figure 14. PAO biofilm treated with blue laser protocol Wavelength 445nm, power 1W, top irradiance 0,6W/cm^2, bottom irradiance 0,3 W/cm^2, fluence 150 J/cm^2, CW, stained and visualized using Laser Scanning Confocal Microscopy.

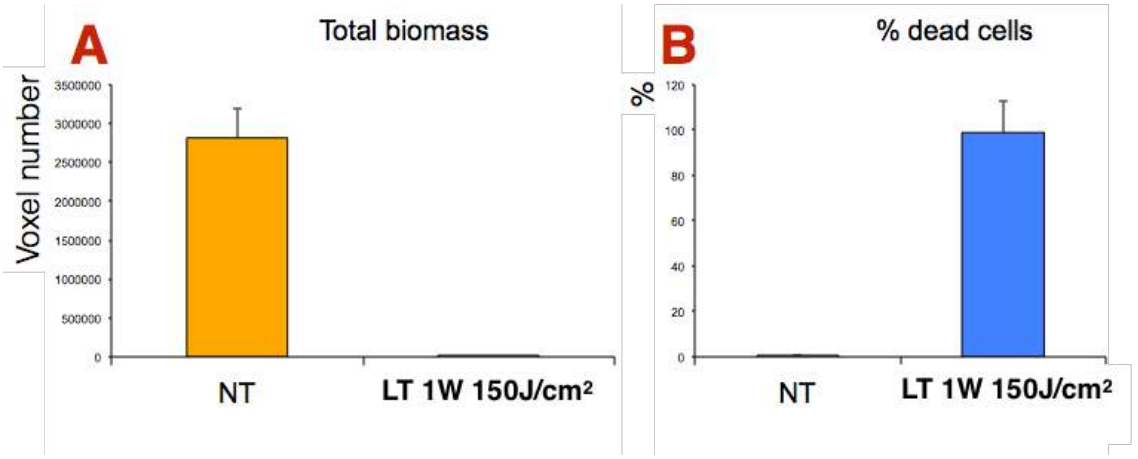

Figure 15. Graph A is showing the total biomass in treated and non treated samples, while Graph B is showing the % of dead cells on total biomass in each group. Data are shown as mean ±SD. Mann-Whitney U Test LT versus NT significant with p<0,0001 for both total biomass and % of dead cells.

The same protocol in terms of power density and fluence has been employed using infrared (IR) laser light: Wavelength 970nm, power 1W, top irradiance 0,6W/cm^2, bottom irradiance 0,3 W/cm^2, fluence 150 J/cm^2, CW. The results are represented in Figure 16 and the total biomass and % of dead cells compared to non treated samples are showed in Figure 17. This experiment showed how IR laser irradiation, performed using the same parameters that

showed maximum efficacy with the Blue laser, haven't affected biomass stability and bacterial viability compared to non treated samples.

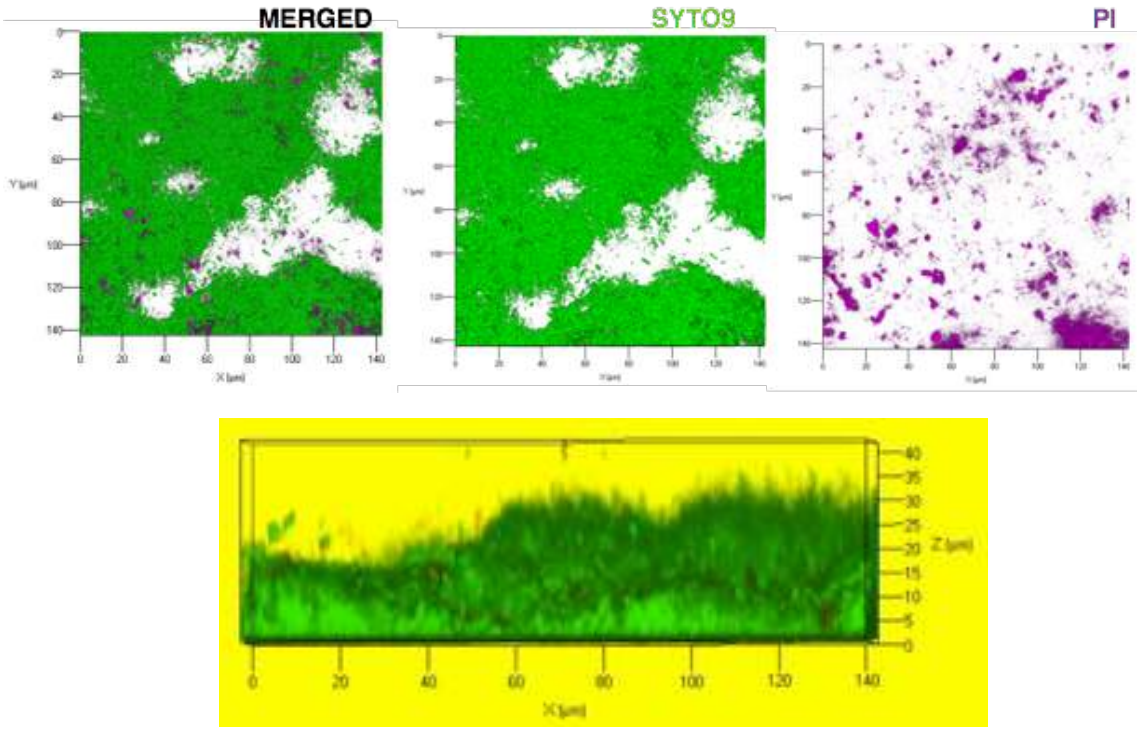

Figure 16. PAO biofilm treated with IR laser protocol wavelength 970nm, power 1W, top irradiance 0,6W/cm^2, bottom irradiance 0,3 W/cm^2, fluence 150 J/cm^2, CW, stained and visualized using Laser Scanning Confocal Microscopy.

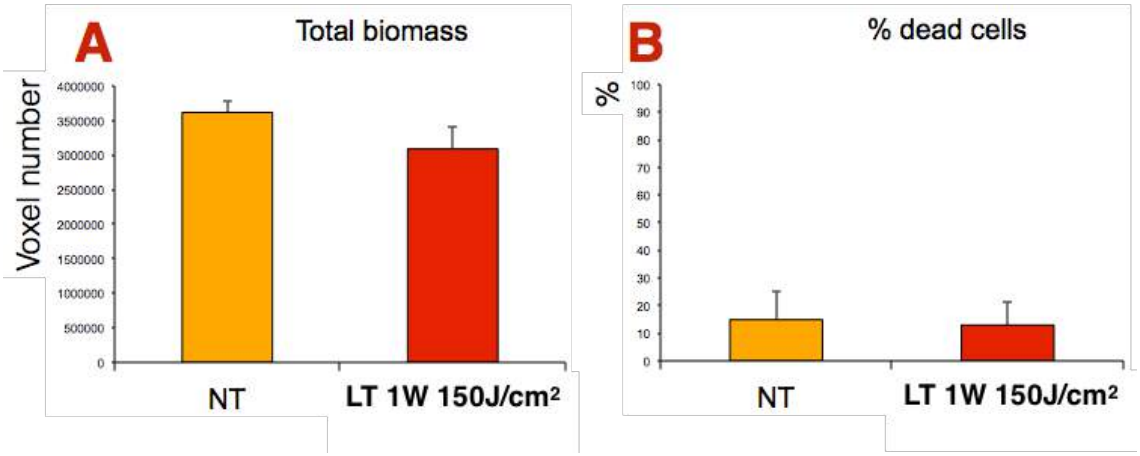

Figure 17. Graph A is showing the total biomass in treated and non treated samples, while Graph B is showing the % of dead cells on total biomass in each group. Data are shown as mean ±SD. Mann-Whitney U test LT versus NT not significant for both total biomass and % of dead cells.

Furthermore, to evaluate biofilm growth inhibition, a flow cell has been irradiated shortly after inoculation with the protocol Wavelength 445nm, power

1W, top irradiance 0,6W/cm^2, bottom irradiance 0,3 W/cm^2, fluence 150 J/cm^2, CW, and biofilm growth has been monitored over time: at 24h, 48h and 72h after irradiation. Figure 18 shows the images of the flow cell acquired at a 63x magnification using an optical microscope.

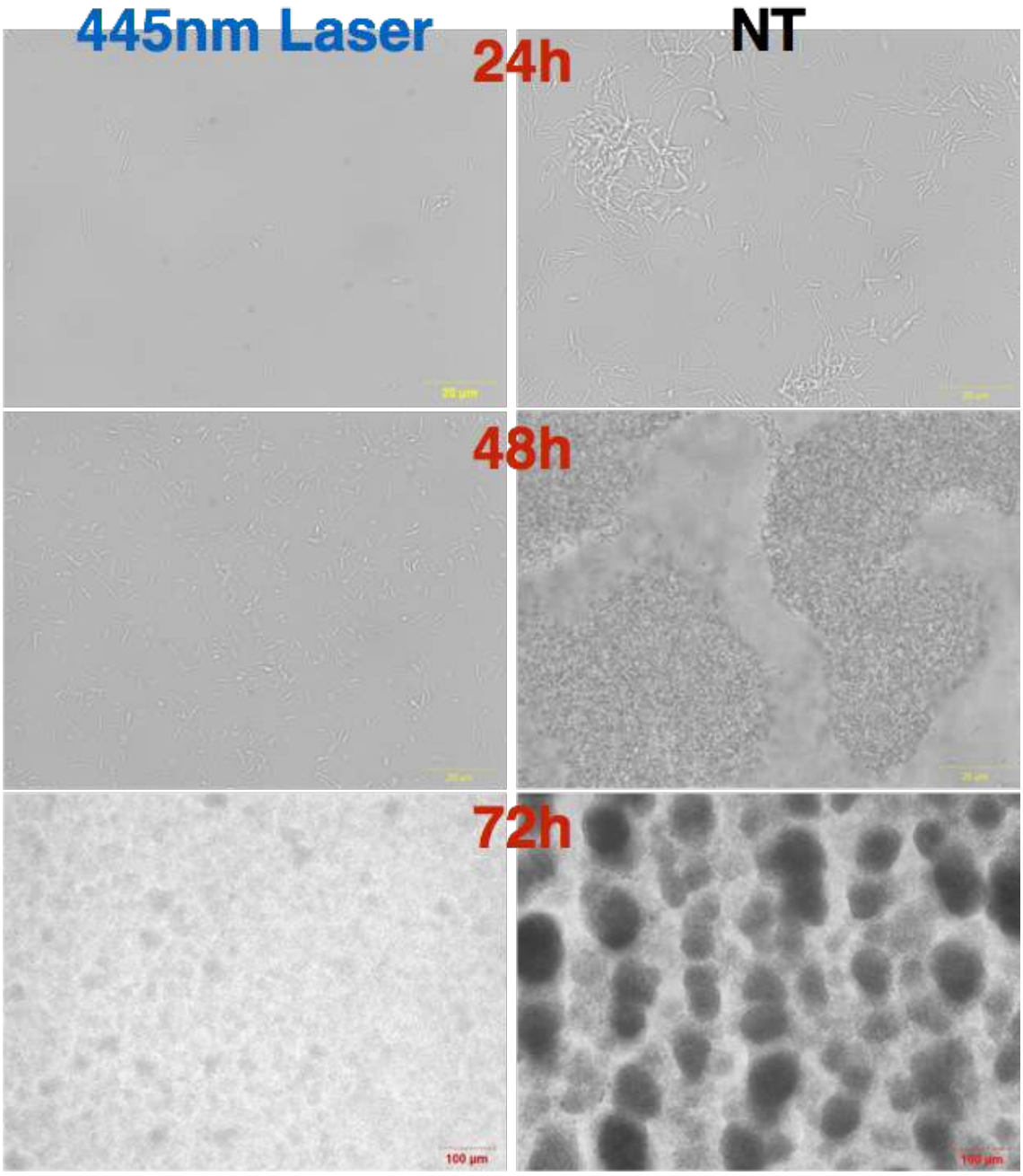

Figure 18. Images acquired using optical microscope showing flow cells treated with the protocol Wavelength 445nm, power 1W, top irradiance 0,6W/cm^2, bottom irradiance 0,3 W/cm^2, fluence 150 J/cm^2, CW shortly after inoculation and then visulalized 24h, 48h and 72h after one treatment compared with a non treated sample inoculated at the same time.

The images taken are clearly showing a reduction in the number of viable bacteria after 24h, which persists in later time points. 72h after inoculation and treatment, the surviving bacteria have been able to proliferate and organize a biofilm structure, which remains less developed compared to non treated samples. The hill-like structures “mushrooms” are visible as in the non treated samples, but remain smaller and less organized.

After 72h, the biofilm has been stained with the same techniques used in previous experiments and volumetric data has been acquired. Figures 19 and 20 show representative images of the stainings and 3Dimensional reconstructions of the treated and non treated samples, while Figure 21 shows the total biomass and % of dead cells comparing the two groups.

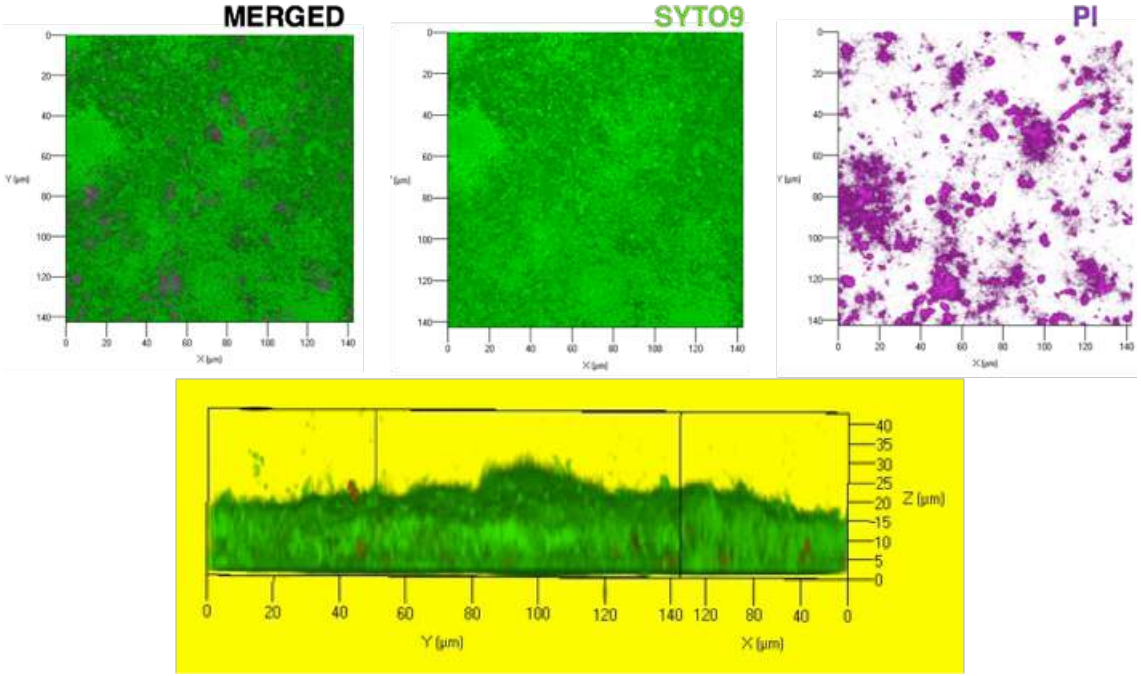

Figure 19. PAO biofilm treated with blue laser protocol Wavelength 445nm, power 1W, top irradiance 0,6W/cm^2, bottom irradiance 0,3 W/cm^2, fluence 150 J/cm^2, CW, shortly after inoculation in the flow cell. After 72h, the biofilm has been stained and visualized using Laser Scanning Confocal Microscopy.

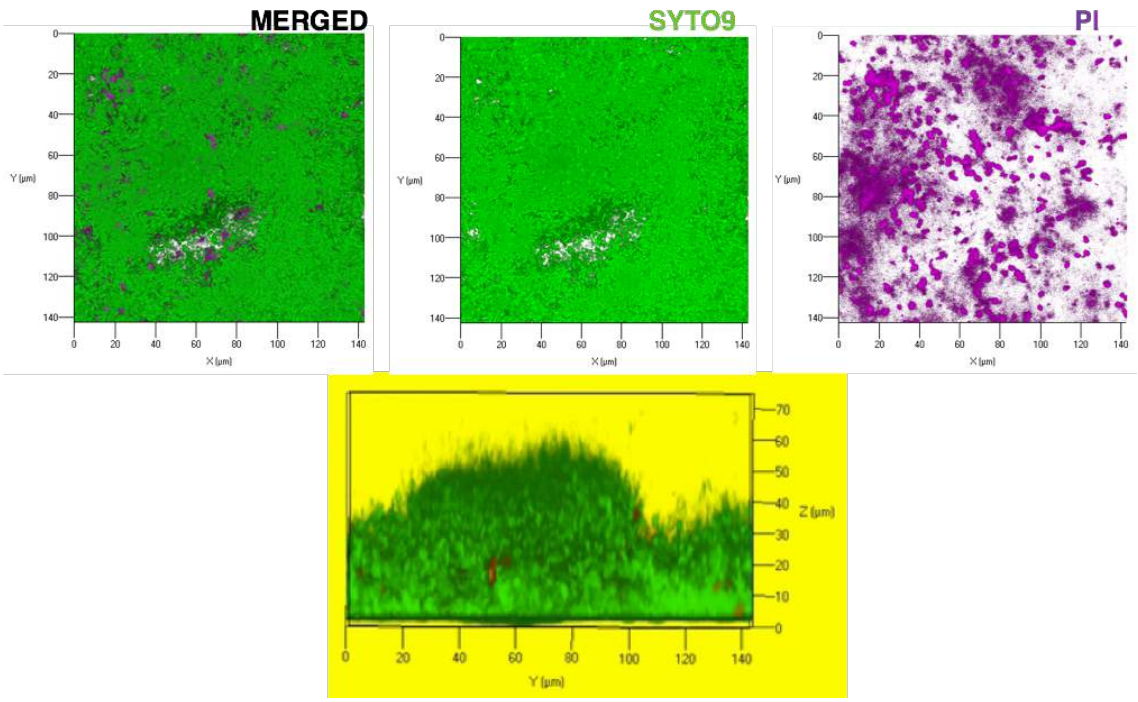

Figure 20. Non treated PAO biofilm stained and visualized 72h after inoculation using Laser Scanning Confocal Microscopy.

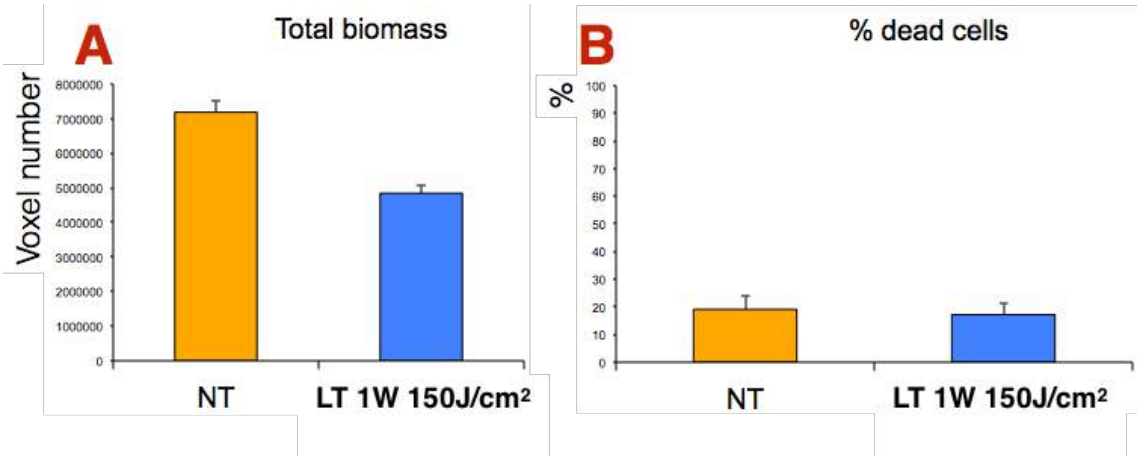

Figure 21. Graph A is showing the total biomass in treated and non treated samples, while Graph B is showing the % of dead cells on total biomass in each group. Data are shown as mean ±SD. Mann-Whitney U Test LT versus NT significant with p<0,0001 only for total biomass.

The results of voxel counting are consistent with the aspect of biofilms visualized using the optical microscope: 72h after a single laser irradiation, the remaining bacteria have proliferated but haven't been able to form the biomass structure as non treated bacteria. The number of dead cells inside the biofilm

doesn't differ significantly between the two groups as expected, since all dead cells are washed out due to the constant flow of fresh growth medium.

1.4 Scanning Electron Microscopy imaging and analysis

SEM images have been obtained using different magnifications (300x, 2400x, 20.000x). PAO have been inoculated on sterile cover plates and then irradiated using the following protocols: Wavelength 445nm, power 1W, irradiance 0,3W/cm^2, fluence 150 J/cm^2 and 75 J/cm^2, CW; Wavelength 970nm, power 1W, irradiance 0,3W/cm^2, fluence 150 J/cm^2 and 75 J/cm^2, CW. Figure 22 shows images regarding the protocols involving blue laser light (445nm), while Figure 23 shows images regarding infrared laser light (970nm).

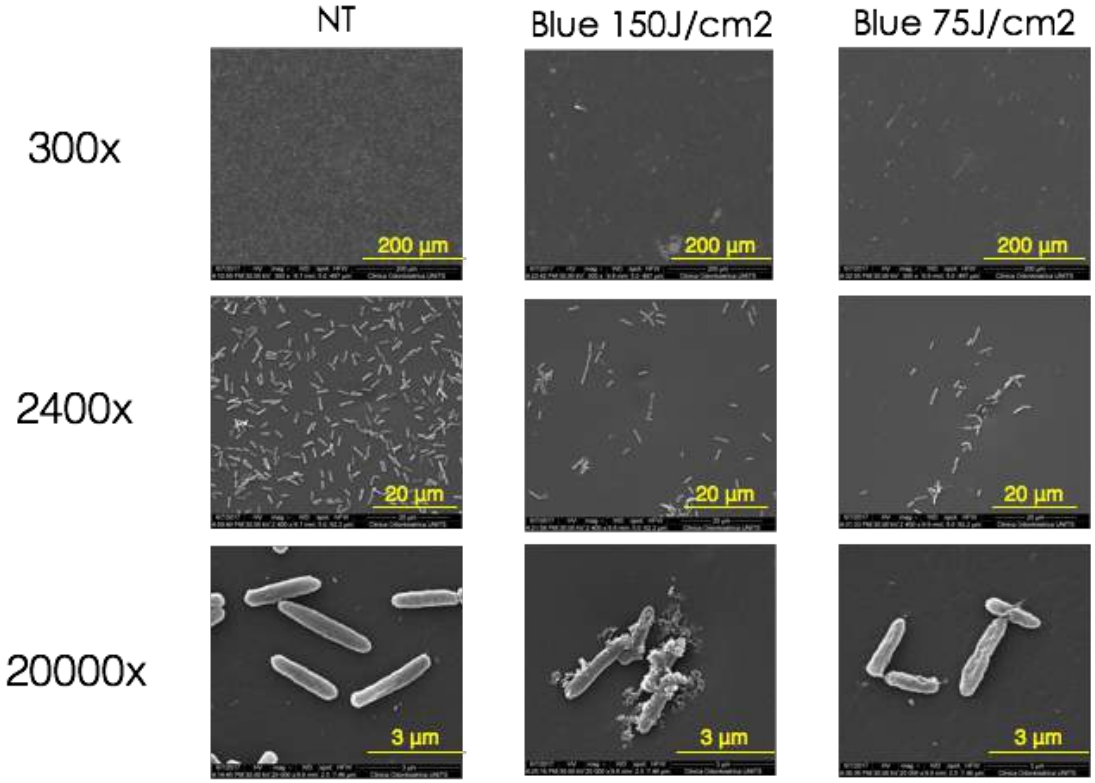

Figure 22. Images acquired using SEM showing blue laser treated and non treated PAO at different magnifications.

In the pictures acquired using 300x and 2400x magnifications regarding bacteria treated with blue laser, it is easily noticed how a large number of bacteria have been detached and washed away after laser treatment. In the largest magnification (20000x), severely damaged bacteria can be observed.

Multiple blebs on the outer membrane and perturbed membrane morphology are clearly visible on the remaining bacteria.

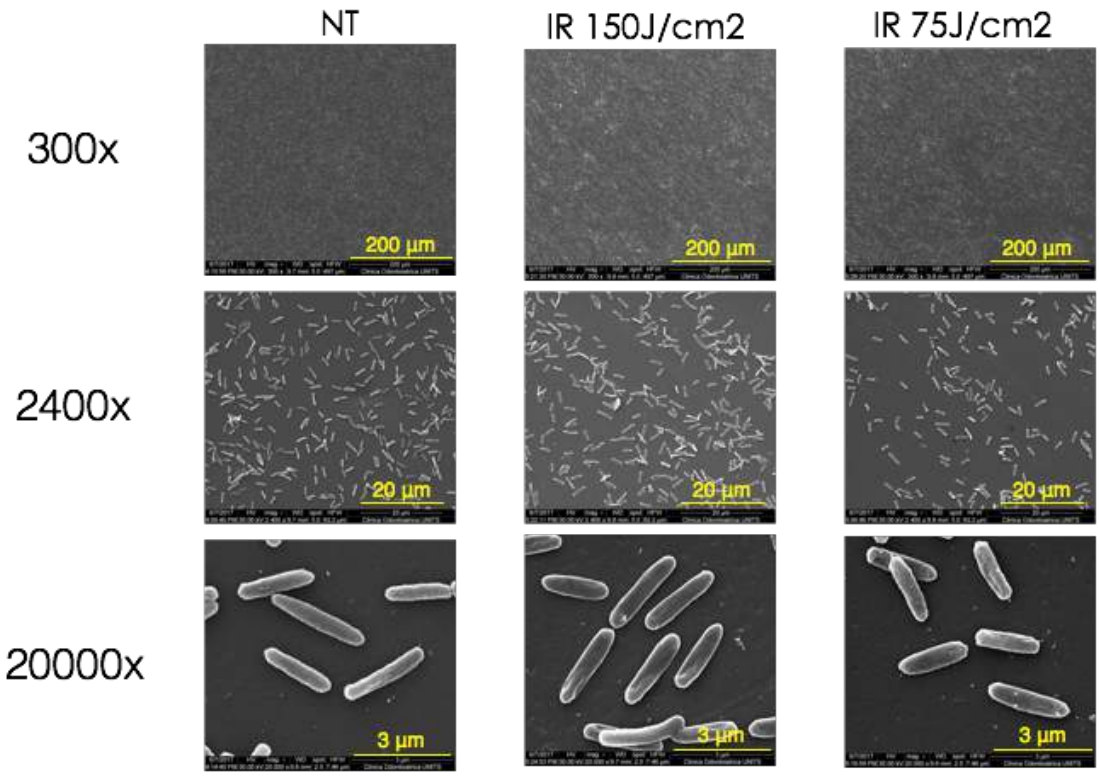

Figure 23. Images acquired using SEM showing infrared laser treated and non treated PAO at different magnifications.

In the pictures regarding bacteria treated with infrared laser with the same protocols in terms of power density ad fluence, there are no visible differences in cell quantity or morphology compared to non treated samples.

Scanning Electron Microscopy is a usually considered a qualitative technique which allows to visualize cell morphology and membrane changes. To obtain quantitative results and numerically compare the experimental groups, the 300x magnification images taken from quadruplicates have been analyzed using the ImageJ software. Every image has been binarized and the quantity of white pixels, corresponding to the surface covered by bacteria, has been obtained. Subsequently, statistical analysis has been performed to compare the bacterial density of the treated samples with non treated ones. The results of the analysis are showed in Figure 24. The results showed how both of the blue laser

protocols were able to decrease significantly the bacterial density ($p<0,0001$ for both protocols), whereas the infrared protocols haven't showed any significant changes in density compared to non treated samples. Looking at the mean proportions considering non treated samples as 100%, while the infrared 150J/cm^2 protocol caused a slight decrease in bacterial density, the infrared protocol with fluence 75J/cm^2 was able to stimulate bacterial proliferation resulting in a moderate increase in bacterial density (120,75% compared to non treated samples). However, these differences were statistically not significant.

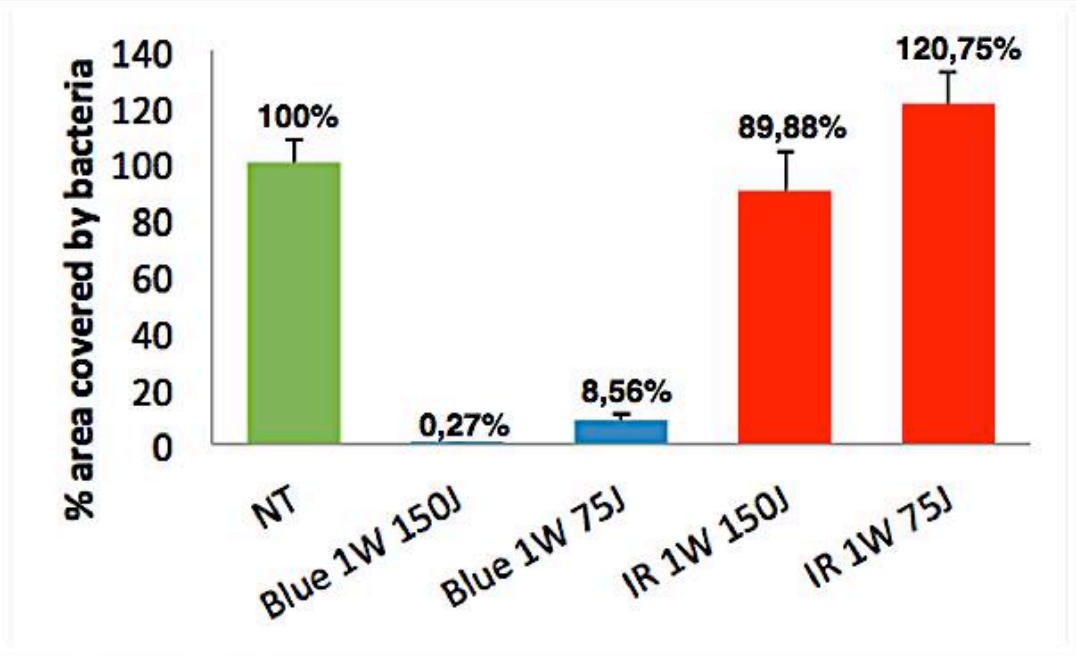

Mann-Whitney test
NT versus Blue (75J and 150J): $p<0,0001$
Blue (75J and 150J) versus IR (75J and 150J): $p<0,0001$
NT versus IR (75J and 150J): NS

Figure 24. Graphical representation of the results of the SEM images analysis using ImageJ software in order to calculate the % of area covered by bacteria in each sample. Data are shown as mean ±SD.

2. Evaluation of the antimicrobial mechanism of action

2.1 Monitoring of the temperature at sites of irradiation

It is known that a temperature between 60 and 70°C is needed to kill several bacterial species including PAO. To investigate whether the blue laser protocols employed in previous experiments could provoke such temperature increase on sites of irradiation thus providing a photothermal antimicrobial effect, the temperature changes at sites of irradiation have been measured using a thermographic camera. Results regarding power densities power 0,2W irradiance 0,12W/cm^2, power 0,3W irradiance 0,18W/cm^2, power 0,4W irradiance 0,24W/cm^2, power 0,5W irradiance 0,3W/cm^2 are shown in Figure 25. Results regarding power 1W irradiance 0,49W/cm^2 obtained with both the ENT and Zoom tip are shown in Figure 26. The pictures show how the increase of irradiance causes a slight progressive increase in temperature measured at spots of irradiation. However, the temperature remains always within the range of viability conditions for PAO. The maximum temperature registered was 33,7°C, obtained applying power 1W irradiance 0,49W/cm^2 using the Zoom tip.

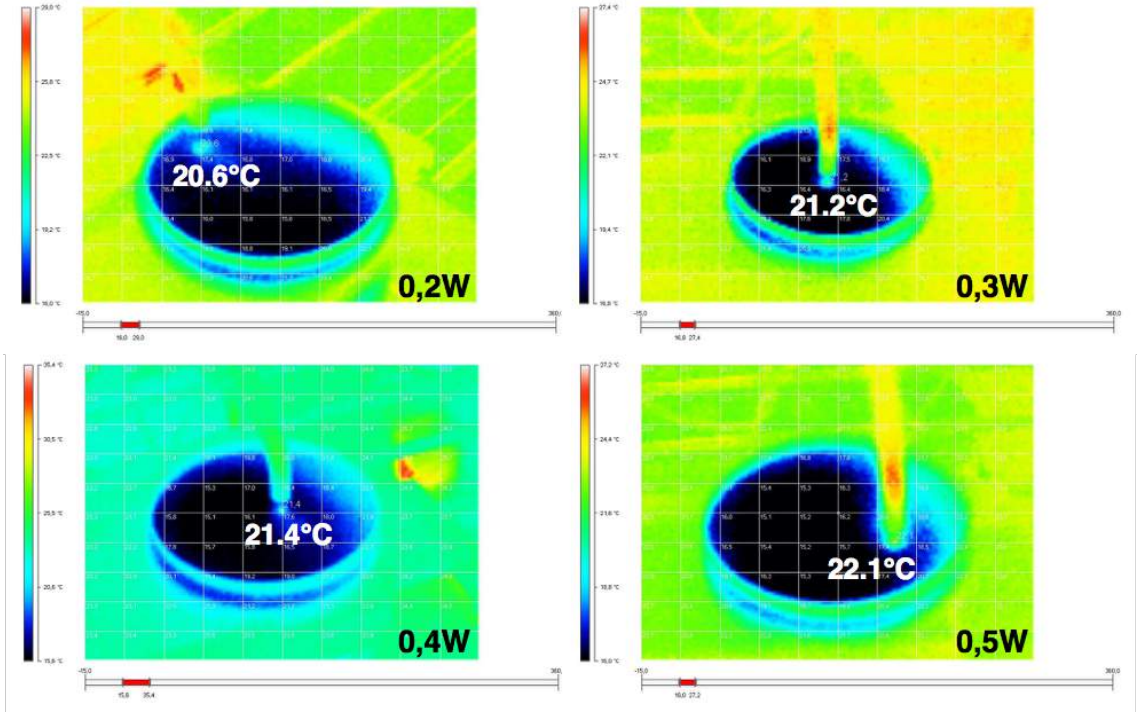

Figure 25. Picture showing temperature measured at irradiation spots during laser irradiation with different power densities.

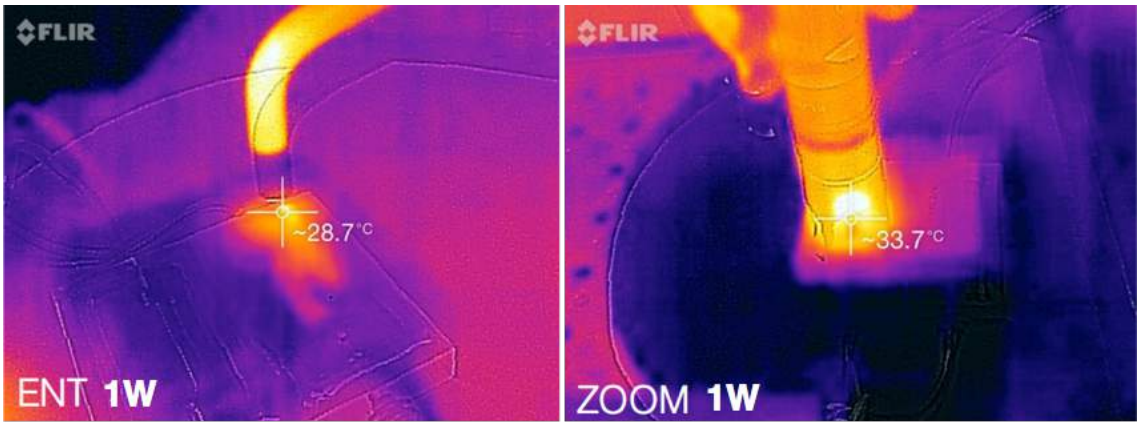

Figure 26. Picture showing temperature measured at irradiation spots during laser irradiation with 1W power with different tips.

2.2 Measurement of the Total Oxidant Status

Oxidative stress is believed to be the main antimicrobial mechanism of action of blue light against several bacterial species including PAO. To evaluate changes in the oxidative stress in bacterial suspensions following laser treatment, we measured the Total Oxidant Status (TOS) shortly after laser irradiation using the protocol wavelength 445nm, power 0,3W irradiance 0,18W/cm^2, fluence 120 J/cm^2, CW. The results are shown in Figure 27 and demonstrate how the oxidant status increased significantly after laser treatment compared to non treated bacteria.

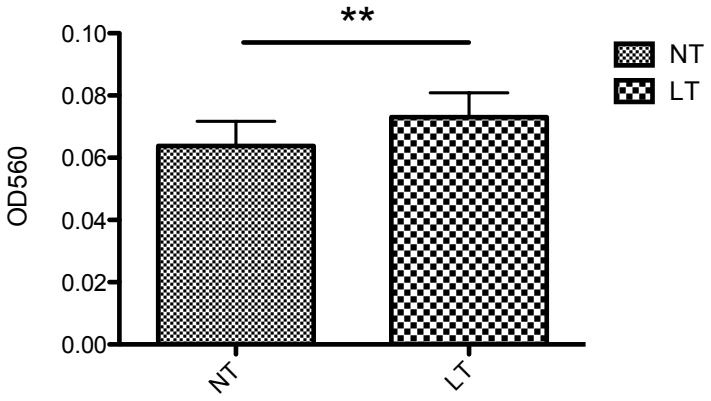

Figure 27. Graph representing the Total Oxidant Status levels in treated (LT) and non treated (NT) PAO suspensions. Data are shown as mean ±SD. ** Mann-Whitney U-test p<0,001

2.3 Evaluation of the antimicrobial effect adding an antioxidant compound

To further confirm the crucial role of oxidative stress generation in the mechanism of antimicrobial action of blue laser light, we repeated the survival experiment on planktonic bacteria using a protocol which has been effective before (wavelength 445nm, power 0,3W irradiance 0,18W/cm^2, fluence 120 J/cm^2, CW), with the addition of ascorbic acid as natural scavenger of reactive oxygen species. The results are shown in Figure 28.

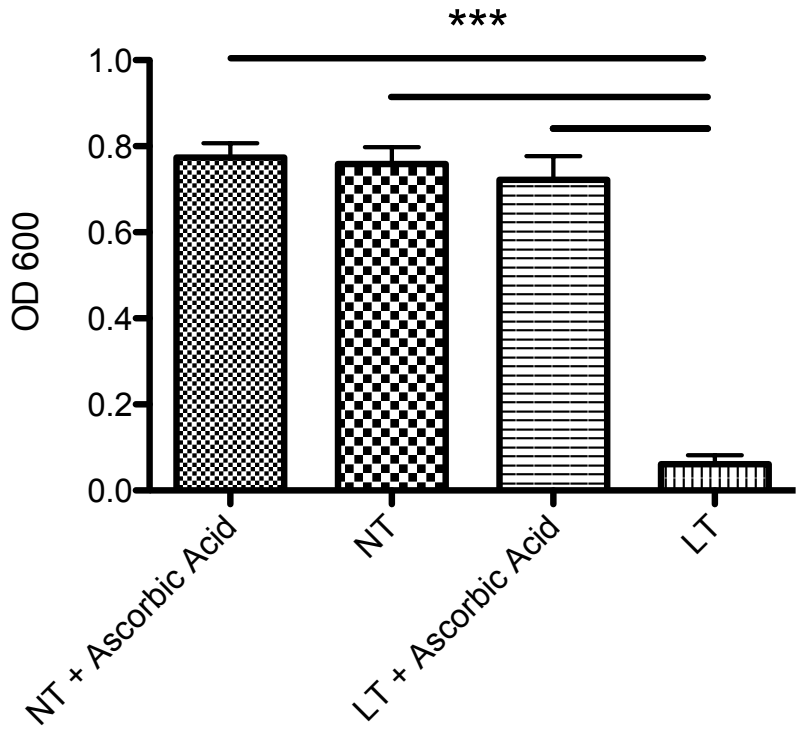

Figure 28. Graph representing bacterial survival and growth levels in treated (LT) and non treated (NT) PAO suspensions. Data are shown as mean ±SD. Kruskal-Wallis p<0,0001; ***Mann-Whitney all vs LT p<0,0001.

The addition of the potent ROS scavenger ascorbic acid with a 40μM concentration was able to rescue irradiated PAO from growth inhibition and death. In fact, it is clearly visible from the graphical representation that while irradiated PAO wells showed a complete eradication of bacteria 24h after treatment as expected, the bacteria inside the wells with ascorbic acid proliferated in the same way as the non treated ones.

2.4 Evaluation of the antimicrobial effect of blue LED light

To test whether another source of blue light could exert a similar antimicrobial activity, thus confirming a possible photochemical effect rather than photothermal, a planktonic growth curve assay has been performed using a blue LED light source providing 380-490nm light. Due to technical limitations in the LED light source used, we limited the analysis to two powers and irradiances (0,3W with 0,18W/cm^2 and 0,5W with 0,3W/cm^2) and two fluencies (60J/cm^2 and 120J/cm^2) and we compared the results with those obtained using blue laser as described in Paragraph 1 of this Chapter. The results regarding fluence 60J/cm^2 are described in Table 6 and Figure 29.

Table 6. T0-24 representent time points (hours) after irradiation. Values represent OD_{600} of bacterial suspensions. NT non treated. *** Mann-Whitney U test vs. NT p<0,0001; * Mann-Whitney U Test vs NT p<0,01.

LED 60J/cm^2	**0,3W**	**0,5W**	**NT**
T0	0	0	0
T6	0	0	0
T12	0,016*	0,04*	0,115
T18	0,032*	0,06*	0,551
T24	0,106*	0,097*	0,553
p-value (Friedman)	**p=0,019**	**NS**	**<0,0001**

LASER 60J/cm^2	**0,3W**	**0,5W**	**NT**
T0	0	0	0
T6	0	0	0,006
T12	0***	0***	0,177
T18	0***	0***	0,288
T24	0***	0***	0,288
p-value (Friedman)	**NS**	**NS**	**<0,0001**

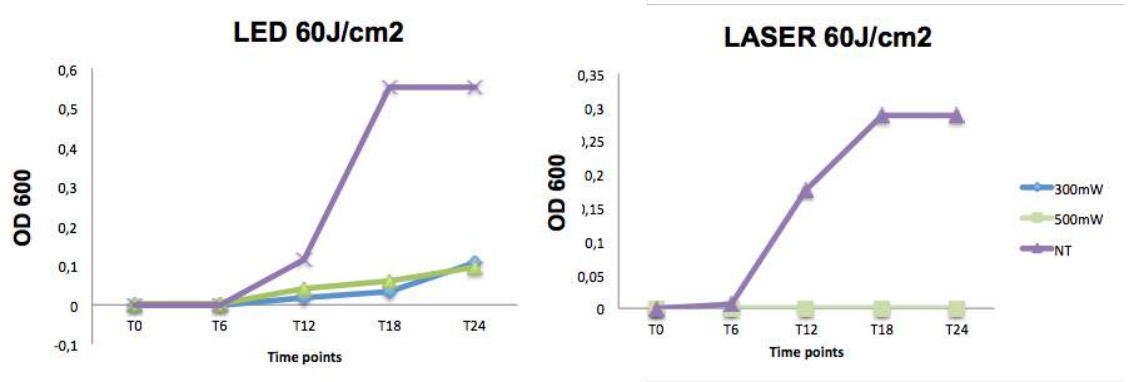

Figure 29. Graphs summarizing the results of 60J/cm^2 LED and laser protocols.

Both blue LED light protocols employed with 60J/cm^2 fluence have shown to be able to partially inhibit bacterial growth, considering that at T12, T18 and T24 (12, 18 and 24 hours after irradiation) there is a significant difference between every protocol and non treated wells (p<0,01). There is, however, a significant increase in well torbidity over time (Friedman test p=0,019) in the group treated with 0,3W power, meaning that there wasn't a complete eradication of bacteria. In the group treated with 0,5W power there is also a slight increase in well torbidity over time, which was statistically not significant. Therefore, we can conclude that 60J/cm^2 blue LED light protocols were able to significantly decrease bacterial viability, but weren't enough effective in eradicating completely planktonic bacteria.

The results regarding fluence 120J/cm^2 are showed in Table 7 and Figure 30.

LED 120J/cm^2	**0,3W**	**0,5W**	**NT**
T0	0	0	0
T6	0	0	0
T12	0,004*	0,004*	0,115
T18	0,002*	0,002*	0,551
T24	0,002*	0,002*	0,553
p-value (Friedman)	**NS**	**NS**	**<0,0001**

LASER 120J/cm^2	**0,3W**	**0,5W**	**NT**
T0	0	0	0
T6	0	0	0,006
T12	0***	0***	0,177
T18	0***	0***	0,288
T24	0***	0***	0,288
p-value (Friedman)	**NS**	**NS**	**<0,0001**

Table 7. T0-24 represent time points (hours) after irradiation. Values represent OD_{600} of bacterial suspensions. NT non treated. *** Mann-Whitney U test vs. NT p<0,0001; * Mann-Whitney U Test vs NT p<0,01.

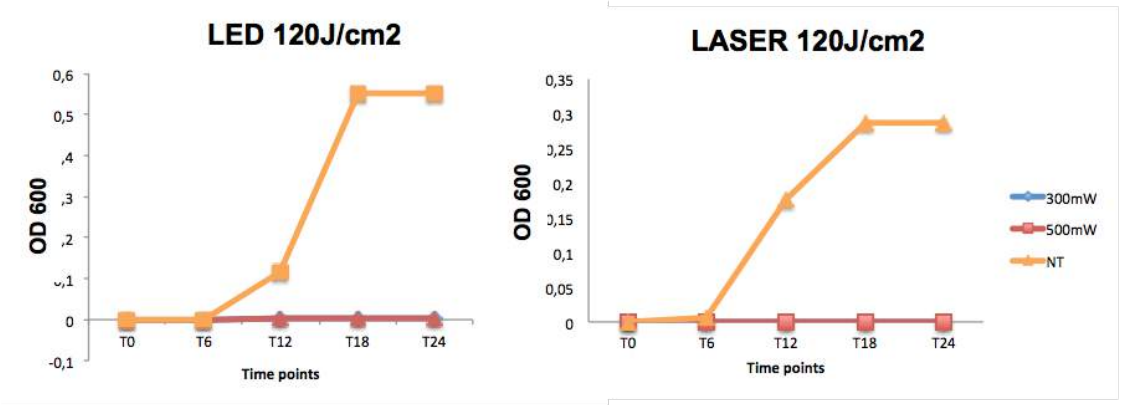

Figure 30. Graphs summarizing the results of 120J/cm^2 LED and laser protocols.

Both blue LED light protocols employed with 120J/cm^2 fluence were able to elicit an effective antimicrobial activity showing an inhibition of bacterial growth over time (Friedman for differences in bacterial growth over time non significant for all tested protocols, while non treated increased significantly with p<0,0001). The employed protocols maintained bacterial inhibition up to 24 hours after irradiation, even if a slight increase in bacterial density can be noticed, but still significantly lower compared to non treated samples.

In addition, the effect of the same protocols in terms of power density and fluence between laser and LED sblue light sources have been compared. The results of statistical analysis are shown in Table 8.

LASER vs. LED	0,3W 60J/cm^2	0,5W 60J/cm^2	0,3W 120J/cm^2	0,5W 120J/cm^2
T0	**NS**	**NS**	**NS**	**NS**
T6	*	**NS**	**NS**	**NS**
T12	*	**NS**	**NS**	**NS**
T18	*	*	*	**NS**
T24	*	*	*	**NS**

Table 8. T0-24 represent time points (hours) after irradiation. * Mann-Whitney U test LT vs LED p<0,01. NS not significant.

The results show that despite the fact that all blue LED protocols were able to inhibit PAO growth over time when compared to non treated samples, their effectiveness was significantly lower compared to the blue laser light. Specifically, the less effective protocol was power 0,3W, irradiance 0,18W/cm^2 and fluence 60J/cm^2, where bacterial density becomes significantly higher in the LED group as soon as at T6. In the samples where the protocols with LED light, power 0,5W, irradiance 0,3W/cm^2, fluence 60J/cm^2 and power 0,3W, irradiance 0,18W/cm^2, fluence 120J/cm^2 have been employed, inhibition of bacterial growth became significantly lower compared to laser light at T18. The only LED protocol which proved to be as effective as the laser one was the one using power 0,5W, irradiance 0,3W/cm^2, fluence 120J/cm^2.

2.5 Irradiation of a mutant library of PAO

To confirm at molecular level the antimicrobial mechanism of action of blue laser light possibly identifying one or a pool of candidate genes encoding for proteins responsible for bacterial susceptibility to blue laser light, we performed the screening of a gene mutant library of PAO. The plates carrying the mutants have been irradiated in a standardized manner using a protocol that has shown antimicrobial activity in previous experiments (power 0,5W irradiance 0,3W/cm^2 fluence 120J/cm^2). After irradiation, the plates were incubated at 37°C and checked after 24 hours for the growth of single colonies in the irradiated areas. After several cycles of irradiation, unfortunately we haven't found any resistant mutant. Figure 31 is showing an example of the irradiated plates where the central area area of complete inhibition of bacterial growth corresponding to the irradiated area is surrounded by proliferating colonies.

Figure 31. Picture showing agar plates used for the random mutant library screening.

3. Safety/Toxicity of blue light irradiation on eukaryotic cell lines

In the experiments performed and described so far we have demonstrated the antimicrobial efficacy of blue laser irradiation on PAO grown on solid surfaces, in planktonic state and in mature biofilms, which would make it a promising approach for wound infections treatment. Since several protocols proved to be effective, before applying this approach *in vivo* it has been of crucial importance to perform different experiments on eukaryotic cell lines to verify whether the same protocols could elicit cytotoxic effects and eventually select one or more protocols to be employed in a mouse model of wound infection.

It is known from literature that blue light has very low penetrability across the skin/mucosa as its effects are limited to the most superficial epidermidal layers. Therefore, we decided to explore its effects on keratinocytes derived from both oral mucosa and skin, as the principal possible application of such approach would be the treatment of skin/mucosa infections. Specifically, human oral mucosa keratinocytes (TR146, model of oral buccal epithelium derived from well-differentiated keratinizing squamous cell carcinoma) and human skin keratinocytes (HaCaT, model of human skin derived from spontaneously transformed aneuploid immortal keratinocyte cell line) have been employed.

3.1 Cell viability and metabolism assays

a. Cell viability assays

The MTT assay has been employed to evaluate cell viability 24h after irradiation with different blue laser protocols. The results regarding the TR146 cell line are showed in Figure 32. It is noticeable that cell viability tends to increase compared to non treated samples at low fluence ($30J/cm^2$) and slightly decrease with the rising of fluence for each power. However, the differences were not significant (Kruskal-Wallis NS, Mann-Whitney U test every treatment protocol versus NT samples NS).

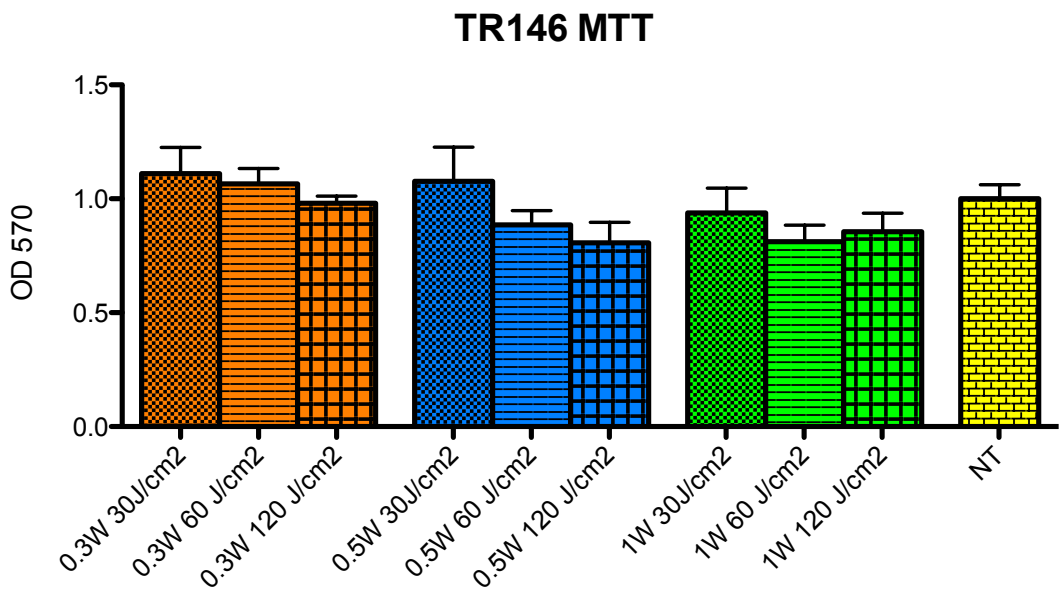

Figure 32. Graph representing cell viability 24h after blue laser irradiation performed using different protocols in terms of fluence, irradiance and power. Data are shown as mean ±SD. Kruskal-Wallis NS.

The results regarding the HaCaT cell line are showed in Figure 33. It is clear how this cell line was more sensitive to blue laser irradiation. The reason may be that the TR146 cell line is neoplastic and therefore more resistant.

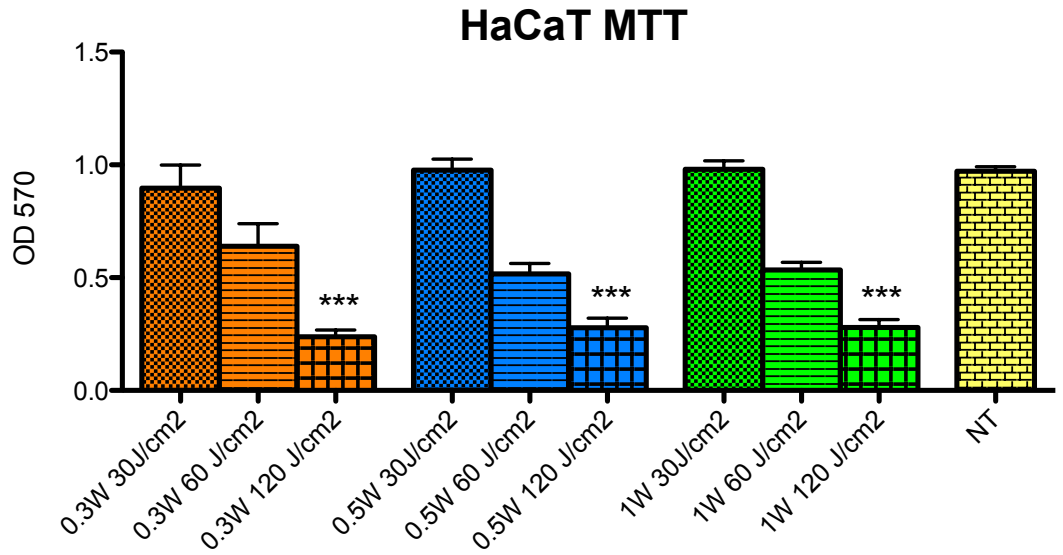

Figure 33. Graph representing cell viability 24h after blue laser irradiation performed using different protocols in terms of fluence and power. Data are shown as mean ±SD. Kruskal-Wallis p<0,0001. ***Dunn's Multiple Comparison Test vs. NT p<0,0001.

Also in this case as the fluence rises, cell viability decreases regardless of power and irradiance. With 30J/cm^2 fluence, cell viability wasn't affected at all. With 60J/cm^2 fluence, the proportion of viable cells decreased (especially for powers 0,5W and 1W), but the differences were not significant compared to non treated samples. For all power densities, cell viability was significantly lower with fluence 120J/cm^2 compared to non treated cells ($p<0,0001$).

Laser light can be provided in continuous wave (CW), as we performed throughout this study, but also in chopped mode with different possible frequencies. We evaluated the possible changes in cell viability in the TR146 cell line following blue laser irradiation with the protocol power 0,5W irradiance 0,175W/cm^2 fluence 40J/cm^2 with different frequencies and the results are represented in Figure 34. It is clear from the graphical representation and confirmed by the statistical analysis (Kruskal-Wallis NS) that changes in the frequency of irradiation did not affect cell viability at all.

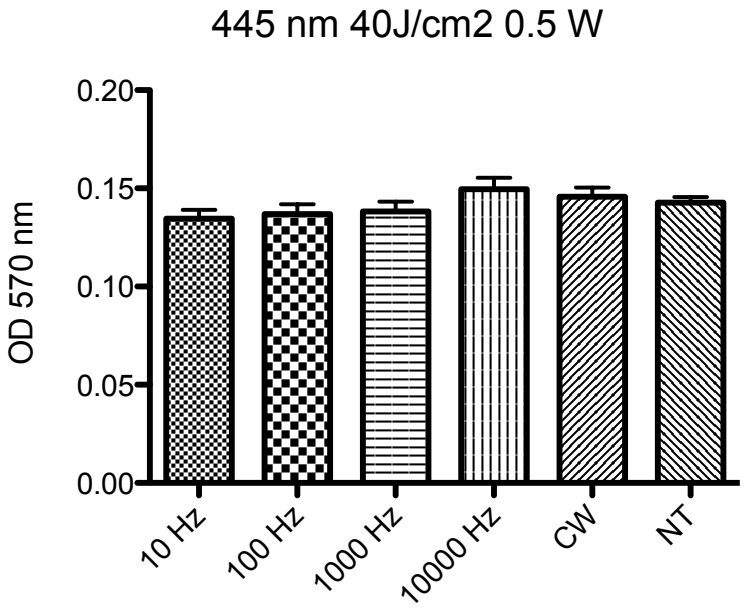

Figure 34. Graph representing cell viability 24h after blue laser irradiation performed using different frequencies with the same protocol in terms of power density and fluence. Data are shown as mean ±SD. Kruskal-Wallis NS.

b. Cell metabolism assays

Cell metabolic activity at different time points and following different blue laser protocols has been assessed through ATP production measurement using the ATPlite luciferase test.

Both TR146 and HaCaT cell lines have been irradiated using the blue laser protocol wavelength 445nm, power 0,5W, power density 0,3W/cm^2 and fluence 40J/cm^2. Results regarding the TR146 cell line are represented in Figure 35. ATP production remains similar to non treated cells 30min after irradiation, decreases significantly 2h later and finally increases significantly 6h after treatment.

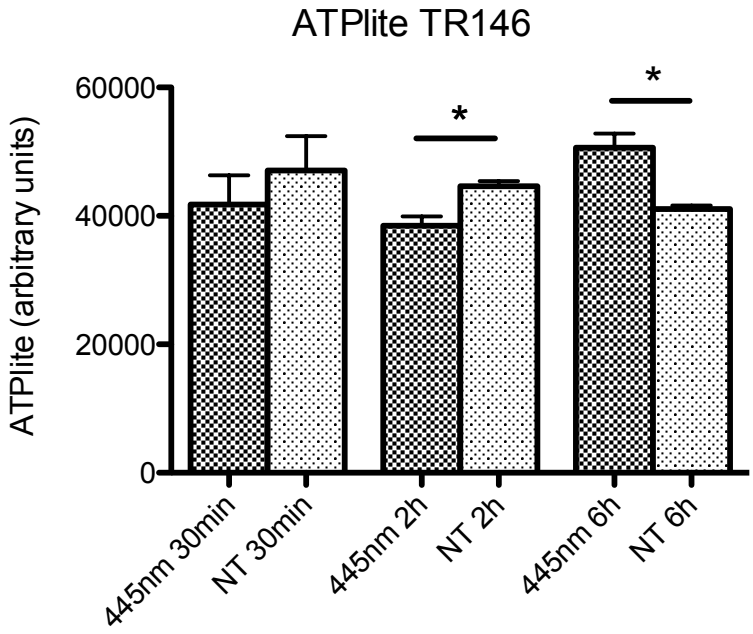

Figure 35. Graph showing ATP content in TR146 oral keratinocytes 30min, 2h and 6h after laser irradiation with the protocol 0,5W, 0,3W/cm^2, 40J/cm^2. NT non treated. * Mann-Whitney U test $p<0,05$.

Results regarding the HaCaT cell line are represented in Figure 36. ATP production remains similar to non treated cells at all time points, although in treated cells it seems slightly lower. However, the differences were statistically not significant.

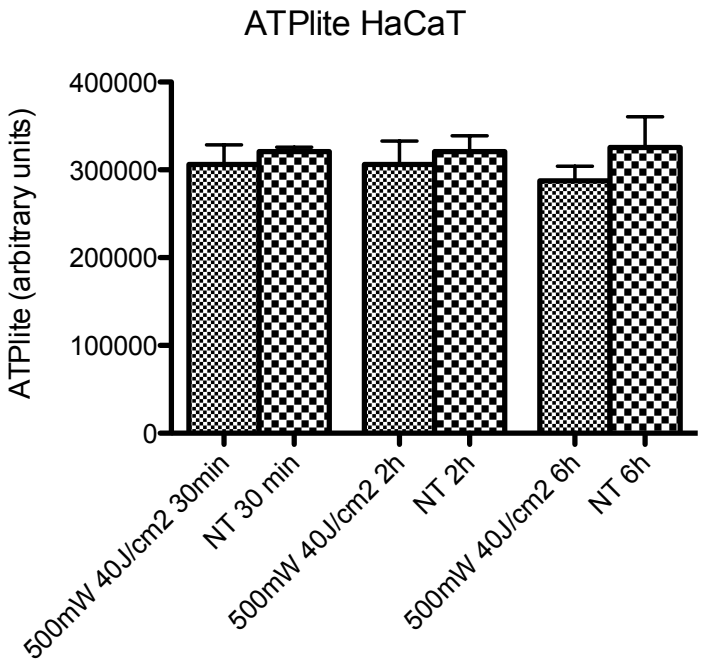

Figure 36. Graph showing ATP content in HaCaT skin keratinocytes 30min, 2h and 6h after laser irradiation with the protocol 0,5W, 0,3W/cm^2, 40J/cm^2. NT non treated. * Mann-Whitney U test p<0,05.

Furthermore, we tested the effect on cell metabolism activity of different bactericidal protocols of blue laser irradiation on the TR146 cell line 30 minutes and 24 hours after irradiation. To avoid possible interferences of laser light with growth medium, we performed the irradiations removing the medium shortly before, and adding fresh medium after treatment. At both time points, we didn't observe any significant differences compared to non treated samples (p>0.05 by Kruskal-Wallis test) as shown in Figure 37.

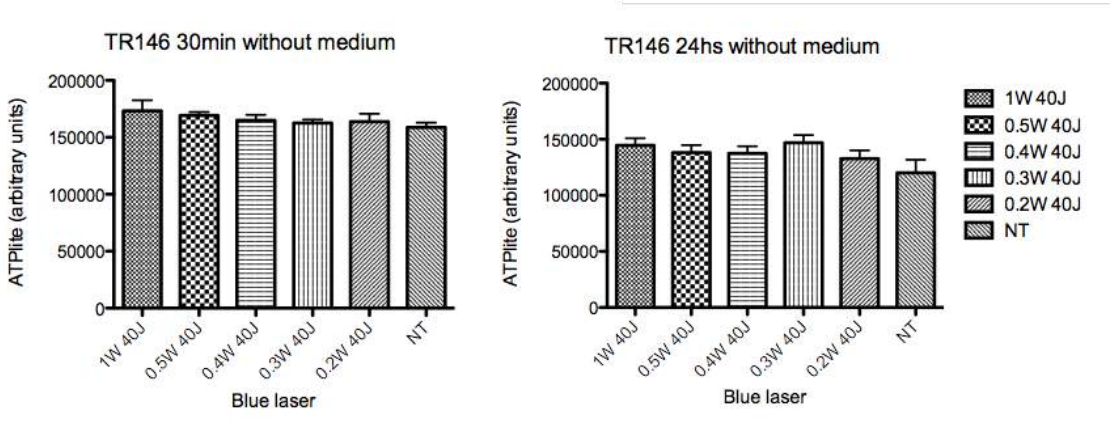

Figure 37. Graphs representing ATP content in TR146 cells 30 minutes and 24 hours after irradiation with different laser protocols removing growth medium.

c. Cell cycle analysis

We performed a cell cycle flow cytometry analysis on both cell types to evaluate possible changes in cell cycle phases distribution of the cells and to detect the proportion of apoptotic cells in the population. The cells were treated using the laser protocol wavelength 445nm power 0,5W irradiance 0,175W/cm^2 fluence 40J/cm^2 and processed 4 hours and 24 hours after laser treatment.

The results regarding the TR146 cell line are showed in Figure 38 and 39. 4 hours after irradiation, the distribution of the cells among the different phases of the cell cycle is homogenous, with slightly less cells in phase S in both groups (treated and non treated). In both groups, there is a very low presence of apoptotic cells, which are higher in the non treated group. There is a moderate number of multinucleate cells, which may represent cell aggregates formed during the analysis.

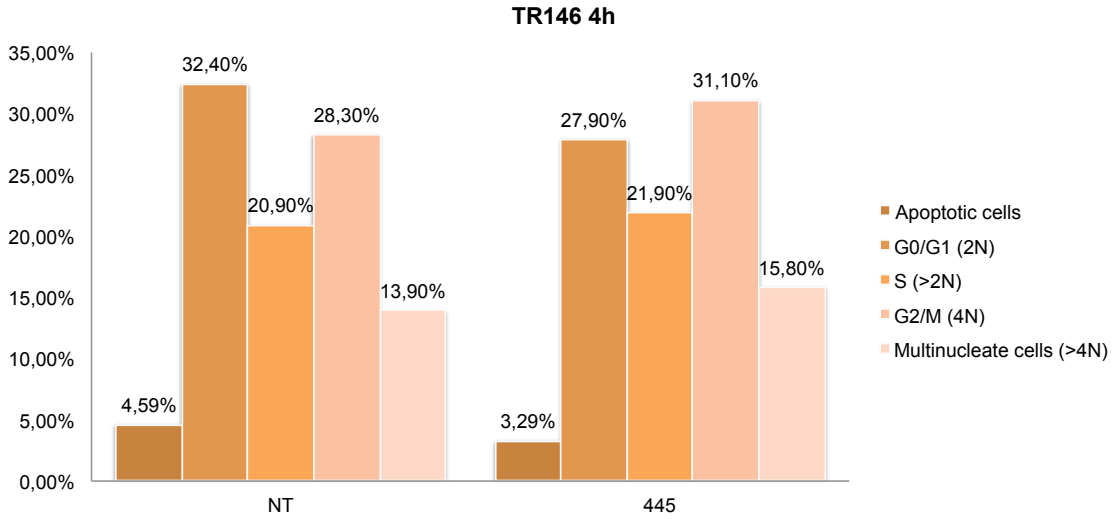

Figure 38. Graphical representation of the results of cell cycle phases distribution of TR146 cells 4 hours after laser treatment.

24 hours after treatment, there are more cells in G0/G1 phase compared to the other phases, which means that the cells are quiescent. There is a higher number of quiescent cells in the laser group compared to the non treated group. The number of apoptotic cells is higher than at 4 hours, but there are no differences between the two groups.

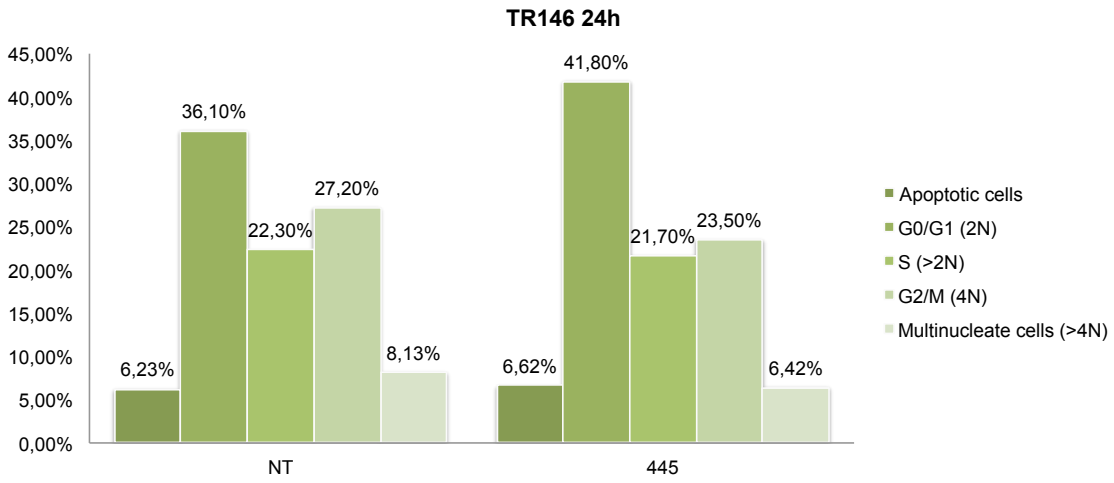

Figure 39. Graphical representation of the results of cell cycle phases distribution of TR146 cells 24 hours after laser treatment.

The results regarding the HaCaT cell line are showed in Figure 40 and 41. 4 hours after irradiation, the number of cells in each phase of the cell cycle (G0/G1, S, G2/M) is very similar in both groups. In both groups, there is a very low presence of apoptotic cells, which are higher in the non treated group as in the TR146 cell line. There is a moderate number of multinucleate cells, which may represent cell aggregates formed during the analysis.

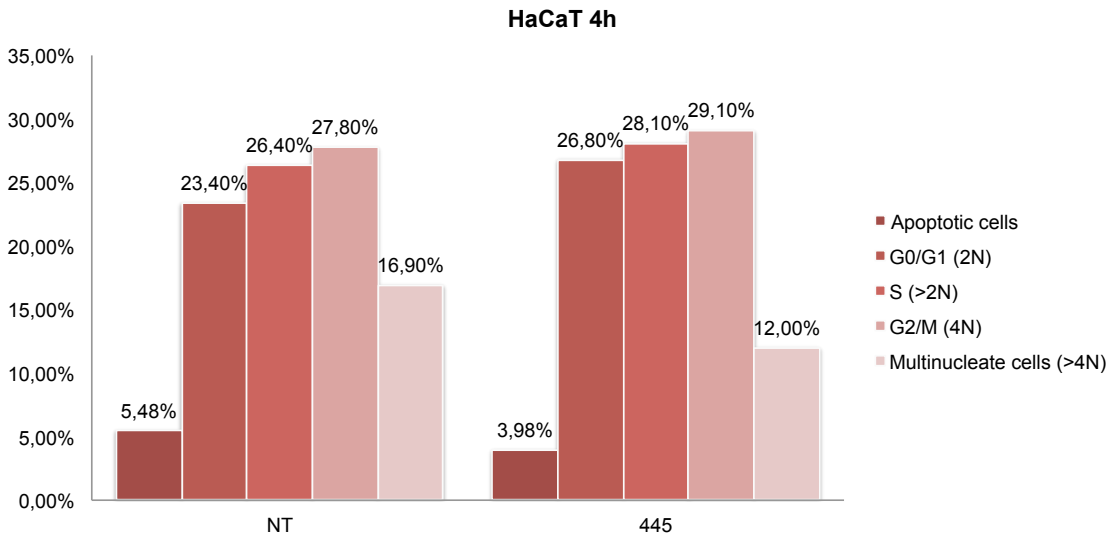

Figure 40. Graphical representation of the results of cell cycle phases distribution of HaCaT cells 4 hours after laser treatment.

24 hours after treatment, there are more cells in both G0/G1 and G2/M phase compared to the S phase. The number of apoptotic cells is lower than at 4 hours, but there are no differences between the two groups. The distribution of cells in the different phases is very similar in the treated and non treated group.

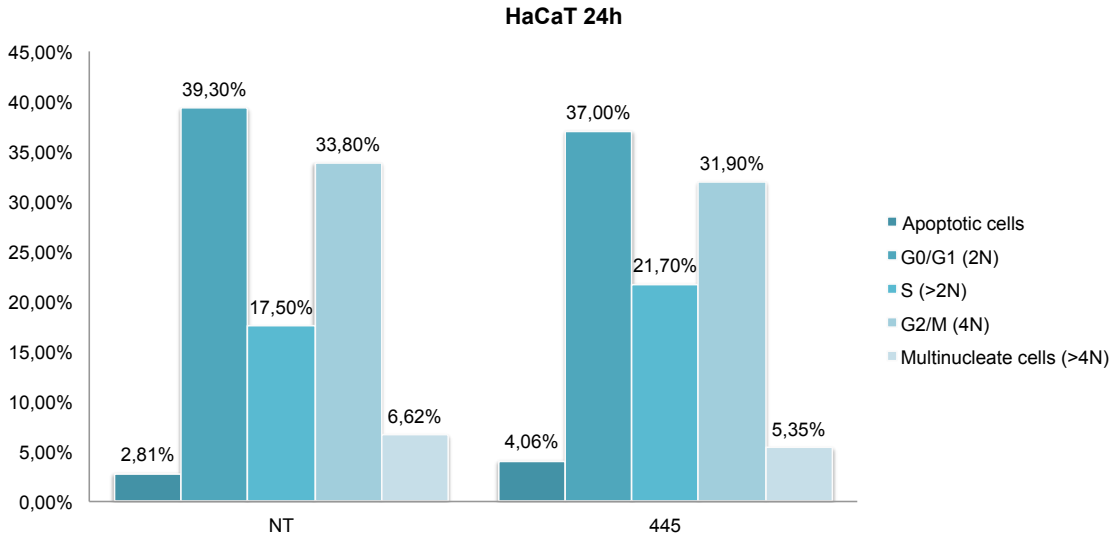

Figure 41. Graphical representation of the results of cell cycle phases distribution of HaCaT cells 24 hours after laser treatment.

d. Mitochondrial transmembrane potential

Cell damage leading to apoptosis is accompanied also by alterations of mitochondrial membrane potential (Δψm), which can be assessed using fluorescent probes in living cells such as JC-1. We measured the possible changes in the healthy/poor health mitochondria ratio expressed as red/green fluorescence intensity ratio measured in flow citometry following laser irradiation with the blue laser protocol wavelength 445nm power 0,5W irradiance 0,175W/cm^2 fluence 40J/cm^2 of TR146 oral keratinocytes.

The results are showed in Figure 42. The ratio between healthy and non healthy mitochondria resulted to be very similar in both groups (Mann-Whitney U-test), although the mean value is slightly higher in the laser treated group.

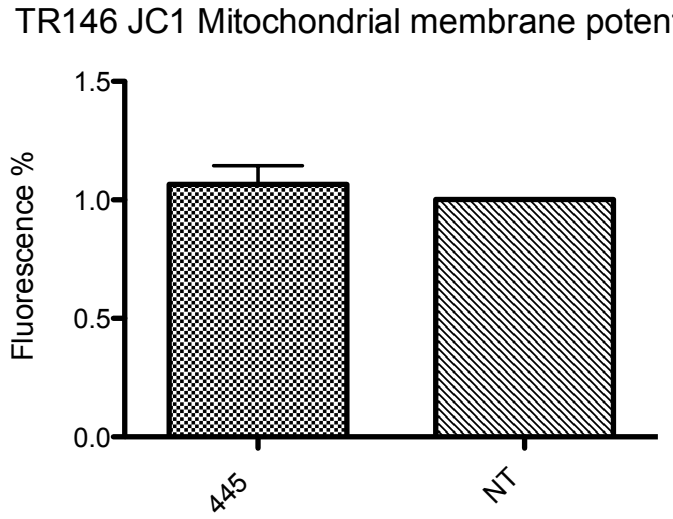

Figure 42. Healthy/poor health mitocondria in laser treated and non treated TR146 cells.

3.2 Gene expression analysis

In this experiment we evaluated the changes in the expression of proteins involved in inflammation and innate immunity mechanisms 30 minutes and 6 hours after laser treatment using the protocol wavelength 445nm power 0,5W irradiance 0,175W/cm^2 fluence 40J/cm^2. Inflammosome molecules include Caspase 1, Interleukin-1b and NLRP3 and are known to be overexpressed after cell damage induced by ultra-violet radiation (UVR) (Seo et al, 2001). Subsequently, the release of pro-inflammatory cytokines activate neighboring healthy cells to secrete antimicrobial peptides and support wound healing processes. For the latter ones we evaluated specifically three antimicrobial peptides (AMPs), known to be expressed at the oral mucosa surfaces: β-defensins 1, 3 and 4 (DEFb1, DEFb3, DEFb4); hBD-1 is constitutively expressed, while hBD-3 and hBD-4 are inducible by pro-inflammatory stimuli and bacteria.

The experiment has been performed on the HaCaT cell line, since TR146 is derived from an oral squamous cell carcinoma and is therefore not suitable for such experiments. Results regarding inflammasome complex gene expression are grouped in Figure 43, whereas those regarding antimicrobial peptides are shown in Figure 44.

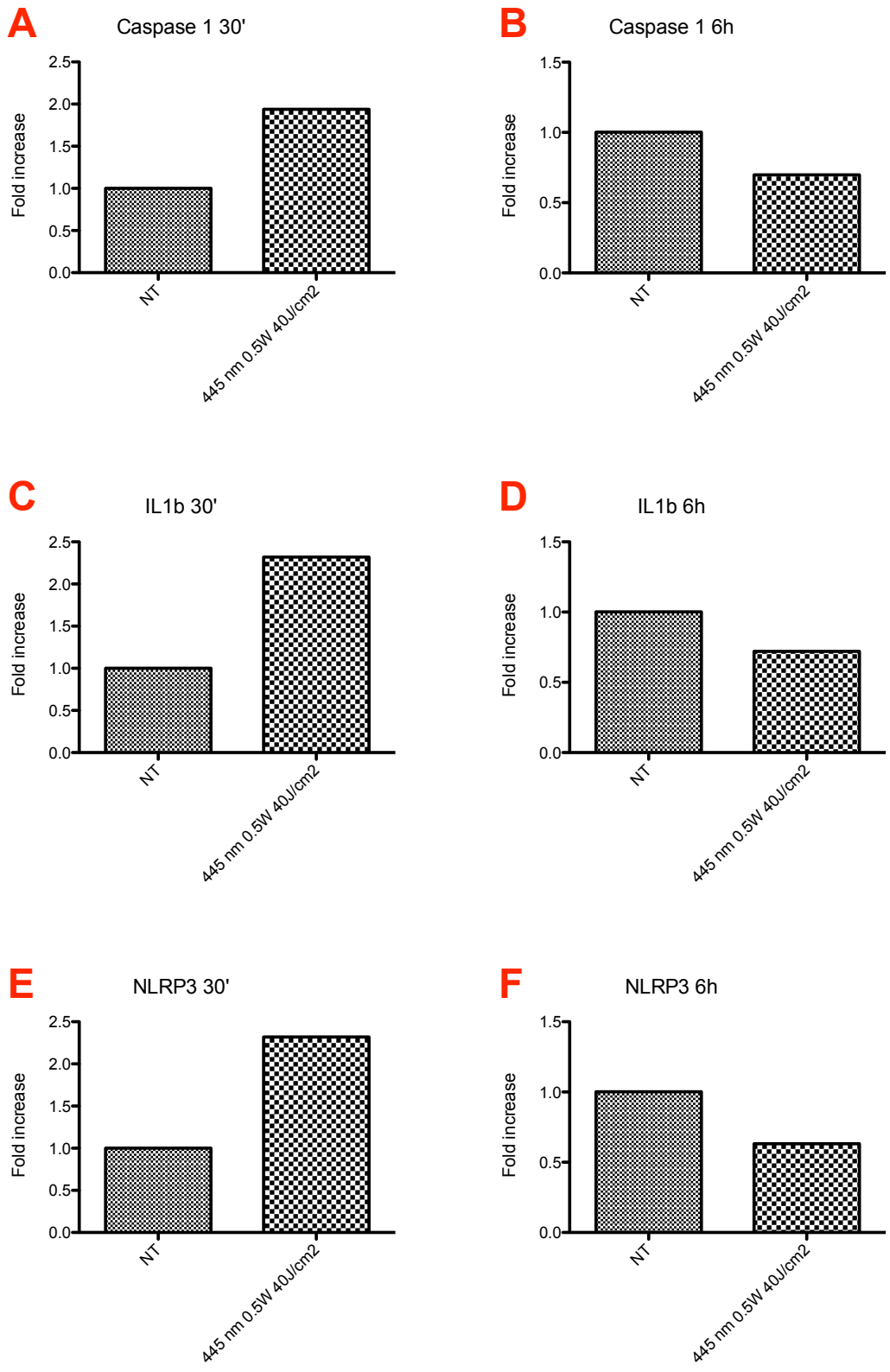

Figure 43. Expression of inflammasome molecules Caspase 1, Interleukin 1b and NLRP3 in HaCaT keratinocytes 30 minutes and 6 hours after laser treatment compared to non treated controls (NT). Results are expressed in mean fold increase compared to constitutive reference genes.

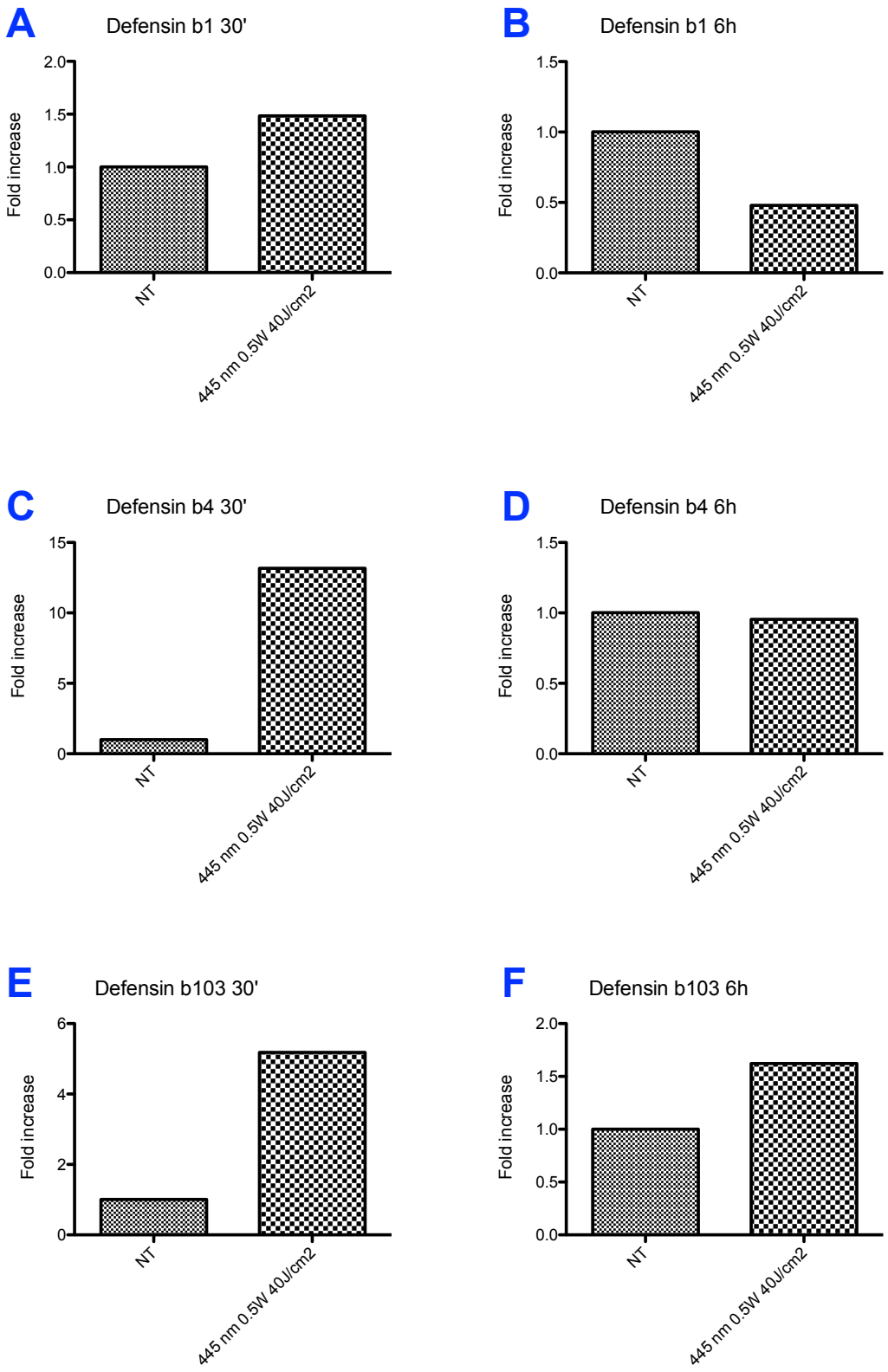

Figure 44. Expression of innate immunity molecules β-defensins 1, 3 and 4 in HaCaT keratinocytes 30 minutes and 6 hours after laser treatment compared to non treated controls (NT). Results are expressed in mean fold increase compared to constitutive reference genes.

The results show how 30 minutes after blue laser exposure all the inflammasome mediators evaluated were overexpressed compared to non treated cells. The treatment stimulates the inflammatory cascade in keratinocytes, which is consistent with data regarding the effect of UVR, the nearest to visible blue part of the electromagnetic radiation. However, after 6 hours the expression is not only normalized, but also suppressed compared to non treated cells. Blue laser irradiation performed with this protocol probably provokes a certain damage rate to eukaryotic cells, similarly to UVR, which appears to be repaired within hours as both cell metabolism and viability don't seem to be affected looking at the MTT and ATPlite results. Considering that higher fluences cause a dose-dependent depletion of viable keratinocytes, the selection of the irradiation protocol appears to be fundamental. In particular, IL1b expression seems to be crucial to induce many repair genes in keratinocytes in a time dependent manner indicating it may be promoting DNA repair enzyme activity after irradiation.

Defensin expression usually follows the inflammosome one, as inflammatory cytokines such as IL1b directly stimulate keratinocytes to release antimicrobial peptides. The results of our gene expression analysis are consistent with this mechanism, as the expression of all three defensins considered increases 30 minutes after blue laser exposure. It is of great interest the fact that especially Defensins b3 and b4 were overexpressed (respectively with 5,18 and 13,17 fold increase), considering that they are antimicrobial peptides active against a wide range of gram positive and gram negative bacteria including multiresistant bacteria. In particular, it has been demonstrated elsewhere that the antimicrobial activity of Defensin b4 is particularly effective towards PAO (Garcia et al, 2001).

4. Assessment of the antimicrobial effect on PAO in vivo in a mouse model of wound infection

Considering all the experiments described so far, we decided to validate the antimicrobial efficacy of blue laser light irradiation in vivo in a mouse model of PAO wound infection. Mice with skin abrasions were irradiated shortly after infection with a PAO suspension with the protocol wavelength 445nm power 0,3W irradiance 0,105W/cm^2 fluence 60J/cm^2. After 24 hours, both treated and non treated mice were sacrificed and a skin specimen was obtained. Half of the specimen was used to evaluate residual bacterial load, and the other half underwent histological evaluation.

4.1 Bacterial load

Bacterial load was measured for every sample by CFU counting after inoculation on LB agar plates. Examples of colony counts performed using the ImageJ software are shown in Figure 45.

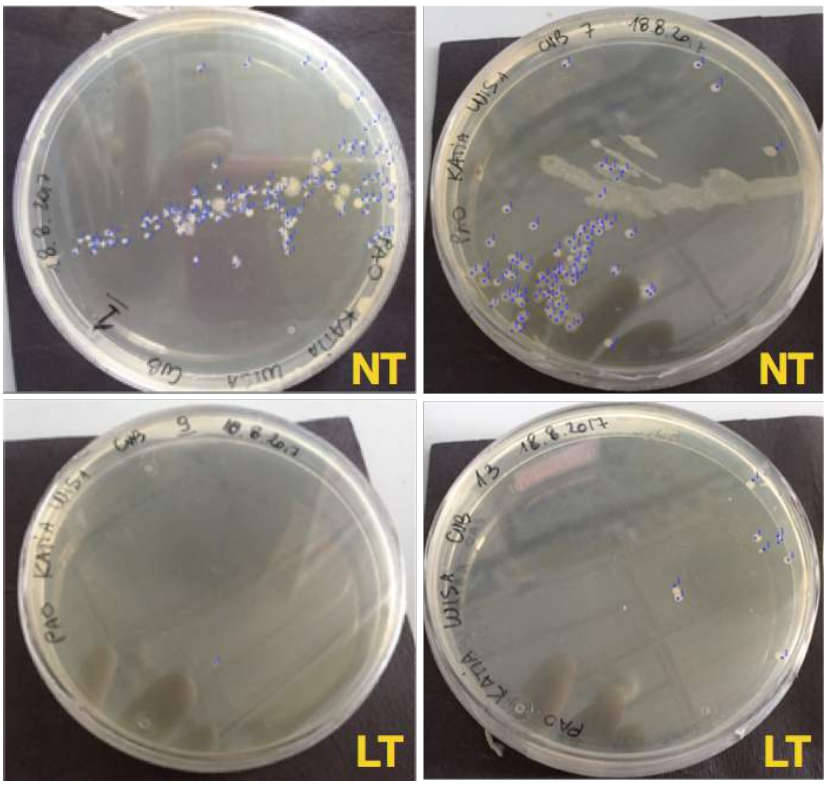

Figure 45. Examples of CFU counts from treated (LT) and non treated (NT) samples.

Figure 46 represents results regarding bacterial load in every sample expressed in CFU/ml. All laser treated samples remained below 3000 CFU/ml, but only in one case (LT3) we obtained a complete eradication of PAO. In non treated samples, the results were heterogeneous but always higher than 2000 CFU/ml.

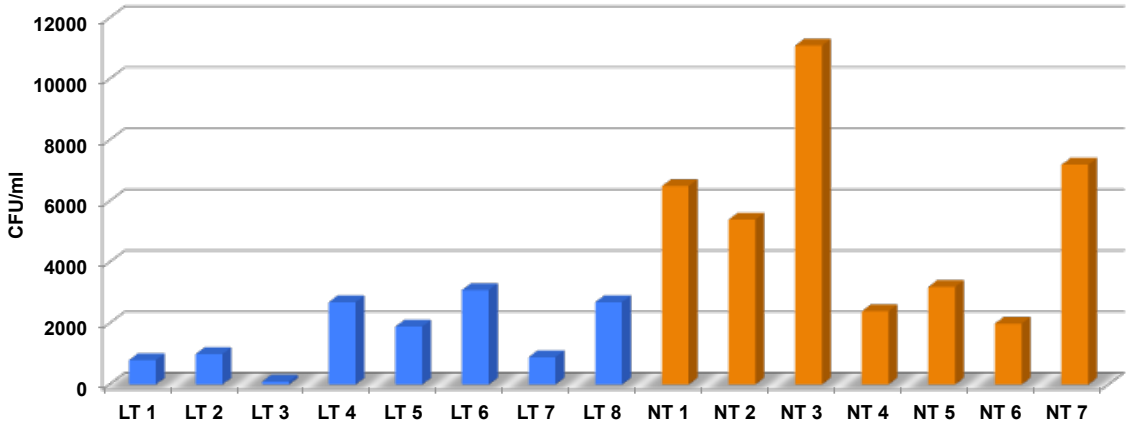

Figure 46. CFU/ml in every animal 24 hours after infection. LT laser treated, NT non treated.

Statistical analysis showed how the mean CFU/ml count in treated animals (16,5 CFU) was significantly lower than in non treated animals (54 CFU) with p=0,0128 as represented in Figure 47.

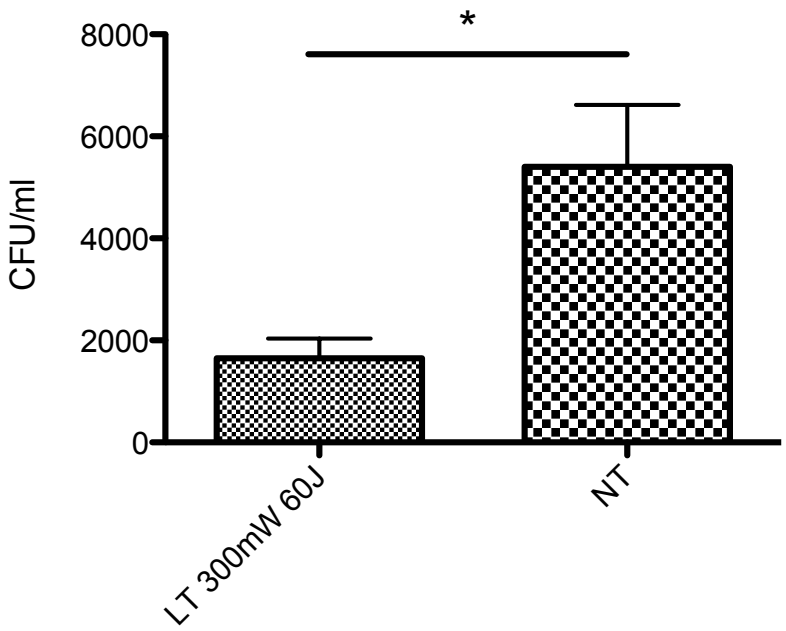

Figure 47. Graph representing PAO CFU/ml in laser treated and non treated animals. * Mann-Whitney U test p=0,0128.

4.2 Histological evaluation

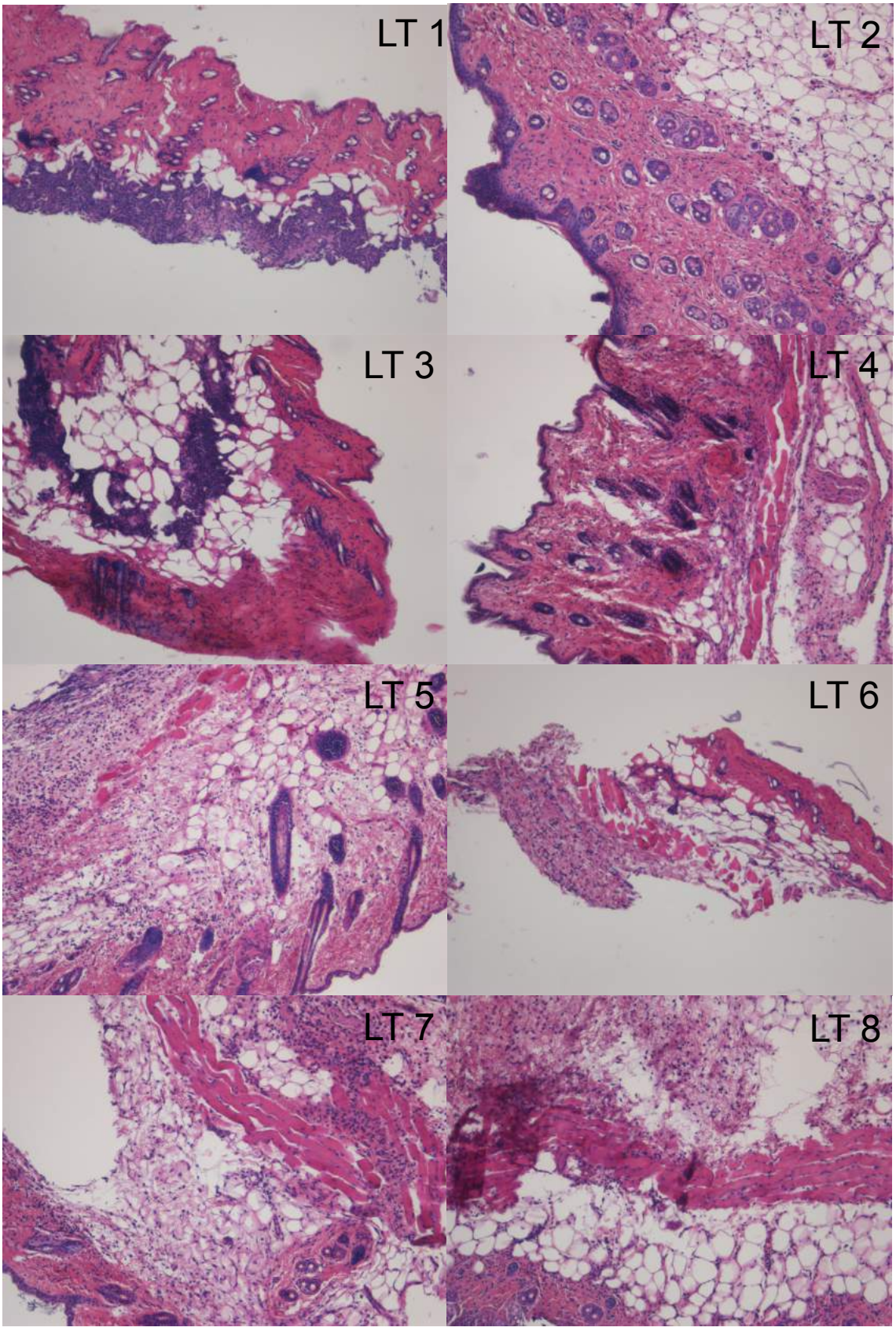

Figure 48. Epidermal, dermal and muscolar tissues stained with hematoxylin and eosin in laser treated animals. (10x magnification)

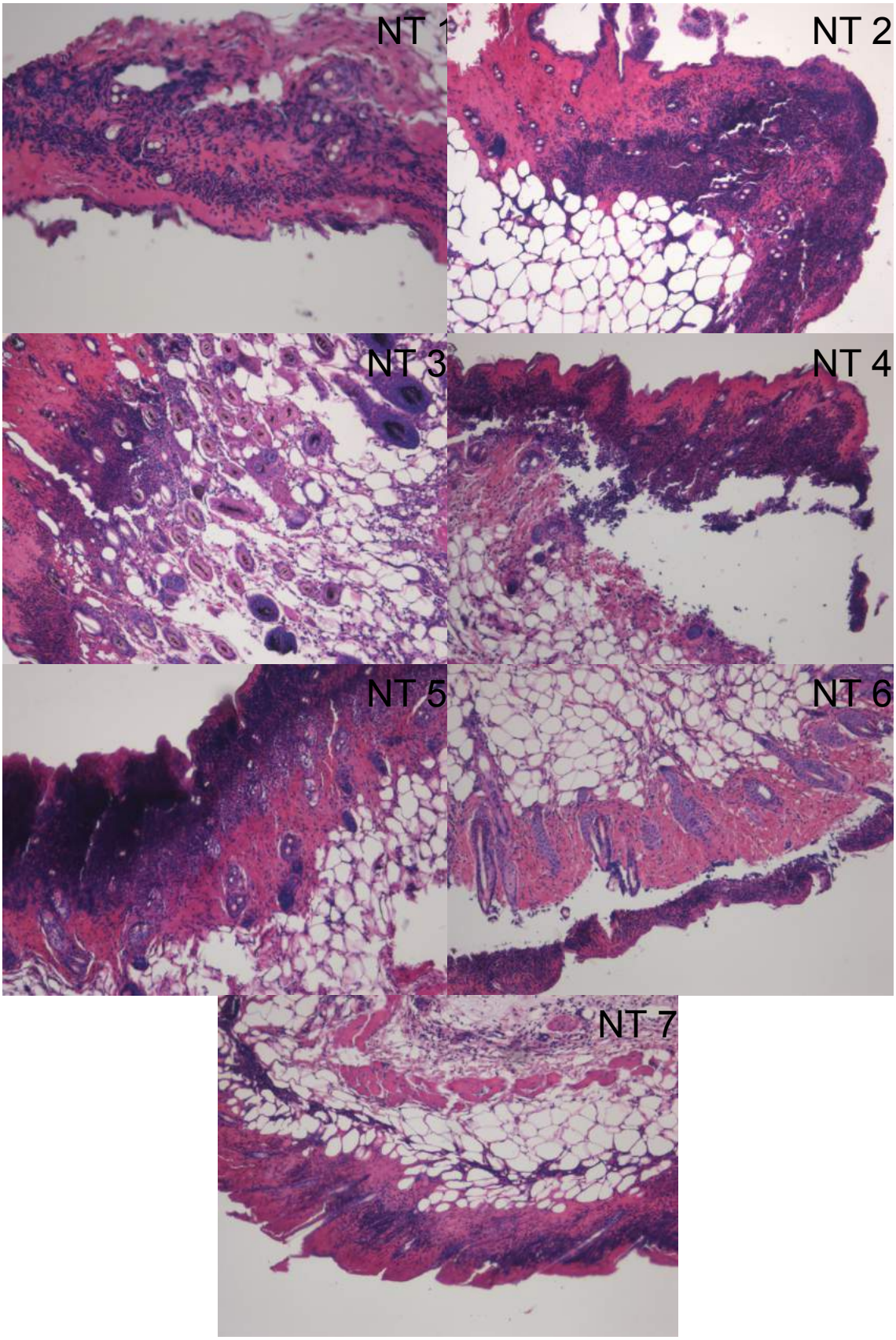

Figure 49. Epidermal, dermal and muscolar tissues stained with hematoxylin and eosin in non treated animals. (10x magnification)

Histological evaluation of the harvested skin samples was performed with the collaboration of an expert pathologist. The maximum depth of visible thermal damage in every sample treated with blue laser was measured and the results are reported in Table 9.

	LT 1	LT 2	LT 3	LT 4	LT 5	LT 6	LT 7	LT 8	**Mean**
pth (µm)	28,6	0	40,9	117,8	0	0	0	0	**23,4±41,4**

Table 9. Maximum depth of thermal damage in every laser treated (LT) sample.

Thermal damage was detectable only in three samples (LT1, LT3 and LT4) and it remained always in the external half of the epithelium layer. Epithelium thickness is reduced in all samples, which is consistent with the abrasions. In samples LT1 and LT3, there is a visible purulent inflammatory infiltrate/abscess probably generated by PAO infiltrating the dermal layer. Since blue laser light effect is superficial, it is plausible that the treatment failed to reduce the infection in the more profound layers. In the other treated samples, there is a modest inflammatory infiltrate throughout epidermal, dermal and ipodermal layers.

In all non treated samples, the epidermal layer is visibly and importantly permeated by inflammatory infiltrate. In sample NT1, inflammation is extended to the muscle. In samples NT2-NT7, inflammation is extended to the ipodermal layer. In all non treated samples, inflammation rate is higher than in laser treated ones, which was the opposite than we expected since the scope of this experiment was principally to evaluate possible thermal damages on laser treated infected abrasions.

5. Photodynamic therapy (PDT) using amphiphilic nanomicells loaded with curcumin activated by sublethal blue laser irradiation

A sub-lethal blue laser protocol has been used in a photodynamic therapy experiment on three types of nanomicelles loaded with curcumin and free curcumin.

5.1 Preparation of the nanomicelles

Nanomicelles were prepared as described in the Materials and methods part. Solutions with DAPMA, SPD and SPM nanomicelles carrying different concentrations of curcumin were obtained following dilutions of DAPMA, SPD and SPM suspensions with known amount of encapsulated curcumin.

5.2 PAO irradiation

Table 10 reports the significance of the difference in OD_{600} between each treatment versus Non treated (NT) and Laser treated (LT) bacteria. Results of PAO growth after 24 hours of incubation with free curcumin at different concentrations and curcumin nanomicelles are showed in Figure 49 (free curcumin), Figure 50 (DAPMA nanomicelles), Figure 51 (SPD nanomicelles) and Figure 52 (SPM nanomicelles). For every type of treatment, 4 samples were treated with blue laser light with the protocol wavelength 445nm, power 0,2W irradiance 0,1W/cm^2, fluence 6J/cm^2 and 4 were not. Bacterial growth after 24 hours was evaluated measuring of the wells at OD=600nm. An OD<0,1 was considered as evidence of PAO eradication/complete growth inhibition.

Bacterial growth for every treatment protocol, with and without laser irradiation, has been compared to non treated bacteria (NT) and to bacteria treated with laser only (LT). In addition, the results for every treatment without laser (-LT) have been compared to the same treatment with laser (+LT).

-LT	CUR 10µM	CUR 20µM	CUR 50µM	DAPMA blank	DAPMA 1µM	DAPMA 500nM	DAPMA 250nM
NT	NS	**	**	NS	**	**	NS
LT	NS	NS	**	*	**	**	**

-LT	DAPMA 100nM	DAPMA 50nM	SPD blank	SPD 1µM	SPD 500nM	SPD 250nM	SPD 100nM
NT	*	NS	NS	**	*	NS	NS
LT	NS	**	**	**	NS	**	**

-LT	SPD 50nM	SPM blank	SPM 1µM	SPM 500nM	SPM 250nM	SPM 100nM	SPM 50nM
NT	NS	*	**	**	**	NS	NS
LT	**	NS	**	**	**	*	NS

+LT	CUR 10µM	CUR 20µM	CUR 50µM	DAPMA blank	DAPMA 1µM	DAPMA 500nM	DAPMA 250nM
NT	**	**	**	**	**	**	**
LT	NS	*	**	NS	**	**	NS

+LT	DAPMA 100nM	DAPMA 50nM	SPD blank	SPD 1µM	SPD 500nM	SPD 250nM	SPD 100nM
NT	*	**	**	**	**	*	**
LT	NS	*	NS	**	NS	**	NS

+LT	SPD 50nM	SPM blank	SPM 1µM	SPM 500nM	SPM 250nM	SPM 100nM	SPM 50nM
NT	NS	**	**	**	**	*	*
LT	**	NS	**	**	**	*	*

Table 10. Significance of the difference in optical density/bacterial growth of each treatment versus Laser treated (LT) and non treated (NT). * Mann-Whitney U test p<0,05. ** Mann-Whitney U test p<0,001. NS Not significant. Red color means OD<0,1.

The laser protocol employed for this experiment proved to be non sublethal, as it reduced significantly bacterial growth compared to non treated bacteria (p=0,0002) without complete eradication. Looking at all treatments, bacterial growth was always lower in the laser treated ones (+LT). Nanomicelles without curcumin haven't shown any antimicrobial effect, so the antimicrobial effect was provided by curcumin itself, which exerted its toxicity once penetrated into microbial cells.

The only treatments that were able to completely eradicate planktonic PAO were DAPMA 1µM -LT, DAPMA 1µM +LT, DAPMA 500nM -LT, DAPMA 500nM +LT, SPD 1µM -LT, SPD 1µM +LT, SPM 1µM -LT, SPM 1µM +LT, SPM 500nM -LT, SPM 500nM +LT, SPM 250nM -LT, SPM 250nM +LT.

Figure 50 shows how free Curcumin wasn't able to completely eradicate bacteria in the suspension at any of the concentrations employed. Curcumin 50µM was the most effective treatment among free curcumin, reducing bacterial growth by half. Curcumin 10µM and 20µM +LT treatments were significantly more effective than –LT.

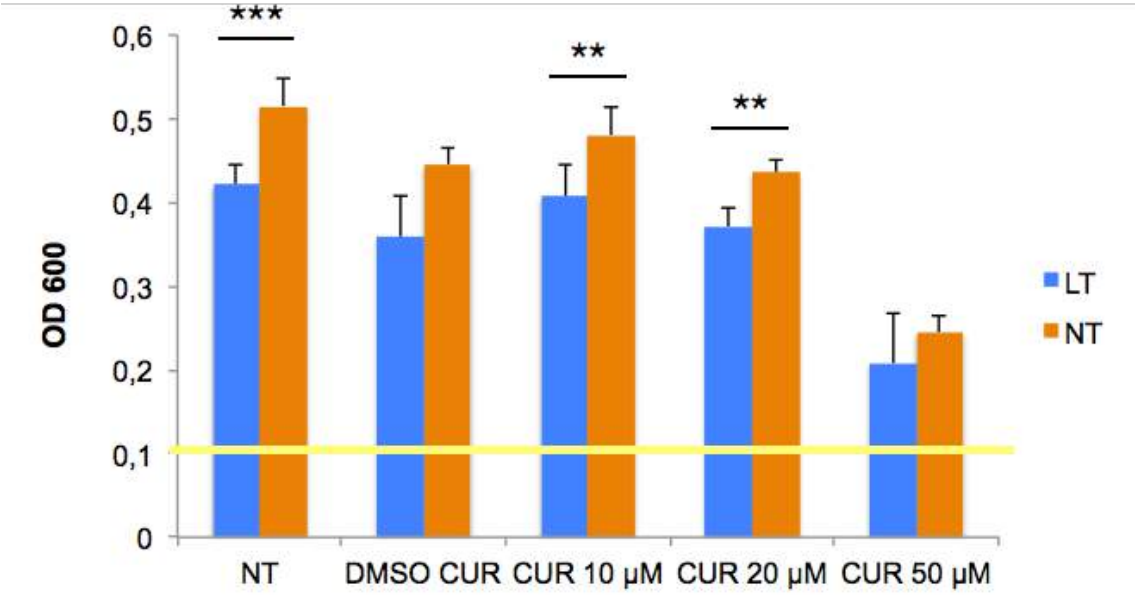

Figure 50. Graph showing mean±DS optical density after 24h of incubation with each treatment. Yellow line at OD=0,1 is considered limit for bacterial eradication. LT: with laser irradiation. NT: without laser irradiation. *** Mann-Whitney U test p<0,0001. ** Mann-Whitney U test p<0,001.

Looking at the results regarding the DAPMA nanomicelles embedding curcumin, they were able to eradicate PAO up to a 500nM concentration. Differences between +LT and -LT were significant only for DAPMA 50nM.

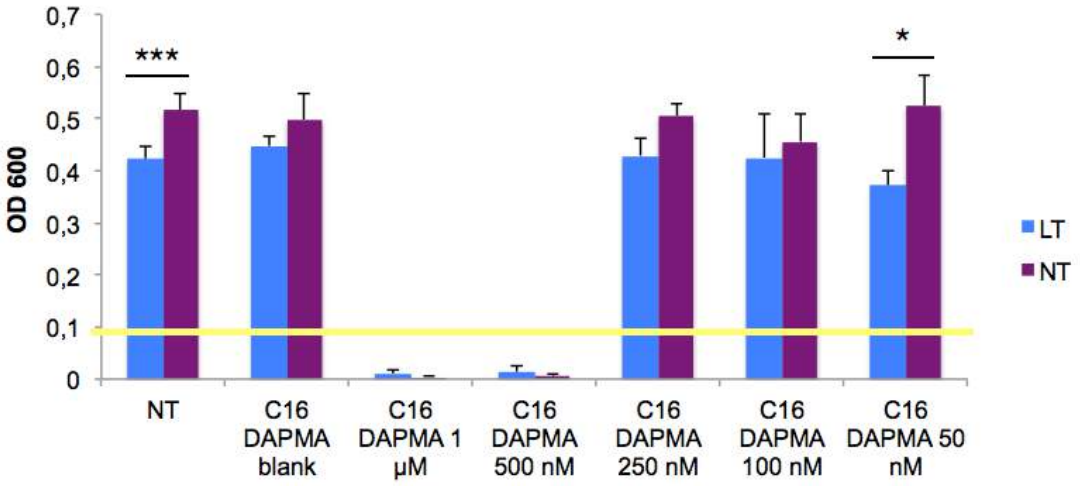

Figure 51. Graph showing mean±DS optical density after 24h of incubation with each treatment. Yellow line at OD=0,1 is considered limit for bacterial eradication. LT: with laser irradiation. NT: without laser irradiation. *** Mann-Whitney U test p<0,0001. * Mann-Whitney U test p<0,05.

The only SPD nanomicelles embedding curcumin concentration that cleared PAO from planktonic suspensions was 1µM. Differences between +LT and -LT were significant for SPD blank, SPD 250nM and SPD 100nM.

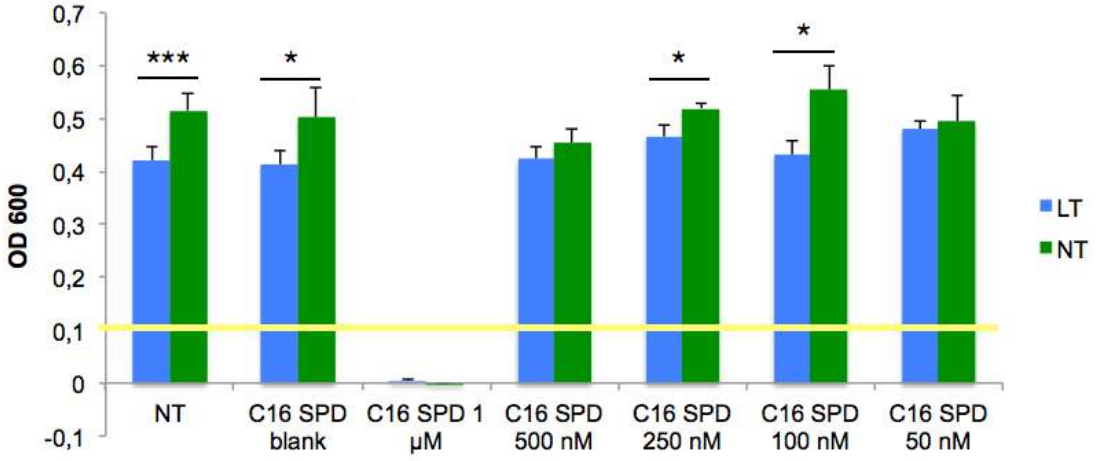

Figure 52. Graph showing mean±DS optical density after 24h of incubation with each treatment. Yellow line at OD=0,1 is considered limit for bacterial eradication. LT: with laser irradiation. NT: without laser irradiation. *** Mann-Whitney U test p<0,0001. * Mann-Whitney U test p<0,05.

SPM nanomicelles were the most effective, probably because of their major affinity with microbial membrane and capacity to delivery curcumin, which appears to exert its antimicrobial effects up to 250nM concentration. There were no differences between +LT and –LT among treatments.

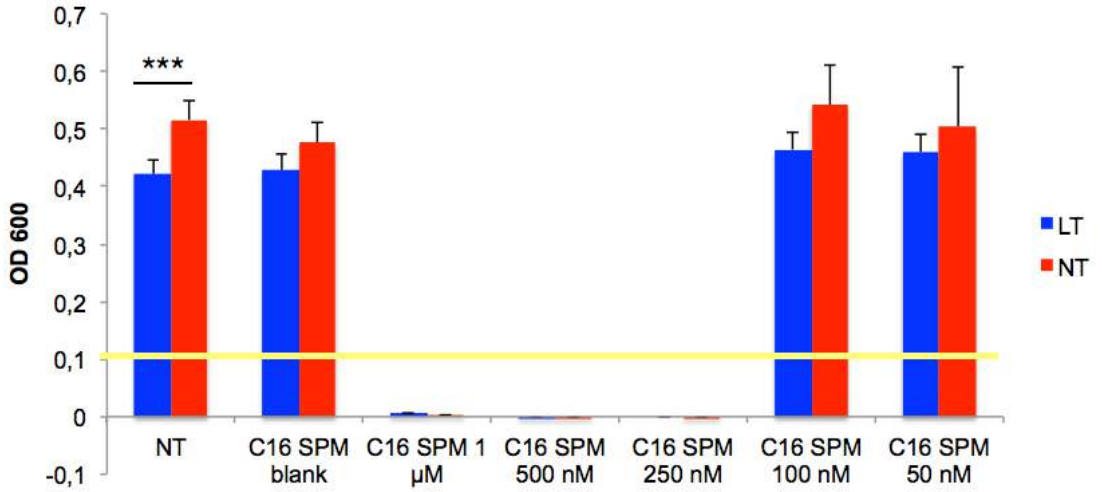

Figure 53. Graph showing mean±DS optical density after 24h of incubation with each treatment. Yellow line at OD=0,1 is considered limit for bacterial eradication. LT: with laser irradiation. NT: without laser irradiation. *** Mann-Whitney U test p<0,0001.

Despite bacterial growth was lower in the laser irradiated treatments (+LT), even if not always significantly, we haven't observed a true activation of curcumin to provide a difference in the final antimicrobial efficacy. For this means, we repeated the experiment chosing only SPM, which were the most effective nanomicelles. We evaluated a possible increase of the antimicrobial effect increasing the fluence in order to stimulate curcumin, using the protocols wavelength 445nm, power 0,2W, irradiance 0,1W/cm^2, fluence 18J/cm^2, and wavelength 445nm, power 0,2W, irradiance 0,1W/cm^2, fluence 30J/cm^2.

The results are reported in Figure 54. Higher fluences were able to stimulate more effectively curcumin in SPM nanomicelles, resulting in a complete inhibition of bacterial growth even at 50nM for both protocols (18J/cm^2 and 30J/cm^2).

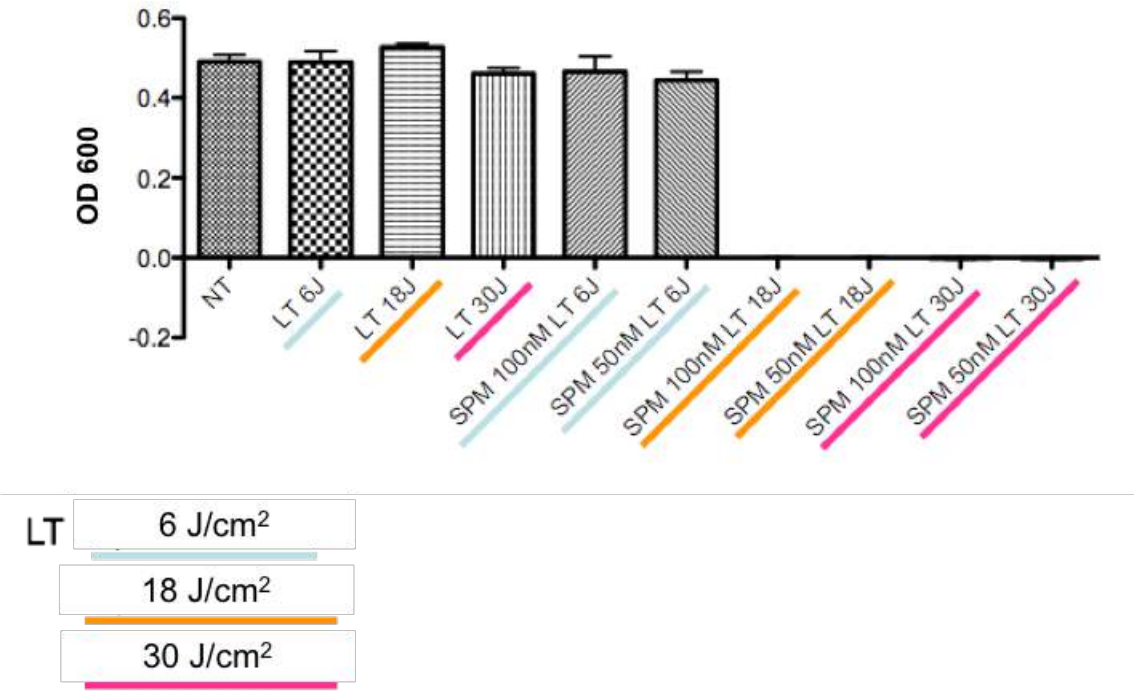

Figure 54. Graph showing mean±DS optical density after 24h of incubation with each treatment.

Discussion

The discovery of antibiotics in the first half of the 20th century was one of the most important advances in the history of medical science. Their use has reduced childhood mortality and increased life expectancy, and they are crucial for the success of invasive surgery and immuno-suppressive treatments such as chemotherapy. Unfortunately, shortly after the beginning of their widespread use, the onset of resistance has been recorded and since then a perpetual race in Achilles and tortoise style is being engaged between pathogen evolution and scientists in pharmacological field. While throughout the past century the development of novel antimicrobials was able to keep pace with pathogen adaptation, in recent years we are facing an increasing antibiotic resistance crisis, which is becoming a more and more important threat and burden for both patients and healthcare providers and the spectre of untreatable infections is becoming a reality. The 2014 World Economic Forum Global Risks reports have listed antibiotic resistance as one of the greatest threats to human health (WEF Global risk records, 2014). It is estimated that in Europe 25,000 people die each year as a result of multidrug-resistant bacterial infections and that this costs the European Union economy €1.5 billion annually (Walker et al, 2011).

The antibiotic resistance crisis has been ascribed to the overuse and misuse of these medications, as well as to a lack of new drug development by the pharmaceutical industry. According to the FDA Center for Drug Evaluation and Research, the number of new antibiotics developed and approved has decreased steadily over the past three decades, dropping from 19 in the 1980-84 interval to 3 in 2005-09 and 6 in 2010-14 (Bartlett et al, 2013).

It is clear that the development of novel antimicrobial strategies and approaches is already of crucial importance and great effort is being made by scientists worldwide to succesfully contribute to this field. Such strategies include the optimization of natural or synthetic antimicrobial paptides, photodynamic therapy, predatory bacteria, phages, gene editing enzymes and metals (Reardon et al, 2015).

Throughout this research work, we explored the possibility to use laser light with a particular wavelength, that is 445nm (visible blue), to exert direct antimicrobial activity without the addition of exogenous photosensitizing agents. The antimicrobial effect of blue light has been described in several studies, some of

them performed on *Pseudomonas aeruginosa* (PAO), on which we decided to focus also our study. PAO is the most common and difficult to eradicate pathogen colonizing the mucosa of cystic fibrosis patients, and causing lethal urinary tract, ear and skin infections in immuno-compromised humans.

We started to evaluate the survival of PAO over time performing planktonic growth curve experiments in planktonic suspensions after blue laser irradiation with increasing irradiances and fluences. Basing on our results, the minimum inhibitory blue laser protocol was power 0,3W irradiance 0,18W/cm^2 and 60J/cm^2 fluence. The same power and irradiance with lower fluence (40J/cm^2) was able to partially inhibit bacterial growth until 12 hours post-treatment, but then bacteria started to grow again and reached the same values in terms of well torbidity 24 hours post single treatment. Interestingly, when we increased the fluence to 60J/cm^2, higher powers and irradiances were less effective than lower. We have to consider that higher irradiances have to be applied for less time to reach the same fluence, following the formula F (fluence)= I (irradiance)*sec. When increasing irradiances were applied to reach fluence 120J/cm^2, all were effective and completely inhibited bacterial growth 24 hours after treatment except for the power 2W irradiance 1,040W/cm^2, which was the one applied for less time. We performed the same experiments applying identical power densities with the highest fluence (120J/cm^2) using red (660nm) and infrared (970nm) laser light, without obtaining any inhibition in bacterial growth compared to non treated bacteria.

Following these results, we can hypothesize that it is the time of irradiation with a specific wavelength (blue, 445nm) that interacts with bacteria and causes death/inhibition of growth.

When we employed similar powers and irradiances with 40J/cm^2 fluence on PAO grown on agar plates, we obtained complete inhibition of PAO growth. We also excluded a possible degradating effect on the Mueller-Hinton agar performing an irradiation of the plate before the inoculation of the bacteria, obtaining a uniform growth. Similarly as in the planktonic growth curve experiment, we evaluated also the effect of infrared (970nm) laser light, without noticing any antimicrobial effect.

The difference between the efficacy of laser protocols on PAO grown in different conditions may relay on the fact that blue light has very low penetration potential, so it is plausible that its effect is mostly superficial. Although blue light is transparent to water, it can be postulated that it undergoes a certain rate of diffraction in the bacterial suspension, needing higher fluences to fully exert its antimicrobial activity.

A similar effect has been described by Bumah et al, describing the dependence of the efficacy of antimicrobial effect of blue LED light on Meticillin Resistant *Staphylococcus aureus* on bacterial density. In fact, as the bacterial density increased, an irradiation from different sides of the culture was needed to reach all the layers (Bumah et al, 2013). In general, the results published in literature are not uniform, due to the different irradiation and treatment protocols described. Guffey and Wilborn performed an experiment evaluating the effect of increasing fluences using blue LED wavelengths (405nm and 470nm) on PAO grown on agar plates, and found a significant reduction in PAO growth at 5J/cm^2 with both wavelengths (Guffey et al, 2006). Rehab et al proved the antimicrobial effect of blue LED light on PAO suspensions, irradiating 40 µl with an irradiance 0,02W/cm^2 for 40 minutes up to 48 J/cm^2 (Amin et al, 2016). When PAO was treated in 96-well plates like in our study, the results were similar as Fila et al obtained complete PAO eradication at fluence 50J/cm^2 (Fila et al, 2017). Considering the results regarding red and infrared laser light, our results disagree with the ones obtained by De Sousa et al, where they obtained a significant inhibition of bacterial growth on agar plates after irradiating a bacterial suspension with diode laser 660nm at fluences of 18 and 24 J/cm^2 and 904nm at fluence 24 J/cm^2 (De Sousa et al, 2017).

One of the key factors in PAO resistance to both conventional antibiotics and components of the host immune system is the fact that, like most of pathogen bacteria, it grows in biofilms, which are complex communities of bacteria embedded in an extracellular matrix composed of proteins, extracellular DNA (eDNA), and exopolysaccharides. In addition, virulence factors are secreted, which inhibit and kill polymorphonuclear leukocytes letting the development of chronic infections, which persist despite apparently adequate antibiotic therapy (Høiby et al, 2015; Alhede et al, 2009; Van Gennip et al, 2009). Therefore, it is

mandatory to develop antimicrobial mechanisms that are able not only to kill bacteria in liquid suspensions or on solid surfaces, but above all to disrupt mature biofilms and/or to significantly inhibit biofilm formation.

Reproducing in laboratory a mature biofilm mimicking in vivo conditions isn't an easy task and may lead to inaccurate and non applicable conclusions. During the last decades, two major in vitro biofilm growth methods have been optimized and are considered the best up to date: microtitre plate assays and flow cells. However, we can still not define them as "gold standard" because of several issues which can not be solved at present time: unlike in vitro conditions, in vivo biofilms are often polymicrobial, grow in media that have different composition of nutrients basing on the anatomical district of formation, often do not grow on solid surfaces and the actual bacterial strains may be phenotipically very different from reference strains. In spite of these factors, in vitro models are still the best way to obtain crucial information for the understanding of biofilm dynamics and the development of novel disruption/inhibition strategies (Roberts et al, 2015).

We evaluated the effect of blue laser irradiation on both biofilm formation models. Firstable, we performed a screening of different protocols in microtitre-based high throughput screening experiments using Calgary biofilm devices and noticed how, in comparison with data from planktonic suspensions and agar plates, higher irradiances with lower fluences were necessary to disrupt the biofilm grown on the plastic pegs. In fact, power 0,4W iradiance 0,24W/cm^2 fluence 40J/cm^2 and power 0,5W irradiance 0,3W/cm^2 fluence 20J/cm^2 were the minimum inhibitory blue laser irradiation protocols. The results are similar to the only study (to our knowledge) investigating the effect of blue light on biofilm grown on Calgary devices: using a blue LED light on different PAO strains, Halstead et al obtained a significant antibiofilm effect with 54J/cm^2 fluence (Halstead et al, 2017).

This experiment allowed us also to select a sublethal laser protocol and evaluate its effect in increasing antibiotic sensitivity of the biofilm. A pre-treatment with a single irradiation of the protocol with power 0,3W irradiance 0,18W/cm^2 and fluence 20J/cm^2 significantly reduced the MIC of two of the currently used antibiotics for the treatment of PAO-sustained cystic fibrosis lung

infection: Tobramycin (MIC reduced from 0,3µg/mL to 0,2µg/mL) and Gentamicin (MIC reduced from 0,9µg/mL to 0,62µg/mL).

When we moved to a more complex model, that is the biofilm growth in flow cells under continuous fresh growth medium flow analyzed with Laser Scanning Confocal Microscopy, we faced the problem of the reduction of power density of the laser light throughout the flow cell. It is still unclear to us whether the reduction was due to the flow cell consituent materials (transparent plexiglass) or the biofilm biomass itself. Therefore, we decided to increase the output power reporting also the power density measured at the opposite side of the flow cell. This experiment showed us clearly how blue laser was effective in both killing microbial cells throughout the biomass, and also in significantly reducing the biomass (power 0,5W, top irradiance 0,3W/cm^2, bottom irradiance 0,15 W/cm^2, fluence 120 J/cm^2, CW) or completely disrupt it (power 1W, top irradiance 0,6W/cm^2, bottom irradiance 0,3 W/cm^2, fluence 150 J/cm^2, CW). The entity of the effect was dose-dependent, and it required the highest power/energy combinations employed so far.

When we applied the highest protocol using infrared laser light (970nm), we obtained an absolute absence of any antibacterial or antibiofilm effect, which was consistent with our previous results but not with literature, where such wavelengths have been employed with positive results. Previously published studies have indeed reported significant inhibition of PAO using 660nm, 830nm, 904 laser light (De Sousa et al, 2016) and 880nm LED (Petrini et al, 2017). It is important to highlight the fact that they used always bacterial suspensions and not biofilms, and that they obtained a reduction, and never complete eradication, of bacteria, which tended to grow again after a certain period of time.

This method allowed us also to evaluate inhibition of biofilm growth following a single irradiation with blue laser over time, obtaining a significant reduction in biomass formation up to 72 hours. It is still unclear whether this effect is due to the reduction of viable cells and consequent delay in biofilm development, or to a possible inhibition involving intra/extracellular signaling pathways sensitive to blue light. To explore such hypothesis, gene expression analysis should be considered in the future.

To our knowledge, this is the first report describing the antimicrobial and antibiofilm effect of blue light using the flow cell technique.

To confirm once more the effectiveness of blue laser irradiation in killing PAO, we performed a hybrid qualitative/quantitative experiment using Scanning Electron Microscopy. The obtained images, taken after non viable bacteria have been washed away during sample processing, are showing us severely damaged bacteria with evident blebs and mottled membranes. In addition, the % of the area covered by bacteria was significantly lower in treated samples compared to non treated and infrared laser-treated ones.

Once demonstrated the antimicrobial and antibiofilm effect *per se*, to exploit it and optimize properly it would be fundamental to understand the underlying molecular mechanisms. Despite the literature in the field is still poor, there is an increasing number of studies showing how the exposure to light in the range of 400-470nm decreases viability in a heterogeneous group of bacteria, including *Pseudomonas aeruginosa*, *Porphyromonas gingivalis*, *Helicobacter pylori*, and methicillin-resistant *Staphylococcus aureus* (MRSA) (Dai et al, 2012; Enwemeka et al, 2009). The antimicrobial mechanism of blue light seems to rely on a photochemichal effect rather than a photothermal one, as the interaction of blue light with endogenous photosensitizing molecules, especially porphyrins and flavins, is believed to provoke the generation of reactive oxygen species (ROS). Specifically, absorption of light brings porphyrin molecules into an excited triplet state, leading to a non-radiative transfer of energy to the chemically stable molecular oxygen. The excited oxygen molecule dissociates into two highly reactive atomic species that damage the integrity of cells, leading eventually to microbial death (Yang et al, 1995).
Firstable, to exclude a possible photothermal effect, using a thermographic camera we assessed that for all tested protocols the temperture at sites of irradiation remained always within the range of viability conditions for PAO. The minimum temperature measured was 20,6°C and the maximum was 33,7°C, which we obtained using the Zoom tip with the highest power and irradiance (power 1W irradiance 0,49W/cm^2).

To support the mechanism of action hypothesis that is the most cited in literature, which hasn't found a definitive confirm though, we performed two experiments evaluating oxidative stress from different points of view: on one side, we measured a significant increase in the level of oxidant species in the growth medium after blue laser irradiation; on the other side, the addition of a potent antioxidant compound such as ascorbic acid was able to completely rescue irradiated PAO from death. We wanted to add strength to these hypothesis finding, among a library of random PAO mutants, a gene or a pool of candidate susceptibility genes. Unfortunately, we didn't find any resistant mutant with this approach.

Since endogenous porphyrins seem to be the intracellular targets of blue light, we are currently preparing PAO knock-out mutants for the genes HemA, HemL and HemF, which are respectively upstream (HeaM and HemL) and downstream (HemF) the molecular chain of porphyrin synthesis, to evaluate both whether deficient PAO are less sensitive to blue light, and whether overproducing PAO are more sensitive as we are expecting.

Finally, to confirm the importance of the wavelength rather then the light source and compare the effect of different blue light sources, we repeated the planktonic growth curve experiment using a blue Light Emitting Diode (LED) source. Blue LED is also the blue light source used for the largest part of the studies exploring the antimicrobial activity of blue light, and it is the only one that has found a widespread clinical application for the topical treatment of acne vulgaris (Wheeland et al, 2011). Due to technical limitations, we were able to use only 0,3W and 0,5W powers, which were also the most effective when employed with laser light. Although LED light showed to have significant antimicrobial properties, which is consistent with literature, its effectiveness was significantly lower compared to blue laser at lower fluences (60J/cm^2). We obtained a complete eradication of planktonic PAO only with the LED protocol with power 0,5W irradiance 0,3W/cm^2 and fluence 120J/cm^2. This result disagrees with the only similar study reported in literature, where the antimicrobial efficacies of blue 405nm laser and LED on *Staphylococcus aureus* were not significantly different (Masson-Meyers et al, 2015).

Lasers and LEDs have several differences: while the main characteristics of lasers are monochromaticity, coherence and unidirectionality, LEDs differ

substantially being slightly polychromatic within a certain range (although they are considered monochromatic compared to other sources, for example halogen lamp), their emission lacks coherence, directionality and collimation. Especially longitudinal coherence seems to play a major role in the possible different biological effects of the two sources, as it is associated with the potential for greater penetration of light in tissue/medium (Karu et al, 2003). The slight, but significant difference demonstrated in our study may suggest that the characteristics of blue laser light make it more suitable for penetrating into a medium, throughout a biofilm or through several layers of bacteria exerting a more powerful and less superficial antimicrobial effect.

Since the ultimate scope of this research would be the development and optimization of a novel approach to treat skin infections and clear resistant biofilms *in vivo*, we evaluated the possible safety/toxicity of several irradiation protocols in vivo on HaCaT skin keratinocytes and oral TR146 keratinocytes. We observed differences between cell lines: TR146 keratinocytes, which are of neoplastic origin, showed a complete resistance to blue laser irradiation at all protocols, whereas HaCaT keratinocytes were more sensitive at high fluences. Furthermore, TR146 cells showed also an increase in cell metabolism in terms of ATP production 30 minutes and 2 hours after irradiation, whereas HaCaT cells showed a slight but not significant decrease at every time point. Cell cycle analysis showed no significant differences in the % of apoptotic cells 4 and 24 hours after irradiation for both cell lines. Also the measurement of mitochondrial transmembrane potential, directly related to cell damage and suffering, hasn't shown changes after blue laser treatment. These results are consistent with those reported in literature (Dai et al, 2013).
We further explored possible intracellular changes in response to blue light promoting/suppressing inflammation through gene expression analysis involving both inflammosome molecules (Caspase 1, Interleukin-1b and NLRP3) and antimicrobial pepitdes (Defensin 1, 3 and 4) 30 minutes and 6 hours after irradiation. As expected, all inflammosome genes are overexpressed 30 minutes after treatment, but then normalize after 6 hours. These results are consistent with those reported by Becker et al, where they found an increase of ROS and overexpression of genes involved in

inflammation pathways shortly after irradiation, which then normalize after 1 hour (Becker et al, 2016).
To our knowledge, this is the first study exploring the expression of defensins in HaCaT keratinocytes following blue light treatment. Defensin expression is usually stimulated by inflammatory cytokines such as IL1b. Since IL1b was overexpressed 30 minutes after treatment, we were expecting an increase in all three defensins that we considered. What surprised us was the persistance of overexpression in Defensin 3 and 4 after 6 hours, which have specific antimicrobial activity against several gram positive and gram negative bacteria. In particular, Defensin 4 appears to be highly effective against PAO (Garcia et al, 2001; Harder et al, 2004). Since a recent study showed how immunosuppressive neutrophils (PMN-II) associated with skin wounds, especially with burn injuries, suppress the expression of defensins increasing susceptibility to various infections including PAO (Kawasaki et al, 2014), this result is of particular interest and will warrant further investigation.

The experiments performed and described so far allowed us to choose a protocol to use in the *in vivo* experiment, trying to find a balance between antimicrobial effects and safety against keratinocytes. We decided to employ the protocol with wavelength 445nm power 0,3W irradiance 0,105W/cm^2 fluence 60J/cm^2.
This experiment confirmed what we evaluated *in vitro* previously, that is the significant decrease in bacterial load on the abrasions 24 hours after treatment. However, we obtained complete eradication of PAO in only one sample. Several possible reasons can be identified: the cross-infection with other animals during the 24 hours post-treatment, a fast penetration of PAO through the damaged tissues which wouldn't allow the blue laser light to reach all microbial cells, or an interference of light with the skin layers. Multiple irradiation sessions should be considered in future experiments.
Apart from testing antimicrobial efficacy, our primary goal was to evaluate possible thermal damages to the irradiated tissue. To our surprise, not only the thermal damage was detectable in only 3 samples and it was of very low entity, but the treated samples showed a huge difference in inflammation rate compared to non treated ones. In fact, in all non treated samples the dermal

and epidermal layers were permeated with a huge inflammatory infiltrate. Also panniculitis was clearly visible in most of the animals. On the other hand, in all laser treated samples the epidermal layer was preserved (apart from the reduced thickness caused by abrasion) and free from inflammatory infiltrate. The only sample showing a modest focal infiltrate together with dermal flogosis was LT3.
The anti-inflammatory properties of photobiomodulation (PBM) are well known and still under investigation, and usually involve red or infrared wavelengths due to their major penetration into skin/mucosal deeper layers (Prindeze et al, 2012). Since it is known that blue light has a very low penetration and its effects are considered superficial, these findings are very interesting and will need further investigation to be thoroughly explained.

It is well known that blue light can be used also to excite photosensitizing molecules in photodynamic therapy (PDT). As happened for a lot of scientific discoveries over centuries, also PDT was accidentally discovered over 100 years ago by Oskar Raab and Hermann von Tappiener when they noticed that *Paramecium spp* protozoans stained with acridine orange died upon exposure to bright light (Raab et al, 1900). Since then, it has been transformed to an anticancer therapy but recently, due to the increasing antibiotic resistance crisis, it is returning into consideration for the treatment of localized infections. PDT is considered quite selective because the photosensitizer uptake is major in highly proliferating cells, such as bacteria or neoplastic cells.
Among the variety of possible photosensitizers, curcumin is on the edge of interest due to its multiple antimicrobial, anti-inflammatory and anti-tumoral effects. Its poor water solubility is limiting clinical applications so far due to consequent reduced bioavailability and instability. In particular, it seems that the antimicrobial activity of curcumin is associated to membrane damage and it acts towards both gram positive and gram negative bacteria, including PAO. However, gram negative bacteria are less sensitive due to the outer bacterial cell membrane restricting permeation of curcumin (George et al, 2009) and at least 100μM concentrations are necessary to significantly decrease PAO viability (Tyagi et al, 2015). This result is consistent with the data that we obtained, since 50μM curcumin concentrations significantly decreased bacterial

growth but weren't enough to eradicate planktonic bacteria. There are no data about the use of free curcumin in antimicrobial PDT towards PAO. Studies conducted on other bacterial species still suggest the need for high concentrations (mM) to exert its effect (Araujo et al, 2014), which may be toxic for surrounding tissues. In our study, we observed statistically significant differences in bacterial growth with the addition of free curcumin followed by laser irradiation, unfortunately without obtaining complete inhibition.

In literature, when curcumin was encapsulated in nanoparticles, its efficacy increased but the minimum inhibitory concentration remained in the range of μM (Atahoun et al, 2016; Trigo Gutierrez et al, 2017).

In our study, we evaluated the antimicrobial efficacy with and without blue laser irradiation of curcumin embedded in three types of amphiphilic self-assembling nanomicelles with palmitic acid as hydrophobe (C_{16}) and three types of cationic ligands, connected using TBTU-mediated peptide coupling, yielding C_{16}-DAPMA, C_{16}-SPD and C_{16}-SPM with nominal ligand charges of +2, +2 and +3 respectively at physiological pH (7.4). Compound C_{16}-DAPMA (+2) has good aqueous solubility, spermidine-based C_{16}-SPD (+2) is slightly less soluble, and spermine-derived C_{16}-SPM (+3) is more difficult to dissolve.

When provided in decreasing concentrations to a PAO planktonic suspension, all three types of curcumin embedding nanomicelles showed antimicrobial efficacy, eradicating PAO at 500nM (C_{16}-DAPMA), 1μM (C_{16}-SPD) and 250nM (C_{16}-SPM) concentrations.

Therefore, spermine-based nanomicelles were the most effective. One possible reason for its effectiveness at such low concentrations (the lowest from those reported in literature so far, to our knowledge) could be the antimicrobial activity of spermine itself, although its MIC is 16mM (Kwon et al, 2007), which is much higher than the concentrations that we employed. In addition, we evaluated the effect of blank nanomicelles (not carrying curcumin), and all types of nanomicelles lacked any antimicrobial effects. The reason for their efficacy is probably their highest charge (+3), which increases significantly their capacity to bind polyanions, as tested experimentally during their characterization (Fechner et al, 2016). Like all gram negative bacteria, also PAO has an outer membrane situated above a thin peptidoglycan layer. Together with the peptidoglycan layer and and periplasm, it constitutes the gram-negative envelope. The outer

membrane possesses proteins, phospholipids, and lipopolysaccharides (LPS) which are asymmetrically distributed as the outer face is constituted with only LPS. LPS contains more charge per unit of surface area than any phospholipid, and most of this charge is anionic at neutral pH because of exposed phosphoryl and carboxyl groups which can be readily ionized. For this reason, the outer face of the outer membrane is highly charged and is highly interactive with cations in the outside milieu (Beveridge, 1999), including, in our case, the positively charged nanomicelles. Being C_{16}-SPM the most positively charged nanomicelles among the ones included in our study, it is reasonable that its interaction with PAO outer membrane is enhanced with respect to the others.
When micelles were irradiated with the blue laser protocol wavelength 445nm, power 0,2W irradiance 0,1W/cm^2, fluence 6J/cm^2 we haven't observed differences in bacterial survival compared to non irradiated ones. However, when we increased fluence to 18J/cm^2 and 30J/cm^2, the MIC of C_{16}-SPM further decreased to 50nM.

In conclusion, throughout this research work we demonstrated how blue laser irradiation alone is able to exert antimicrobial effects towards PAO grown in different conditions and we identified the most effective irradiation parameters. Furthermore, we described also an antibiofilm activity both in disrupting a mature biofilm and in inhibiting biofilm formation. Although further and more molecular-based investigation is warranted, our results suggest, according with literature, a possible role of oxidative stress stimulation for the explanation of bacterial inhibition/death. Comparing blue laser source with LED, laser was significantly more effective. When investigating the possible toxic effects on keratinocytes, we highlighted a stimulation of inflammosome molecules expression as expected, but also an overexpression of highly active antimicrobial peptides (defensins), which persists hours after irradiation, and will surely deserve deeper investigation. The results regarding the experiment in vivo on a mouse model of infected abrasion were both conflicting and surprising: although we obtained a significant reduction in bacterial load in laser treated mice, we haven't obtained complete eradication as we were expecting basing on our previous results. But on the other hand, when observing histological samples to evaluate possible thermal damage, we noticed a huge

difference among samples: while non treated displayed a high inflammation rate permeating epidermal and dermal layers, the laser treated ones had minimum epidermal damage and were almost free of inflammatory infiltrate. While anti-inflammatory properties of red and infrared laser-mediated photomodulation are known and currently under investigation, such effects of blue light haven't been explored yet. Finally, we explored the possible potentiating effect of blue laser sublethal irradiation on three types of amphiphilic nanomicelles loaded with curcumin. We obtained the lowest MIC of curcumin nanoparticles described so far, which further decreased after sublethal blue laser irradiation.

While it is clear that a number of doubts remain unanswered, and several new questions have arised, we believe that the obtained results have pushed a bit further the research in the field, fostering the validation of a novel antimicrobial approach in a moment of increasing resistance crisis.

Acknowledgements

My deepest and most sincere thanks go to my tutor Serena Zacchigna who gave me the possibility to work in such a stimulating and high profile environment as the ICGEB. She constantly helped reviewing my work and enriched it thanks to her observations. My gratitude goes to all the special and talented scientists I met there and elsewhere, who helped me developing this research work: Vittorio Venturi, Iris Bertani, Rossana Bussani, Valentina Martinelli, Simone Vodret, Daniel Passos Da Silva and Matthew Parsek.

During these years, I was lucky enough to meet and collaborate with colleagues from other institutions that helped in a fundamental and precious way: Luisa Zupin, Davide Porrelli, Mario Mardirossian and Jacopo Dus. I hope this is only the beginning of a long lasting and proficient cooperation.

I wish to express my sincere gratitude to my supervisor Roberto Di Lenarda and to Matteo Biasotto for helping me initiate and perform this experience, maintaining also my clinical activity in the field of oral medicine and pathology.

A very special thanks goes to my colleague Giulia Ottaviani, the “mother of lasers”, without whose studies I would not have the possibility to perform my research in the laser field.

Let me also thank all the colleagues and friends, from the Oral Medicine and Pathology Unit Margherita, Valentina, Erica and Maddalena for all the scientific and non-scientific discussions during ladies’ dinners.

My devoted gratitude and endless love is addressed to the special people that constantly enrich my life and make it always full of joy: my parents, my family (true and acquired), and my best friends.

And of course I thank You, my significant other. Your intelligence and rationality stimulate me to constantly improve my results.

But the most important gratitude goes to *Pseudomoas aeruginosa*, for not liking the blue light.

References

Adahoun MA, Al-Akhras MH, Jaafar MS, Bououdina M. Enhanced anti-cancer and antimicrobial activities of curcumin nanoparticles. Artif Cells Nanomed Biotechnol. 2017 Feb;45(1):98-107. Epub 2016 Jan 8.
doi: 10.3109/21691401.2015.1129628

Akbarzadeh A, Rezaei-Sadabady R, Davaran S, et al. Liposome: classification, preparation, and applications. Nanoscale Research Letters. 2013;8(1):102. doi:10.1186/1556-276X-8-102.

Alkilany AM, Murphy CJ. Toxicity and cellular uptake of gold nanoparticles: what we have learned so far? Journal of Nanoparticle Research. 2010;12(7):2313-2333. doi:10.1007/s11051-010-9911-8.

Alhede M, Bjarnsholt T, Jensen PØ, Phipps RK, Moser C, Christophersen L, et al. Pseudomonas aeruginosa recognizes and responds aggressively to the presence of polymorphonuclear leukocytes. Microbiology 2009;155:3500–8. doi:10.1099/mic.0.031443-0.

Almeida RD, Manadas BJ, Carvalho AP, Duarte CB. Intracellular signaling mechanisms in photodynamic therapy. Biochim Biophys Acta. 2004 Sep 20; 1704(2):59-86.

Amin RM, Bhayana B, Hamblin MR, Dai T. Antimicrobial blue light inactivation of Pseudomonas aeruginosa by photo-excitation of endogenous porphyrins: In vitro and in vivo studies. Lasers Surg Med. 2016 Jul;48(5):562-8. doi: 10.1002/lsm.22474. Epub 2016 Feb 18.

Araújo NC, Fontana CR, Bagnato VS, Gerbi ME. Photodynamic effects of curcumin against cariogenic pathogens. Photomed Laser Surg. 2012 Jul;30(7):393-9. doi: 10.1089/pho.2011.3195. Epub 2012 Jun 13.

Araújo NC, Fontana CR, Bagnato VS, Gerbi ME. Photodynamic antimicrobial therapy of curcumin in biofilms and carious dentine. Lasers Med Sci. 2014 Mar;29(2):629-35. doi: 10.1007/s10103-013-1369-3. Epub 2013 Jun 23.

Bai, J., Kim, Y.-T., Ryu, S., and Lee, J.-H. (2016). Biocontrol and Rapid Detection of Food- Borne Pathogens Using Bacteriophages and Endolysins. Front. Microbiol. 7: 474.

Bartlett JG, Gilber t DN, Spellberg B. Seven ways to preserve the miracle of antibiotics. Clin Infect Dis 2013;56(10):1445–1450.

Becker A, Klapczynski A, Kuch N, Arpino F, Simon-Keller K, De La Torre C, Sticht C, van Abeelen FA, Oversluizen G, Gretz N. Gene expression profiling reveals aryl hydrocarbon receptor as a possible target for photobiomodulation when using blue light. Sci Rep. 2016 Sep 27;6:33847. doi: 10.1038/srep33847.

Beveridge TJ. Structures of gram-negative cell walls and their derived membrane vesicles. J Bacteriol. 1999 Aug;181(16):4725-33.

Biener G, Masson-Meyers DS, Bumah VV, Hussey G, Stoneman MR, Enwemeka CS, Raicu V. Blue/violet laser inactivates methicillin-resistant Staphylococcus aureus by altering its transmembrane potential. J Photochem Photobiol B. 2017 May;170:118-124.

Biondi M, Ungaro F, Qualia F, et al. Controlled drug delivery in tissue engineering. Adv Drug Deliv Rev 2008; 60: 229-42.

Bumah VV, Masson-Meyers DS, Cashin SE, Enwemeka CS. Wavelength and bacterial density influence the bactericidal effect of blue light on methicillin-resistant Staphylococcus aureus (MRSA). Photomed Laser Surg. 2013 Nov;31(11):547-53. doi: 10.1089/pho.2012.3461. Epub 2013 Apr 27.

Dai T, Gupta A, Murray CK, Vrahas MS, Tegos GP, Hamblin MR. 2012. Blue light for infectious diseases: Propionibacterium acnes, Helicobacter pylori, and beyond? Drug Resist. Updat. 15:223–236.

Dai T, Gupta A, Huang YY, Yin R, Murray CK, Vrahas MS, Sherwood ME, Tegos GP, Hamblin MR. Blue light rescues mice from potentially fatal Pseudomonas aeruginosa burn infection: efficacy, safety, and mechanism of action. Antimicrob Agents Chemother. 2013 Mar;57(3):1238-45. doi: 10.1128/AAC.01652-12.

Elhissi AMA, Ahmed W, Hassan IU, Dhanak VR, D'Emanuele A. Carbon Nanotubes in Cancer Therapy and Drug Delivery. Journal of Drug Delivery. 2012;2012:837327. doi:10.1155/2012/837327.

Enwemeka CS, Williams D, Enwemeka SK, Hollosi S, Yens D. 2009. Blue 470-nm light kills methicillin-resistant Staphylococcus aureus (MRSA) in vitro. Photomed. Laser Surg. 27:221–226.

Erel O. A new automated colorimetric method for measuring total oxidant status. Clin Biochem. 2005 Dec;38(12):1103-11. Epub 2005 Oct 7.

De Sousa NT, Santos MF, Gomes RC, Brandino HE, Martinez R, de Jesus Guirro RR. Blue Laser Inhibits Bacterial Growth of Staphylococcus aureus, Escherichia coli, and Pseudomonas aeruginosa. Photomed Laser Surg. 2015 May;33(5):278-82. doi: 10.1089/pho.2014.3854.

De Sousa NT, Gomes RC, Santos MF, Brandino HE, Martinez R, de Jesus Guirro RR. Red and infrared laser therapy inhibits in vitro growth of major bacterial species that commonly colonize skin ulcers. Lasers Med Sci. 2016 Apr;31(3):549-56. doi: 10.1007/s10103-016-1907-x. Epub 2016 Feb 17.

Fechner LE, Albanyan B, Vieira VMP, Laurini E, Posocco P, Pricl S, Smith DK. Electrostatic binding of polyanions using self- assembled multivalent (SAMul) ligand displays – structure–activity effects on DNA/heparin binding. Chem. Sci., 2016, 7, 4653.

Ferreyra DD, Reynoso E, Cordero P, Spesia MB, Alvarez MG, Milanesio ME, Durantini EN. Synthesis and properties of 5,10,15,20-tetrakis[4-(3-N,N-dimethylaminopropoxy)phenyl] chlorin as potential broad-spectrum antimicrobial photosensitizers. J Photochem Photobiol B. 2016 May; 158:243-51.

Fila G, Kawiak A, Grinholc MS. Blue light treatment of Pseudomonas aeruginosa: Strong bactericidal activity, synergism with antibiotics and inactivation of virulence factors. Virulence. 2017 Aug 18;8(6):938-958. doi: 10.1080/21505594.2016.1250995. Epub 2016 Oct 20.

Foote, CS Definition of type I and type II photosensitized oxidation. Photochem Photobiol 1991, 54, (5), 659.

Fu W, Forster T, Mayer O, Curtin JJ, Lehman SM, Donlan RM. Bacteriophage cocktail for the prevention of biofilm formation by Pseudomonas aeruginosa on catheters in an in vitro model system. Antimicrob Agents Chemother. 2010 Jan;54(1):397-404. doi: 10.1128/AAC.00669-09. Epub 2009 Oct 12.

Ganz T, Lehrer RI. Antibiotic peptides from higher eukaryotes: biology and applications. Mol Med Today. 1999 Jul;5(7):292-7.

García JR, Krause A, Schulz S, Rodríguez-Jiménez FJ, Klüver E, Adermann K, Forssmann U, Frimpong-Boateng A, Bals R, Forssmann WG. Human beta-defensin 4: A novel inducible peptide with a specific salt-sensitive spectrum of antimicrobial activity. FASEB J, 15 (2001), pp. 1819-1821.

George S, Hamblin MR, Kishen A. 2009. Uptake pathways of anionic and cationic photosensitizers into bacteria. Photochem Photobiol Sci 8(6):788–795.

Goel A, Kunnumakkara AB, Aggarwal BB. Curcumin as "Curecumin": from kitchen to clinic. Biochem Pharmacol. 2008 Feb 15;75(4):787-809. Epub 2007 Aug 19.

Gold, M. H. Therapeutic and Aesthetic Uses of Photodynamic Therapy Part five of a five-part series: ALA-PDT and MAL-PDT What Makes Them Different. J Clin Aesthet Dermatol 2009, 2, (2), 44-7.

Grönqvist A, Wiström J, Axner O, Monsen TJ. Bactericidal effect of pulsed 1,064 nm Nd:YAG laser light on Staphylococcus epidermidis is of photothermal origin: an in vitro study. Lasers Surg Med. 2000;27(4):336-40.

Guffey, J.S., Wilborn, J., 2006. In vitro bactericidal effects of 405-nm and 470-nm blue light. Photomedicine and Laser Surgery 24, 684–688.

Halstead FD, Thwaite JE, Burt R, Laws TR, Raguse M, Moeller R, Webber MA, Oppenheim BA. Antibacterial Activity of Blue Light against Nosocomial Wound Pathogens Growing Planktonically and as Mature Biofilms. Appl Environ Microbiol. 2016 Jun 13;82(13):4006-16. doi: 10.1128/AEM.00756-16. Print 2016 Jul 1.

Hamblin MR, Hasan T. Photodynamic therapy: a new antimicrobial approach to infectious disease? Photochem Photobiol Sci. 2004 May; 3(5):436-50.

Hamblin MR. Mechanisms and applications of the anti-inflammatory effects of photobiomodulation. AIMS biophysics. 2017;4(3):337-361.
doi:10.3934/biophy.2017.3.337.

Harder J, Meyer-Hoffert U, Wehkamp K, Schwichtenberg L, Schröder JM. Differential gene induction of human beta-defensins (hBD-1, -2, -3, and -4) in keratinocytes is inhibited by retinoic acid. J Invest Dermatol. 2004 Sep;123(3):522-9.

Hirshfield, I.N., Terzulli, S., and O'Byrne, C. (2003). Weak organic acids: a panoply of effects on bacteria. Sci. Prog. 86: 245–269.

Irschik H, R. Jansen, K. Gerth, G. Höfle, H. Reichenbach. The sorangicins, novel and powerful inhibitors of eubacterial RNA polymerase isolated from myxobacteria. J. Antibiot., 40 (1987), pp. 7-13

Jawhara S, Mordon S. Monitoring of bactericidal action of laser by in vivo imaging of bioluminescent E. coli in a cutaneous wound infection. Lasers Med Sci (2006) 21: 153–159.

Kamma JJ, Vasdekis VG, Romanos GE. The effect of diode laser (980 nm) treatment on aggressive periodontitis: evaluation of microbial and clinical parameters. Photomed Laser Surg 2009: 27: 11–19.

Karu TI (2003) Low power laser therapy. In: Vo-Dinh T (ed) Biomedical photonics handbook. CRC Press, Boca Raton, pp 48-1–48-25.

Kawasaki T, Nakamura K, Jeschke MG, Kogiso M, Kobayashi M, Herndon DN, Suzuki F. Impaired ability of burn patient neutrophils to stimulate β-defensin production by keratinocytes. Immunol Cell Biol. 2012 Sep;90(8):796-801. doi: 10.1038/icb.2012.3. Epub 2012 Mar 6.

Kong FY, Zhang JW, Li RF, Wang ZX, Wang WJ, Wang W. Unique Roles of Gold Nanoparticles in Drug Delivery, Targeting and Imaging Applications. Molecules. 2017 Aug 31;22(9). pii: E1445. doi: 10.3390/molecules22091445.

Koseva NS, Rydz J, Stoyanova EV, Mitova VA. Hybrid protein-synthetic polymer nanoparticles for drug delivery. Adv Protein Chem Struct Biol. 2015;98:93-119. doi: 10.1016/bs.apcsb.2014.12.003. Epub 2015 Mar 13.

Krishnamurthy M, Moore RT, Rajamani S, Panchal RG. Bacterial genome engineering and synthetic biology: combating pathogens. BMC Microbiology. 2016;16:258. doi:10.1186/s12866-016-0876-3.

Kutter EM, Kuhl SJ, and Abedon ST. Re-establishing a place for phage therapy in western medicine. Future Microbiol. 2015;10(5):685-8.
doi: 10.2217/fmb.15.28.

Kwon DH, Lu CD. Polyamine effects on antibiotic susceptibility in bacteria. Antimicrob Agents Chemother. 2007 Jun;51(6):2070-7. Epub 2007 Apr 16.

Høiby N, Bjarnsholt T, Moser C, Bassi GL, Coenye T, Donelli G, et al. ESCMID guideline for the diagnosis and treatment of biofilm infections 2014. Clin Microbiol Infect 2015;21 Suppl 1:S1–25. doi:10.1016/j.cmi.2014.10.024.

Mardirossian M, Grzela R, Giglione C, Meinnel T, Gennaro R, Mergaert P, Scocchi M. The host antimicrobial peptide Bac71-35 binds to bacterial ribosomal proteins and inhibits protein synthesis. Chem Biol. 2014 Dec 18;21(12):1639-47. doi: 10.1016/j.chembiol.2014.10.009. Epub 2014 Nov 13.

Masson-Meyers DS, Bumah VV, Biener G, Raicu V, Enwemeka CS. The relative antimicrobial effect of blue 405 nm LED and blue 405 nm laser on methicillin-resistant Staphylococcus aureus in vitro. Lasers Med Sci. 2015 Dec;30(9):2265-71. doi: 10.1007/s10103-015-1799-1. Epub 2015 Sep 11.

McVay, C.S., Velásquez, M., and Fralick, J.A. (2007). Phage therapy of Pseudomonas aeruginosa infection in a mouse burn wound model. Antimicrob. Agents Chemother. 51: 1934–8.

Mitra KA. Drug Delivery (book) 2015; chapter 10, page 244. Jones and Bartlett learning.

Moreno-Vega AI, Gómez-Quintero T, Nuñez-Anita RE, Acosta-Torres LS, Castaño V. Polymeric and Ceramic Nanoparticles in Biomedical Applications. Journal of Nanotechnology, vol. 2012, Article ID 936041, 10 pages, 2012. doi:10.1155/2012/936041.

Moritz A, Gutknecht N, Doertbudak O, Goharkhay K, Schoop U, Schauer P, Sperr W. Bacterial reduction in periodontal pockets through irradiation with a diode laser: a pilot study. J Clin Laser Med Surg. 1997 Feb;15(1):33-7.

Moritz A, Schoop U, Goharkhay K, Schauer P, Doertbudak O, Wernisch J, Sperr W. Treatment of periodontal pockets with a diode laser. Lasers Surg Med. 1998;22(5):302-11.

Müller R, Wink J. Future potential for anti-infectives from bacteria - how to exploit biodiversity and genomic potential. Int J Med Microbiol. 2014 Jan;304(1):3-13. doi: 10.1016/j.ijmm.2013.09.004. Epub 2013 Sep 4. Review.

Munita JM, Arias CA. Mechanisms of Antibiotic Resistance. Microbiology spectrum. 2016; 4(2):10.1128/microbiolspec.VMBF-0016-2015. doi:10.1128/microbiolspec.VMBF-0016-2015.

Nagoba BS1, Selkar SP, Wadher BJ, Gandhi RC. Acetic acid treatment of pseudomonal wound infections--a review. J Infect Public Health. 2013 Dec;6(6):410-5. doi: 10.1016/j.jiph.2013.05.005. Epub 2013 Jul 30.

O'Toole, G., and Kolter, R. Initiation of biofilm formation in Pseudomonas fluorescens WCS365 proceeds via multiple, convergent signalling pathways: A genetic analysis. Mol. Microbiol. 1998; 28:449-461.

Passarella S, Karu T. Absorption of monochromatic and narrow band radiation in the visible and near IR by both mitochondrial and non-mitochondrial photoacceptors results in photobiomodulation. J Photochem Photobiol B. 2014 Nov;140:344-58. doi: 10.1016/j.jphotobiol.2014.07.021. Epub 2014 Aug 21.

Petrini M, Trentini P, Tripodi D, Spoto G, D'Ercole S. In vitro antimicrobial activity of LED irradiation on Pseudomonas aeruginosa. J Photochem Photobiol B. 2017 Mar;168:25-29. doi: 10.1016/j.jphotobiol.2017.01.020. Epub 2017 Jan 24.

Prindeze NJ, Moffatt LT, Shupp JW. Mechanisms of action for light therapy: a review of molecular interactions. Exp Biol Med (Maywood). 2012 Nov;237(11):1241-8. doi: 10.1258/ebm.2012.012180.

Raab O. Ueber diewirkung fluoreszierender stoffe auf infusori. Z Biol 1900; 39:524-36.
Roberts, A.E.L., Kragh, K.N., Bjarnsholt, T. & Diggle, S.P., The limitations of in vitro experimentation in understanding biofilms and chronic infec- tion, Journal of Molecular Biology (2015), doi: 10.1016/j.jmb.2015.09.002

Reardon S. Bacterial arms race revs up. Nature 2015; 521:402-3.

Riley MA, Wertz JE. Bacteriocins: evolution, ecology, and application. Annu. Rev. Microbiol. 2002; 56, 117–137 10.1146/annurev.micro.56.012302.161024

Rkein, A. M.; Ozog, D. M. Photodynamic therapy. Dermatol Clin 2014, 32, (3), 415-25, x.

Roe AJ, McLaggan D, Davidson I, O'Byrne C, Booth IR. Perturbation of anion balance during inhibition of growth of Escherichia coli by weak acids. J Bacteriol. 1998 Feb;180(4):767-72.

Rossolini GM, Arena F, Pecile P, Pollini S. Update on the antibiotic resistance crisis. Curr Opin Pharmacol. 2014 Oct;18:56-60.

Schoop U, Kluger W, Moritz A, Nedjelik N, Georgopoulos A, Sperr W. Bactericidal effect of different laser systems in the deep layers of dentin. Lasers Surg Med. 2004;35(2):111-6.

Seo SJ, Ahn SW, Hong CK, Ro BI. Expressions of beta-defensins in human keratinocyte cell lines. J Dermatol Sci. 2001 Nov;27(3):183-91.

Slavin YN, Asnis J, Häfeli UO, Bach H. Metal nanoparticles: understanding the mechanisms behind antibacterial activity. Journal of Nanobiotechnology. 2017;15:65. doi:10.1186/s12951-017-0308-z.

Sloss JM, Cumberland N, Milner SM. Acetic acid used for the elimination of Pseudomonas aeruginosa from burn and soft tissue wounds. J R Army Med Corps. 1993 Jun;139(2):49-51.

Taylor PK, Yeung AT, Hancock RE. Antibiotic resistance in Pseudomonas aeruginosa biofilms: towards the development of novel anti-biofilm therapies. J Biotechnol. 2014 Dec 10;191:121-30.

Tomasinsig L, Skerlavaj B, Papo N, Giabbai B, Shai Y, Zanetti M. Mechanistic and functional studies of the interaction of a proline-rich antimicrobial peptide with mammalian cells. J Biol Chem. 2006 Jan 6;281(1):383-91.

Trigo Gutierrez JK, Zanatta GC, Ortega ALM, Balastegui MIC, Sanitá PV, Pavarina AC, Barbugli PA, Mima EGO. Encapsulation of curcumin in polymeric nanoparticles for antimicrobial Photodynamic Therapy. PLoS One. 2017 Nov 6;12(11):e0187418. doi: 10.1371/journal.pone.0187418. eCollection 2017.

Tyagi P, Singh M, Kumari H, Kumari A, Mukhopadhyay K (2015) Bactericidal Activity of Curcumin I Is Associated with Damaging of Bacterial Membrane. PLoS ONE 10(3): e0121313. doi:10.1371/journal.pone.0121313

Van Gennip M, Christensen LD, Alhede M, Phipps R, Jensen PØ, Christophersen L, et al. Inactivation of the rhlA gene in Pseudomonas aeruginosa prevents rhamnolipid production, disabling the protection against polymorphonuclear leukocytes. APMIS 2009;117:537–46. doi:10.1111/j.1600-0463.2009.02466.x.

Walker, D. & Fowler, T. Annual Report of the Chief Medical Officer: Volume Two, 2011: Infections and the Rise of Antimicrobial Resistance (Department of Health, 2011).

Wheeland RG, Dhawan S. 2011. Evaluation of self-treatment of mild-to-moderate facial acne with a blue light treatment system. J. Drugs Dermatol. 10:596 – 602.

World Economic Forum. Global Risks 2014 Report
http://www.weforum.org/reports/global-risks-2014-report (2014).

World Health Organization; 2014. Antimicrobial resistance: global report on surveillance 2014.
http://www.who.int/drugresistance/documents/surveillancereport/en/

Yang H, Inokuchi H, Adler J. Phototaxis away from blue light by an Escherichia coli mutant accumulating protoporphyrin IX, Proc. Natl. Acad. Sci. USA 92 (1995) 7332-7336.

Yin R, Agrawal T, Khan U, et al. Antimicrobial photodynamic inactivation in nanomedicine: small light strides against bad bugs. Nanomedicine (London, England). 2015;10(15):2379-2404. doi:10.2217/nnm.15.67.

Yount NY, Bayer AS, Xiong YQ, Yeaman MR. Advances in antimicrobial peptide immunobiology. Biopolymers. 2006;84(5):435-58.

Zanetti M. The role of cathelicidins in the innate host defenses of mammals. Curr Issues Mol Biol. 2005 Jul;7(2):179-96.